

Master thesis

Hugo S. Velásquez Leiva

Structural design optimization of an aircraft composite wing-box using curvilinear stiffeners

*Fakultät Technik und Informatik
Department Fahrzeugtechnik und Flugzeugbau*

*Faculty of Engineering and Computer Science
Department of Automotive and
Aeronautical Engineering*

Hugo S. Velásquez Leiva

**Structural design optimization of an
aircraft composite wing-box using
curvilinear stiffeners**

Masterarbeit eingereicht im Rahmen der Masterprüfung

im Studiengang Flugzeugbau
am Department Fahrzeugtechnik und Flugzeugbau
der Fakultät Technik und Informatik
der Hochschule für Angewandte Wissenschaften Hamburg

in Zusammenarbeit mit:
Deutsches Zentrum für Luft- und Raumfahrt
Institut für Faserverbundeleichtbau und Adaptronik
Lilienthalplatz 7
38108 Braunschweig

Erstprüfer/in: Prof. Dr.-Ing. Michael Seibel
Zweitprüfer/in: Prof. Dr.-Ing. Wilfried Dehmel

Abgabedatum: 24.06.2014

Zusammenfassung

Hugo S. Velásquez Leiva

Thema der Masterthesis

Strukturoptimierung unter Verwendung von krummlinigen Versteifungselementen zur Faserverbund-Tragflächenauslegung

Stichworte

Vorwärts gepfeilter Flügel, Faserverbundwerkstoffe, aeroelastic tailoring, krummlinige Stringer, Optimierung, FEM, glued contact, Bézier Kurve, Nastran SOL105, Nastran SOL400, PCL Patran

Kurzzusammenfassung

In dieser Arbeit werden die Gurtplatten eines vorwärts gepfeilten Faserverbund-Flügels mit krummlinig verlaufenden Versteifungselementen versteift. Es wird untersucht, welchen Einfluss solche Versteifungselemente auf das Strukturverhalten haben (insbesondere hinsichtlich aeroelastic tailoring) im Vergleich zu den üblicherweise geradlinig und parallel verlaufenden Stringer. Die Strukturanalyse erfolgt mit Hilfe der Finite-Elemente-Methode. Die krummlinig verlaufenden Versteifungselemente sind durch polynomiale Funktionen definiert und bieten eine große Entwurfsflexilität. Die Strukturkomponenten des FE Modells sind mittels Kontaktmethoden („permanent glued contact“) gekoppelt, welche die Verbindung von nicht-koinzidenten Vernetzungen ermöglichen. Ein voll-parametrisches FEM ist entwickelt und in eine überspannende Strukturoptimierungsprozedur eingebunden, welche geometrische (z.B. Stringerpositionen) und laminatspezifische (Schichtdicken) Entwurfsvariablen enthält. Die Auslegungskriterien Masse, Stabilität und Steifigkeit (Flügeldurchbiegung und –torsion) werden berücksichtigt.

Hugo S. Velásquez Leiva

Title of the paper

Structural design optimization of an aircraft composite wing-box using curvilinear stiffeners

Keywords

Forward swept wing, composite, aeroelastic tailoring, curvilinear stiffeners, optimization, FEM, glued contact, Bézier curves, Nastran SOL105, Nastran SOL400, PCL Patran

Abstract

Inside this report the concept of stiffening the wing covers of a forward swept wing with curvilinear stringers is presented. The objective is to investigate the influence of such curvilinear stiffeners on the structural behavior, especially w.r.t. aeroelastic tailoring capabilities and in comparison to traditional stiffener arrangements that are straight and/or parallel to front or rear spar. For structural analysis purposes a state-of-the-art finite element model software is used. The curvilinear stringer paths are defined using polynomial functions providing large design flexibility. The wing FEM is assembled using contact methods (“permanent glued contact“) that enables to join the curvilinear stringers to the wing covers both having dissimilar meshes. For optimization purposes a fully parametric FEM is generated and embedded into an overarching design optimization procedure that includes geometrical (e.g. stringer positions) and composite (ply thickness) design variables. The optimization process includes structural design objectives like mass, buckling behaviour and wing deformations (bending and twisting).

Declaration Statement

I declare that I have authored this master thesis independently, that I have not used other than the declared sources / resources, and that I have explicitly marked all material which has been quoted either literally or by content from the used sources.

Name: HUGO S. VELASQUEZ LEIVA

Matriculation Number: 1948499

Signed:



Location, date: Hamburg, 20.06.14

Table of Contents

List of Figures	3
List of Tables	6
List of Symbols, Indices and Abbreviations	8
1 Introduction	1
1.1 Overview of the research project AeroStruct – ForSwing.....	1
1.2 Problem definition and motivation.....	1
1.3 Outline of subsequent chapters.....	3
2 Literature review	5
2.1 Optimization of metal and composite aircraft wing-box structures	5
2.2 Aeroelastic tailoring and forward swept wing.....	6
2.3 Curvilinear stiffening components.....	7
3 Finite-element modeling and assembly method	8
3.1 Geometry and finite-element properties of the forward swept wing model	8
3.2 Overview of finite-element assembly methods.....	10
3.3 Theoretical background and implementation of permanent glued contact method...	11
3.4 Validation of permanent glued contact method.....	15
3.4.1 Assessment of buckling behavior	16
3.4.2 Assessment of elastic deformations	21
3.5 Further considerations about the permanent glued contact method	24
4 Finite-element parameterization and automation	27
4.1 Parameterization concept of curvilinear stiffeners.....	27
4.2 Further parameterized properties	32
4.3 Implementation and automation in MSC.Patran	32
5 Optimization framework	36
5.1 General overview of optimization process	36
5.1.1 Software and architecture.....	36
5.1.2 Parametric Thickness Distribution Procedure (PTDP)	37
5.1.3 Optimization platform Optimus	39
5.2 Optimization problem definition	40
5.2.1 Design variables.....	41
5.2.2 Design responses.....	42
6 Preliminary structural assessment	44
6.1 Definition of parameter study.....	44
6.2 Results of parameter study.....	47

7	Structural optimizations	50
7.1	Definition of optimization models and overall settings.....	50
7.1.1	Optimizations A (elastic deformations)	51
7.1.2	Optimizations B (elastic deformations, limited wing cover thicknesses)	53
7.1.3	Optimizations C (buckling behavior)	55
7.2	Optimization results.....	56
7.2.1	Optimizations A	56
7.2.2	Optimizations B	62
7.2.3	Optimizations C	66
8	Conclusions and outlook	69
	References	72
	Appendix A	77
	Appendix B	78
	Appendix C	79
	Appendix D	80
	Appendix E	81
	Appendix F	86
	Appendix G	87

List of Figures

Fig. 1-1 Overview of different stringer configurations	2
Fig. 1-2 Example of dissimilar meshes for lower cover and stringers	3
Fig. 2-1 Three-Columns-Concept for solving MDO-optimization problems [17]	6
Fig. 3-1 Forward swept wing geometry (adapted from [49])	9
Fig. 3-2 Finite-element modeling of forward swept wing (adapted from [49])	9
Fig. 3-3 Definition of fastener and spot weld connection [35]	10
Fig. 3-4 Permanent glued contact examples	11
Fig. 3-5 Contact problem representation [41]	12
Fig. 3-6 Contact detection and tolerances [43]	13
Fig. 3-7 Detail of isogrid plate FE model	14
Fig. 3-8 MPC input created automatically for permanent glued contact	14
Fig. 3-9 Parallel plate configuration	16
Fig. 3-10 Isogrid plate configuration	17
Fig. 3-11 Comparison of eigenvalues λ of parallel plate (model A)	17
Fig. 3-12 Comparison of eigenvalues λ of parallel plate (model B)	18
Fig. 3-13 Comparison of eigenvalues λ of isogrid plate (model A)	19
Fig. 3-14 Comparison of eigenvalues λ of isogrid plate (model B)	20
Fig. 3-15 Plate models used for assessment of elastich deformation	22
Fig. 3-16 Deformation plot of parallel plate	23
Fig. 3-17: Deformation plot of isogrid plate	23
Fig. 3-18 Definition of contact bodies in forward swept wing model	24
Fig. 3-19 Example of a contact status fringe plot	25
Fig. 3-20 Wing deformation plot for load case 1	25
Fig. 4-1 Definition of support zones for creating curvilinear stiffeners	27
Fig. 4-2 Creation of curves (splines) between support zones	28
Fig. 4-3 Projection of curvilinear paths onto FE model	28

Fig. 4-4	Fourth order Bézier curve representation (adapted from [46]).....	29
Fig. 4-5	Application of Bézier curve within support zone #1	30
Fig. 4-6	Overview of the three Bézier curves of the design model.	30
Fig. 4-7	Four different stringer configurations in the FE wing model	31
Fig. 4-8	Automated PATRAN model generator (adapted from [49])	33
Fig. 4-9	Input file containing the airfoil coordinates	34
Fig. 4-10	Input file containing wing load information (coefficients)	34
Fig. 4-11	Structure of input file <i>wing_corner_nodes.txt</i>	35
Fig. 4-12	Structure of the output file <i>wing_buckling_nodes.txt</i>	35
Fig. 5-1	General overview of optimization framework (adapted from [49])	36
Fig. 5-2	Overview of PTDP-module and FEA (adapted from [49]).....	37
Fig. 5-3	Overview of AECP-module and function calls (adapted from [49])	37
Fig. 5-4	Parametric thickness description for upper cover [50].....	38
Fig. 5-5:	Detail of <i>dummy.bdf</i> before parametric thickness description	39
Fig. 5-6	Detail of <i>dummy.bdf</i> after parametric thickness description	39
Fig. 5-7	Optimization problem definition within Optimus GUI	40
Fig. 5-8	Structure of a *.optimal file containing the optimal results	40
Fig. 6-1	Wing bending results of configuration 3.	47
Fig. 6-2	Wing torsion results of configuration 3	47
Fig. 6-3	Wing bending results of configuration 4	48
Fig. 6-4	Wing torsion results of configuration 4	48
Fig. 7-1	Comparison of optimal mass of <i>A-models</i>	57
Fig. 7-2	Mass breakdown of model <i>4_WBC600_WTC05_01</i>	57
Fig. 7-3	Optimal thickness values of model <i>4_WBC600_WTC05_01</i>	58
Fig. 7-4	Elastic deformations of optimum design	58
Fig. 7-5	Optimal mass as a function of allowable bending value w_{max}	59
Fig. 7-6	Optimal thickness distribution of 0°-layers using curvilinear stiffeners.....	60
Fig. 7-7	Comparison of optimal mass values using only the upper torsion limit.....	60

Fig. 7-8 Torsion angle of optimal designs using only the upper torsion limit.....	61
Fig. 7-9 Comparison of optimal mass of <i>B-models</i>	62
Fig. 7-10 Optimal thickness values of model 2_ <i>WBC600_WTC005_001</i>	63
Fig. 7-11 Mass breakdown of model 2_ <i>WBC600_WTC005_001</i>	63
Fig. 7-12 Optimal thickness values of model 3_ <i>WBC600_WTC005_001</i>	64
Fig. 7-13 Elastic deformations of optimal design of model 3_ <i>WBC600_WTC005_001</i> ...	65
Fig. 7-14 Mass breakdown of model 3_ <i>WBC600_WTC005_001</i>	65
Fig. 7-15 Comparison of optimal mass of <i>C-models</i>	66
Fig. 7-16 Comparison of buckling modes between configurations 1 and 4.....	67
Fig. 7-17 Optimal thickness values of model 1_ <i>LBC10_GBC12</i>	68

List of Tables

Table 3-1 Wing geometric values	8
Table 3-2 Entries and parameters for contact definition in MSC.Nastran [35]	15
Table 3-3 Selected eigenmodes of parallel plate (model A)	18
Table 3-4 Selected eigenmodes of parallel plate (model B)	19
Table 3-5 Selected eigenmodes of isogrid plate (model A)	20
Table 3-6 Selected eigenmodes of isogrid plate (model B)	21
Table 3-7 Comparison of displacement results of parallel plate	23
Table 3-8 Comparison of displacement results of isogrid plate	23
Table 3-9 Comparison of maximum wing displacements	26
Table 4-1 List of parameterized properties of the FE wing model (adapted from [49])	32
Table 4-2 Description of PATRAN model generator modules (adapted from [49])	33
Table 5-1: Nomenclature (labels) of geometric design variables	41
Table 5-2 Nomenclature (labels) of composite design variables	41
Table 6-1 Basic wing model configurations	44
Table 6-2 Wing models with straight divergent stiffeners	45
Table 6-3 Wing models with curvilinear stiffeners	46
Table 6-4 Comparison of results of different models	49
Table 7-1 Fundamental properties of structural model	50
Table 7-2 Composite design variables of <i>A-models</i>	51
Table 7-3 Geometrical design variables of <i>A-models</i>	52
Table 7-4 Composite design variables of <i>B-models</i>	53
Table 7-5 Geometrical design variables of <i>B-models</i>	54
Table 7-6 Composite design variables of <i>C-models</i>	55
Table 7-7 Geometrical design variables of <i>C-models</i>	56
Table 7-8 Values of geometrical DVs of <i>A-models</i> using configuration 4	59
Table 7-9 Values of geometrical DVs of model <i>2_WBC600_WTC005_001</i>	62

Table 7-10 Values of geometrical DVs of model 3_WBC600_WTC005_001	64
Table 7-11 Values of geometrical DVs of <i>C-models</i>	66

List of Symbols, Indices and Abbreviations

Latin symbols

a	Length
A_j	Multipoint constraint coefficient
b	Width; Wing half span
b'	Wetted wing half span
$B_{i,n}(v)$	Bernstein polynomial
c	Chord length
C_Z	Aerodynamic normal coefficient
$C_{M,25}$	Aerodynamic pitching moment coefficient at 25% chord line
C_j	Component number for grid point j
$C(v)$	Bézier curve function
d	Diameter
$D1, D2$	Contact tolerances
E	Young's modulus
F	Force
\underline{F}	Vector of grid point forces equivalent to internal element stresses
G	Shear modulus
G_j	Grid point identification number
h	Height
i	Iteration step; Listing index
j	Grid point index
k	Layer index
$\underline{\underline{K}}_T$	Stiffness matrix (tangential)
l	Length
m	Mass; Identification index
m_{25}	Pitching moment per unit span
M_{25}	Pitching moment
n	Bernstein polynomial function degree; Contact normals;
n_z	Load factor
$\underline{\underline{N}}$	Matrix of contact conditions
\underline{N}_{xy}	Shear flow
P_i	Control points of Bézier curve/surface
\underline{P}	Vector of external grid point forces

q_z	Normal load per unit span
r	Radius
R	Rotational degrees-of-freedom
$R_{ }^t, R_{ }^c$	Allowable strength of an orthotropic layer in longitudinal (fiber) direction t = tension; c=compression
R_{\perp}^t, R_{\perp}^c	Allowable strength of an orthotropic layer in transverse direction t = tension; c=compression
$R_{\perp }$	Allowable shear strength of an orthotropic layer
\underline{R}	Out-of-balance-vector
\underline{R}_c	Vector of grid point contact forces of the system
S	Wing area
s_i	Stringer index
t	Layer thickness; Time
(t/c)	Thickness-to-chord ratio
T	Translational degrees-of-freedom
\underline{U}	Vector of grid point displacements
u_j	Degree-of-freedom correspondent to component number
v	Bernstein coordinate parameter
w	Wing bending
x	Cartesian coordinate x
\bar{x}	Constraint factor for buckling
y	Cartesian coordinate y
z	Cartesian coordinate z

Greek symbols

α	Torsion angle
γ	Stringer position angle (w.r.t to longitudinal axis)
∂	Derivation
Δ	Delta, difference
$\underline{\Delta}$	Vector of material overlapping (penetration)
ε	Strain (compression)
λ	Eigenvalue; Lagrange-multiplier
$\underline{\lambda}$	Vector of grid point contact forces of the touching body
Λ	Aspect ratio
ν	Dihedral angle
ν_{12}	Poisson ratio of an orthotropic layer
ρ	Density

ρ_{KS}	Exponential parameter of Kreisselmeier-Steinhauser function
Φ_{25}	Sweep angle related to 25% chord line
Φ	Contact problem equation

Indices

$()_{11}$	Parameter related to longitudinal (fiber) direction of an orthotropic layer
$()_{22}$	Parameter related to transverse direction of an orthotropic layer
$()_{12}$	Parameter related to the plane 1-2 of an orthotropic layer
$()_{13}$	Parameter related to the plane 1-3 of an orthotropic layer
$()_{23}$	Parameter related to the plane 2-3 of an orthotropic layer
$()_f$	Parameter related to fuselage
$()_k$	Parameter related to layer k of a laminate
$()_r$	Parameter related to wing root
$()_t$	Parameter related to wing tip
$()_{aggr}$	Parameter related to an aggregated (condensed) value
$()_{allow}$	Parameter related to allowable value
$()_{max}$	Parameter related to maximum value
$()_{nom}$	Parameter related to nominal value
$()_{wet}$	Parameter related to a wetted surface
$()_{FS}$	Parameter related to front spar
$()_{RS}$	Parameter related to rear spar
$()_z$	Parameter related to z-direction
<u>()</u>	Single underlined characterizes a vector
<u><u>()</u></u>	Double underlined characterizes a matrix
^t ()	Parameter related to time t
$()^i$	Parameter related to iteration step i

Abbreviations

A320	Airbus aircraft model A320
A350	Airbus aircraft model A350
AECP	Analysis Evaluation and Constraints Procedure
BMIAP	Buckling Mode Identification and Aggregation Procedure
BMWi	Federal Ministry of Economic Affairs and Energy
CFC	Carbon fiber composite
CFD	Computational fluid dynamics
DLR	German Aerospace Center
DOF	Degree-of-freedom
DV	Design variable
EDCP	Elastic Deformation Constraint Procedure
FA	Institute of composite structures and adaptive systems
FS	Front spar
FEA	Finite-Element-Analysis
FE, FEM	Finite-Element, Finite-Element-Method
ForSwing	Forward swept wing
FWD	Forward (flight direction)
HAW	Hamburg University of Applied Sciences
GUI	Graphical user interface
GBC	Global buckling constraint
LBC	Local buckling constraint
LL	Limit load
LC	Load case
LS	Lower skin
LuFo IV	Luftfahrtforschungsprogramm IV
MPC	Multipoint constraint
NLF	Natural laminar flow
NLPQL	Non-Linear Programming by Quadratic Lagrangian
PCL	Patran Command Language
PCOMP	Property card for defining composite materials
PMG	PATRAN Model Generator
PTDP	Parametric Thickness Distribution Procedure
RB	Ribs
RBE	Rigid body element
RS	Rear spar

SU	Stringers of upper cover
SL	Stringers of lower cover
SOL	Nastran solution type
UD	Uni-directional
UL	Ultimate load
US	Upper skin
WBC	Wing bending constraint
WTC	Wing torsion constraint

1 Introduction

1.1 Overview of the research project AeroStruct – ForSwing

AeroStruct is a research and technology project granted by the German Federal Ministry for Economic Affairs and Energy (BMWi) as part of LuFo IV from 2012-2015. Its main objective is the multidisciplinary (structure, aerodynamics, flow technology), integrated, numerically based design of aircraft primary structures and as such enable to integrate flexibility and efficiency into the design process.

The optimum design of a forward swept wing made of composite materials (“ForSwing”) is one of the four use cases of AeroStruct. For this purpose, a coupled aero-structural optimization process is being developed by the German Aerospace Center – Institute of Aerodynamics and Flow Technology (DLR-AS) – as the project coordinator, with the Institute of Composite Structures and Adaptive Systems (DLR-FA) and Hamburg University of Applied Sciences (HAW) responsible for the structural optimization branch.

The general objective of ForSwing is to design a forward swept wing with highest aerodynamic performance, using natural laminar flow characteristics and CFC-materials. The work packages under HAW responsibility deal with the development of the optimization model considering among others CFC-specific failure criteria, buckling phenomena and aeroelastic tailoring. The optimization model includes both geometric (e.g. position of ribs) and composite (e.g. thickness of laminate plies) design variables.

This thesis is carried out within the context of ForSwing. It represents an extension of the investigations performed so far by introducing the concept of curvilinear stiffeners into the optimization process.

1.2 Problem definition and motivation

A conceptual study conducted by DLR showed that a forward swept wing design enables for a so-called natural laminar flow (NLF) over a wide extent of the wing during cruise flight, thus reducing the drag and fuel consumption in comparison to conventional transport aircraft [1]. This is a very promising idea, especially now in times of continuously growing fuel prices. However, in order to make such a wing configuration possible, major challenges in the different aircraft disciplines (aerodynamics, flight mechanics, stress, etc.) must be overcome. One of them is the structural design that must be able to comply with very strict requirements. Numerical optimization methods are therefore employed to find the best suitable structural design.

In this context the idea arose of extending the structural design capabilities from those defined so far for ForSwing. This idea concretized in broadening the allowable design domain of the stiffened wing covers. Fig. 1-1 gives an overview of different stringer configurations. In the configuration used so far within ForSwing, all stringers start at the wing root and run out at the wing tip. The distance between the stringers decreases according to the positions of the spars (cf. Fig. 1-1a). A more common stiffener arrangement is shown in Fig. 1-1b, where the stringers are parallel to one spar and because of the wing taper, some of them run out at different locations of the wing span [2]. This kind of arrangement is used, for example, in the A320 [3].

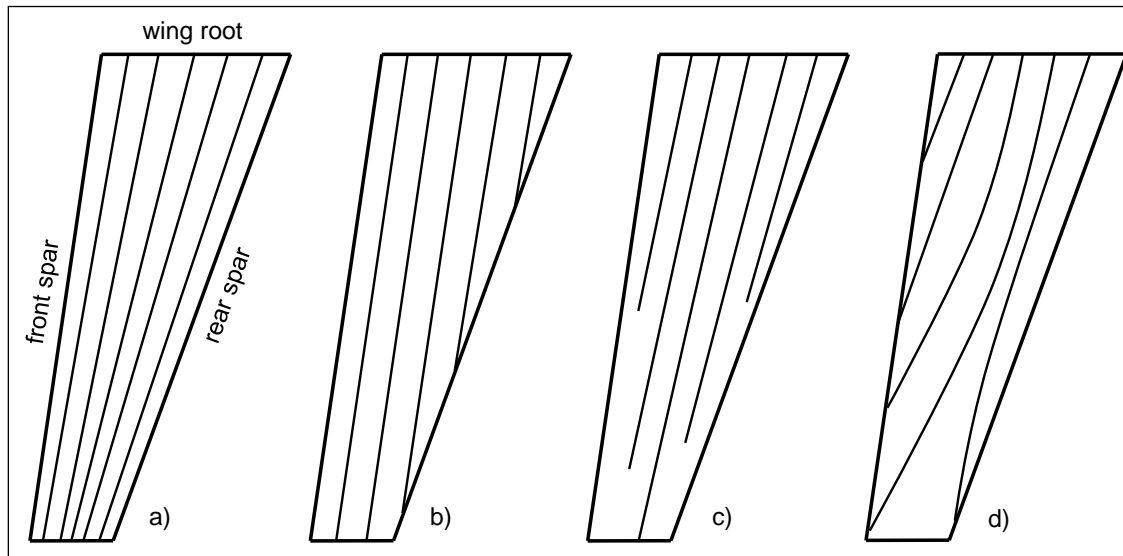


Fig. 1-1 Overview of different stringer configurations

Fig. 1-1c shows an arrangement, in which the stringers are not parallel to either spar and systematically run out before reaching the wing tip. This kind of arrangement is used, for example, in the A350 [4].

The arrangements (a), (b) and (c) share the common fact of using straight stringers (in an organized pattern) for stiffening the wing covers. Within this thesis the concept of using curvilinear stiffeners, such as depicted in Fig. 1-1d, is presented. The objective is to investigate the influence of curvilinear stiffeners on the structural behaviour of a forward swept wing design, especially w.r.t. aeroelastic tailoring capabilities and in comparison to traditional stiffener arrangements. The idea behind the concept of curvilinear stiffeners is to use the stringers not only to stiffen the wing covers but also to control the wing elastic deformations. For this, the configurations (a), (b) and (d) using blade stiffeners will be investigated.

Due to the geometric complexity and the design requirements to be considered (e.g. elastic deformations, buckling behavior) the structural analysis is to be performed by means of the finite-element-method. In this thesis the industry standard MSC.Nastran is used. The structural analysis model is to be adequately parameterized and integrated into a numerical optimization procedure. The latter derives from the optimization procedure developed for ForSwing. Hence, a focal point of the thesis is the comparison of optimum wing designs using traditional and curvilinear stiffener arrangements.

The curvilinear stringer paths represent a challenging task w.r.t. an adequate meshing of the FE model. Generating congruent meshes (i.e. coincident nodes) between the stringers and the covers is a very tedious process, especially taking into account that the stringer geometry (i.e. paths) may change during the optimization process. It might not be assured that the automated structural analysis model procedure creates always a smooth, uniform mesh for the covers. The solution is to mesh the different regions independently. Therefore another focal point of the thesis is the investigation of a robust and precise enough FE assembly method for joining the stringers to the wing covers both having dissimilar meshes (cf. Fig. 1-2).

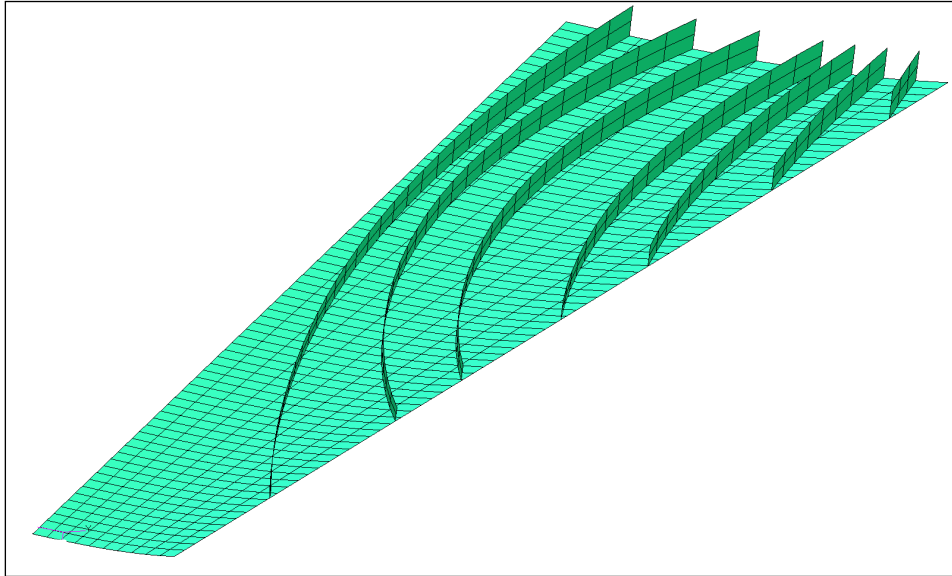


Fig. 1-2 Example of dissimilar meshes for lower cover and stringers

The work steps to be performed in this thesis can be summed up as follows:

- a) Investigation of a suitable FE assembly method for modeling the wing structure
- b) Development and implementation of a parameterization concept for modeling the curvilinear stiffeners
- c) Definition of an optimization framework and performing structural optimizations of a forward swept wing. For this, geometrical and composite design variables are to be used as well as the design responses mass (to be minimized), wing bending, torsion and buckling.
- d) Comparison of the results using traditional and curvilinear stiffener arrangements, especially w.r.t. elastic deformations.

1.3 Outline of subsequent chapters

The thesis is made up of the following chapters:

- Ch. 2
Literature review

Chapter 2 gives an overview of past and current work concerning relevant topics related to this thesis. A brief literature review about structural optimization of wing-box structures, curvilinear stiffening members and aeroelastic tailoring is given.

- Ch. 3
Finite-element modeling and assembly method

Chapter 3 describes the geometry and finite-element properties of the forward swept wing model. It also provides an insight into different FE assembly methods and details due to its advantageous properties the permanent glued contact method. The

theoretical background, validation and implementation of permanent glued contact are shown.

- Ch. 4
Finite-element parameterization and automation

Chapter 4 explains the concept used for the parameterization of the curvilinear stiffeners. Further properties of the parameterized wing model are also described as well as the implementation and automation within the post-processing software MSC.Patran.

- Ch. 5
Optimization framework

Chapter 5 provides an insight into the architecture of the optimization framework. Based on several flowcharts, the main components and modules are described. Furthermore, the optimization GUI, design variables and design constraints are presented.

- Ch. 6
Preliminary structural assessment

Chapter 6 deals with a preliminary parameter study in which the elastic deformations of a reference wing model are investigated using different stiffener configurations. This preliminary assessment is performed upfront the optimizations in order to explore the design domain and identify relevant interactions.

- Ch. 7
Structural optimizations

Chapter 7 describes the used optimization models and overall settings. The results of several optimizations using traditional and curvilinear stiffener arrangements are shown. Special emphasis is put on the comparison of the optimal results concerning the elastic deformations and buckling behaviour.

- Ch. 8
Conclusions and outlook

Chapter 8 wraps up the investigation performed in this thesis. A brief summary and conclusions about the used methodology and results are given as well as an outlook concerning future research.

2 Literature review

In this chapter a literature review about relevant topics related to this thesis is given. An overview of past and current work regarding structural optimization with emphasis on metal and composite wing-box structures is presented. The application of curvilinear stiffening components is also reviewed alongside with work involving forward swept wing designs and aeroelastic tailoring.

2.1 Optimization of metal and composite aircraft wing-box structures

Structural optimization can be considered as a discipline with the aim of enhancing the structural properties of a component w.r.t. a set of given requirements. The dimensioning of lightweight structures (in modern civil aircraft increasingly manufactured from composite materials) is a challenging task, especially in early design phases, because there are a large number of design parameters and at the same time a variety of design requirements to comply with. In this context, robust and efficient optimization methods and tools are predestined to be applied in order to find optimum structural designs.

Almost a hundred years ago *Michell* [5] already developed a design theory for finding optimal truss structures. The fundamentals of modern structural optimization, developed in the second half of the 20th century, can be found in the works of *Haftka et al.* [6], *Arora* [7] or *Kirsch* [8]. These works describe in detail relevant optimization concepts, methods and formulations for constrained and unconstrained problems.

For optimizing wing-box structures very different approaches and methods can be found in the literature. The most common optimization objective is the minimization of the weight, while the most common design constraints are displacements, strength and buckling stability. *Starnes* and *Haftka* [9] conducted optimizations of a multispar high aspect ratio wing by introducing the above mentioned constraints through penalty functions. *Starnes* and *Haftka* obtained minimum-mass designs using Newton's method as search algorithm and compared the results using composites and aluminum. They came to the conclusion that composite designs show an advantage over aluminum designs because they are often able to satisfy additional constraints with small mass increments. *Hürlimann* [10] conducted in his dissertation the structural sizing of an aluminum tail plane rudder using an analytical buckling criterion as the design constraint. To overcome the geometrical limitations of the analytical buckling methods, he suggested the use of a FEM-based buckling criterion that allowed for a larger wing mass reduction.

Venter and *Sobieszcanski-Sobieski* [11] optimized a typical long range transport aircraft wing using a two-level approach and a non-gradient based, probabilistic search algorithm. The aerodynamic optimization takes place at the system level, while the structural optimization is done as a subproblem one level below. The used particle swarm algorithm proved to find a reliable optimum. *Liu et al.* [12] used a different two-level approach for optimizing a simple composite wing-box: at wing-level ply thickness optimization based on response surfaces was performed, while at panel level the number of plies and stacking sequence was genetically optimized. *Hansen* [13] performed a multilevel optimization of a blended wing body aircraft using an evolutionary strategy at the top level for optimizing the wing topology and a gradient-based optimization at the second level for optimizing the thicknesses. They showed that a separation of the topology variables from the sizing variables in two different levels is more efficient than mixing them in one optimization task. A two-level optimization strategy is also performed by *Zhao et al.* [14] for large-scale composite wing structures. The objective is the minimization of the structural efficiency (i.e. efficiency factor calculated based on the failure

coefficients of buckling and strength). An FE model is used for the load extraction, buckling loads are calculated using an energy method and a surrogate model, and empirical formulas are used for static strength.

Chintapalli et al. [15] developed a preliminary optimization routine for optimizing aircraft stiffened panels. The upper skin-stringer panels are optimized under analytical local and global buckling constraints using SQP-methods, while the lower panels are optimized under fatigue constraints based on the linear elastic fracture mechanics theory. *Almeida and Awruch* [16] used an adapted genetic algorithm, associated with FEM as the structural solver, for the design optimization of composite panels. In their examples, the minimization of two objectives (e.g. weight and deflection) is simultaneously conducted.

For solving large, multidisciplinary optimization problems *Eschenauer et al.* [17] proposed a systematic approach called the “3-Columns-Concept”, where the three columns are the structural model, the optimization algorithm and optimization model (cf. Fig. 2-1). This is the concept underlying the optimization procedure used in this thesis. Regarding the implementation and application of optimization algorithms extensive publications have been made, for example, by *Schittkowski* [18, 19]. In his work gradient-based algorithms, such as the SQP-methods used in this thesis, are investigated in detail.

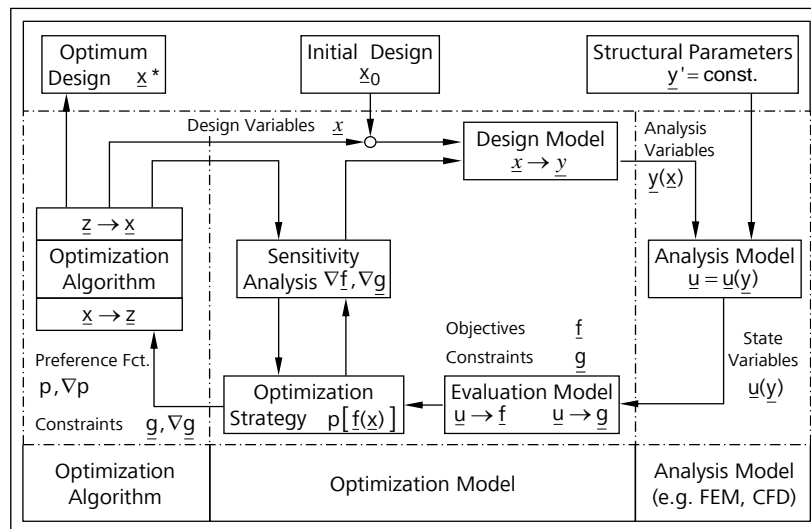


Fig. 2-1 Three-Columns-Concept for solving MDO-optimization problems [17]

2.2 Aeroelastic tailoring and forward swept wing

The structural deformations of a wing are of utmost importance for the aircraft performance, be it for example the achievement of a certain aerodynamic value or – like within ForSwing – the extension of a natural laminar flow. *Shirk et al.* [20] describe the concept of aeroelastic tailoring as “the embodiment of directional stiffness into an aircraft structural design to control aeroelastic deformation, static or dynamic, in such a fashion as to affect the aerodynamic and structural performance of that aircraft in a beneficial way”.

Weisshaar [21] demonstrated that using anisotropic materials (e.g. CFC) with the proper fiber orientations has a significant effect on static aeroelastic characteristics of a forward swept wing such as torsion divergence (i.e. divergence speed). This is best achieved when the main directional stiffness of the covers is turned forward w.r.t. the wing longitudinal axis. *Isogai* [22] performed experimental studies with wind tunnel models and also showed that by aeroelastic tailoring the flutter/divergence characteristics can be improved. *Kruse et al.* [1] conducted a

conceptual study in which the torsional divergence of the forward swept wings of a transonic transport aircraft is successfully suppressed by placing the main fiber direction of upper and lower skins at a certain angle relative to the wing longitudinal axis.

Gleichmar [23] optimized in his dissertation a glider wing using the bending-twist coupling of composite materials to minimize the torsion deformation. For this he employed a Response Surface Approximation method being the design variables the main stiffness orientation of the cover laminates. *Kobler* [24] conducted in his thesis the optimization of a composite wing using evolutionary strategies and aeroelastic tailoring in order to minimize the torsion deformation as well. More information can also be found in the work of *Guo et al.* [25]. Using a genetic algorithm and a gradient-based method they optimized composite layups of a backward swept wing resulting in an increase of the flutter speed.

2.3 Curvilinear stiffening components

The classic structural design of an aircraft wing-box uses simple components as straight spars and stringers. Nevertheless, several publications have been made that deal with more complex geometrical forms and arrangements. *Dems et al.* [26] investigated disks and plates stiffened by curvilinear rib-stiffeners and derived analytical sensitivity expressions for variations of shape and cross-section. *Brubak et al.* [27] presented a semi-analytical buckling strength analysis of plates with arbitrarily oriented stiffeners under in-plane loading. Geodesically stiffened panels were investigated, among others, by *Gürdal* and *Gendron* [28]. Isogrid arrangements, which have been successfully used in the spacecraft industry, can be traced back to 70's [29].

Slemp et al. [30] performed the design, optimization and evaluation of an integrally stiffened aluminum panel with curved stiffeners. The panel was first optimized against buckling load, yielding and crippling and then manufactured and tested under a combined compression-shear load. In his dissertation *Locatelli* [31] implemented curvilinear spars and ribs (so-called *SpaRibs*) in the design process of supersonic aircraft wing-box. Using a MatLab-based optimization framework and a particle swarm method he performed sizing and topology optimization for different *SpaRibs* parameterization techniques. Different optimum designs are obtained for the different parameterization methods used. *Kobayashi et al.* [32] developed a biologically inspired methodology based on so-called cellular division to generate structural topology. For a generic fighter aircraft wing-box the optimization result was a complex, curved internal structure.

Curvilinear stiffening components broaden the design space in the quest for dimensioning advanced engineering structures and systems.

3 Finite-element modeling and assembly method

As briefly explained in Ch. 1, a focal point of the thesis is the investigation of a finite-element assembly method for joining the stiffeners to the wing covers both having dissimilar meshes. First, the geometry and finite-element properties of the structural analysis model are described. Then, a small overview of current FE assembly methods is given. Finally, one of these methods –permanent glued contact– is investigated in detail. A theoretical background and the results of different simulations using this method are given as well as important considerations.

3.1 Geometry and finite-element properties of the forward swept wing model

The forward swept wing model consists of a traditional two-spar wing-box structure and is divided for the purposes of this thesis into six different regions: upper cover, lower cover, front spar, rear spar, ribs, and stringers (blade stiffeners). The geometry and dimensions of the wing derive from the ForSwing data set and are shown in Table 3-1 and Fig. 3-1. The wing has a trapezoidal cantilever design without a kink or longitudinal twist.

Wing area [m ²]	132.0
Aspect ratio [-]	9.71
Taper ratio [-]	0.371
Sweep angle [°]	-19.8
Dihedral angle [°]	4.0
Relative NLF-airfoil thickness [%]	11.5
Front spar position [%]	15.0
Rear spar position [%]	58.0
Fuselage radius [m]	2.0

Table 3-1 Wing geometric values

All structural elements of the wing are modeled using only 2D quadrilateral finite elements (CQUAD4). Triangular elements (CTRIA3) are avoided for being constant strain elements and therefore less accurate. To obtain a good accuracy, either a large number of them (very fine meshes) or higher order elements (e.g. CTRIA6) must be used [33].

With respect to the blade stiffeners, only the vertical flanges (and not the stringer feet) are modeled. The used CFC-laminates must lie within the geometrical aerodynamic contour. Therefore all element normal vectors of the upper and lower covers show to the inside of the wing-box and the laminate offset values are zero. In order to make the boundary conditions more realistic, the center wing box is also modeled but not optimized. Here, the airplane symmetry plane is clamped. Furthermore, the vertical (z-) translation at the interfaces between the center wing box and the spars is constrained. Regarding the wing loading, equivalent transversal forces F_z and pitching moments M_{25} are calculated at multiple wing stations based on the aerodynamic coefficients distribution. These external loads are transferred into the structure by means of rigid body elements (RBE3) placed at every rib station. An overview of the FE model can be seen in Fig. 3-2.

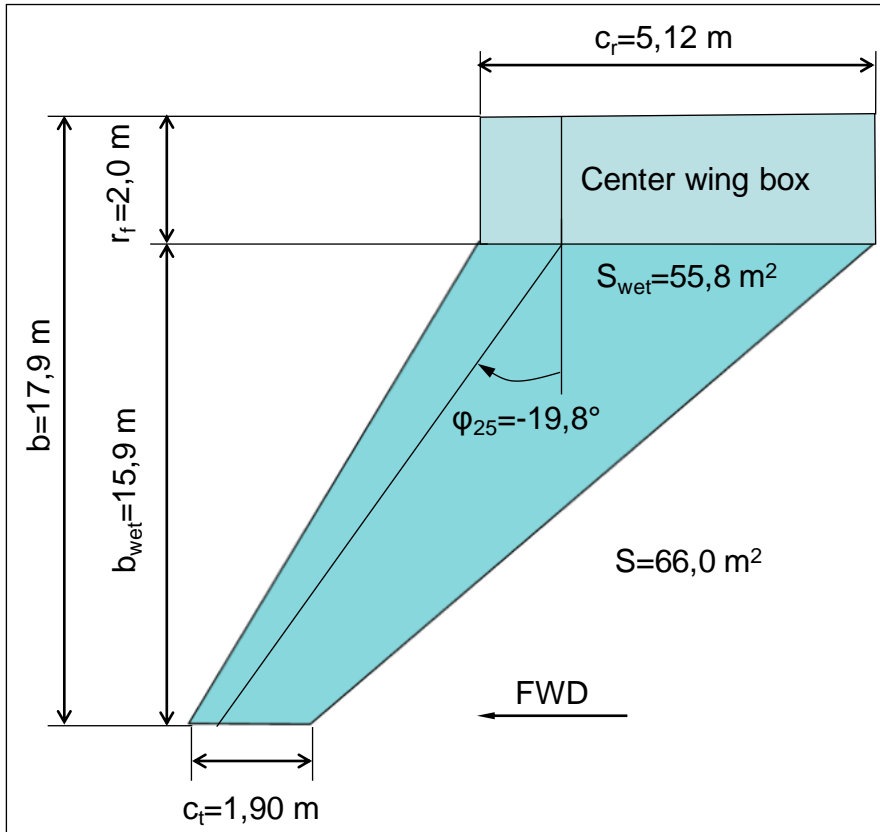


Fig. 3-1 Forward swept wing geometry (adapted from [49])

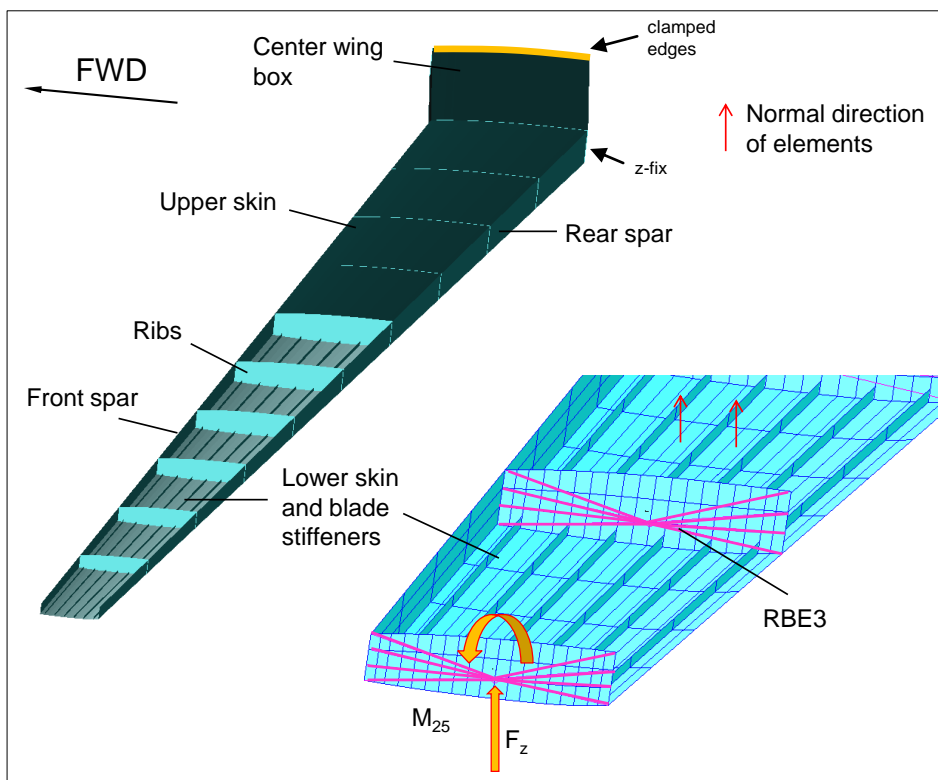


Fig. 3-2 Finite-element modeling of forward swept wing (adapted from [49])

Within an optimization the FE model is generated automatically by the so-called PMG module (PATRAN model generator, cf. Ch. 4.3) based on the current values of the geometric parameters. Each time the model is updated, the procedure must be able to mesh the wing covers with a good quality despite the position of the curvilinear paths. Aligning nodes between skins and stringers so they are coincident is an exhaustive process. It implies very often defining transitions or splitting elements (cf. Appendix A). Performing this automatically increases the programming complexity of this thesis to a very high extent. Even if this is achieved, there is no guarantee that a qualitative uniform mesh will be created and during an optimization it is not possible to manually check and make improvements. The solution to this conundrum is to mesh the skins and stringers independently (cf. Fig. 1-2) and afterwards assembly them together for structural analysis.

3.2 Overview of finite-element assembly methods

In the literature different methods can be found for joining FE components together with dissimilar meshes. In this thesis the methods provided by MSC.Software are portrayed since MSC.Nastran is used as the structural solver. Other structural solvers offer however very similar methods.

MSC.Software offers three types of connectors: fasteners (CFAST), spot weld (CWELD) and seam weld (CSEAM) [34]. The advantage of the first two types is that they rely on a geometrical position in space. This means that only a point or a node must be defined (GS in Fig. 3-3) and the procedure will automatically project it on the surfaces regardless of their meshing definitions. The points GA and GB define the axis of the connector, so that dissimilar meshes can be attached. Internally multi-point-constraint equations are used to define the connection.

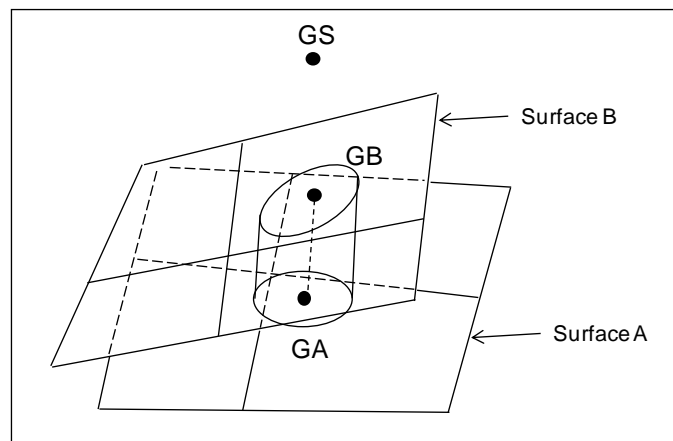


Fig. 3-3 Definition of fastener and spot weld connection [35]

Information about the use of CWELD can be found, for example, in the work of *Palmonella et al.* [36]. They analyzed the influence of different parameter settings on the structural dynamic behavior of a benchmark structure and give general guidelines for an optimum implementation. In [37] a review of available spot weld models in the literature is given. On the other hand, the CFAST method has been used successfully in the modeling of complex structures such as in the work of *Jegley and Velicki* [38] in which a test article of a hybrid wing body vehicle was simulated.

However for the definition of these connector types several inputs are needed such as the connector diameter, the material (CWELD) or the translational/rotational stiffness values

(CFAST) [35]. In addition to this, the number of connectors and distance between each other must also be defined. All these inputs have an enormous influence on the performance of the assembly. To investigate the optimal settings for the forward swept wing model used in this thesis is not viable due to the large number of variables. In this context another assembly method, the so-called “permanent glued contact” [34, 39], seems as a very good alternative. Not only does this technology reduce the need to align incongruent nodes, but there is also no need to define connector properties. Instead two different components are simply “glued” together (cf. Fig. 3-4). The complexity of the assembly process is hence reduced in comparison to the spot weld or fastener method.

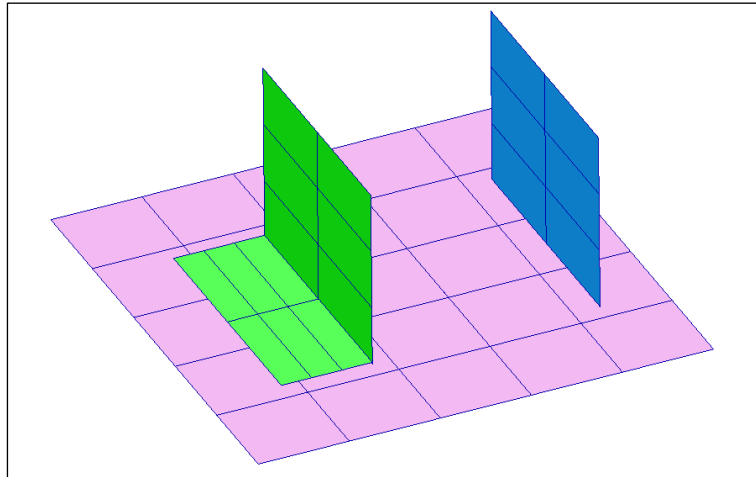


Fig. 3-4 Permanent glued contact examples.
Shell face-to-face (left) and shell edge-to-face (right)

Permanent glued contact offers a fast and relative easy setup. It also enables an accurate stiffness and load transfer [34]. Because of these reasons, this method is chosen for the finite-element modeling within this thesis and analyzed in detail in the following subchapters.

3.3 Theoretical background and implementation of permanent glued contact method

Permanent glued contact corresponds to a type of problems referred to as *contact problems* and, thus deals with bringing two bodies in space together that were previously not touching each other and analyzing their interdependencies.

A geometrical contact problem requires at least two different bodies, one of them called the *slave* and the other one called the *master*. This defines the contact direction, i.e. the grid points of the slave body will seek for contacting the surface of the master body. In doing so, the slave grid points may come in perfect contact with the master surface, penetrate it or not touch it at all [40]. Fig. 3-5 shows a schematic representation of a 2D contact problem.

A simple method for solving contact problems is the method of the *Lagrange-multipliers* λ . Here, the contact problem is converted into a constrained extreme value problem which can be solved using the multipliers. *Klein* [41] outlines this method by means of a simple clamped beam problem. For solving more complex problems iterative methods are employed. The general iterative solution of non-linear problems with contact is given below [41]:

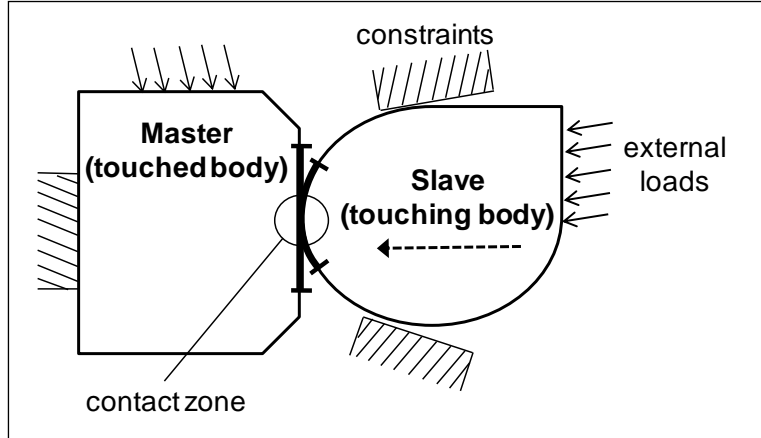


Fig. 3-5 Contact problem representation [41]

In a non-linear static system the equilibrium formulation for a given time t is given by

$${}^t\mathbf{P} - {}^t\mathbf{F}(\mathbf{U}) = 0 \quad (3.1)$$

where \mathbf{P} is the vector of the external grid point forces, \mathbf{F} the vector of the grid point forces equivalent to the internal element stresses and \mathbf{U} the vector of the grid point displacements.

If for the time $t + \Delta t$ there is a contact, then the general non-linear system of equations of the contact problem becomes

$${}^{t+\Delta t}\mathbf{P} - {}^{t+\Delta t}\mathbf{F}(\mathbf{U}) - {}^{t+\Delta t}\mathbf{N}^t \cdot {}^{t+\Delta t}\underline{\lambda} = 0 \quad (3.2)$$

with the constraint

$${}^{t+\Delta t}\mathbf{N} \cdot {}^{t+\Delta t}\underline{\lambda} = {}^{t+\Delta t}\underline{\Delta} \quad (3.3)$$

- ${}^{t+\Delta t}\mathbf{N}$ is the matrix of contact conditions from the geometric examination of contact zone
- ${}^{t+\Delta t}\underline{\lambda}$ is the vector of the grid point contact forces of the touching body
- ${}^{t+\Delta t}\underline{\Delta}$ is the vector of the material overlapping (penetration).

Eq. (3.2) is formally defined as

$${}^{t+\Delta t}\Phi(\mathbf{U}, \underline{\lambda}) := {}^{t+\Delta t}\mathbf{P} - {}^{t+\Delta t}\mathbf{F}(\mathbf{U}) - {}^{t+\Delta t}\mathbf{N}^t \cdot {}^{t+\Delta t}\underline{\lambda} = 0 \quad (3.4)$$

With the partial derivatives

$$\frac{\partial \Phi}{\partial \mathbf{U}} = -\mathbf{K}_T(\mathbf{U}) \quad (3.5)$$

$$\frac{\partial \Phi}{\partial \underline{\lambda}} = -\mathbf{N}^t$$

and the acronyms

$$\begin{aligned}\Delta \underline{\mathbf{U}}^{(i)} &:= {}^{t+\Delta t} \underline{\mathbf{U}}^{(i)} - {}^{t+\Delta t} \underline{\mathbf{U}}^{(i-1)} \\ \Delta \underline{\lambda}^{(i)} &:= {}^{t+\Delta t} \underline{\lambda}^{(i)} - {}^{t+\Delta t} \underline{\lambda}^{(i-1)} \\ {}^{t+\Delta t} \underline{\mathbf{R}}_c^{(i-1)} &= - {}^{t+\Delta t} \underline{\mathbf{N}}^{t,(i-1)} \cdot {}^{t+\Delta t} \underline{\lambda}^{(i-1)}\end{aligned}\quad (3.6)$$

the constitutive system of equations for the contact problem becomes

$${}^{t+\Delta t} \begin{bmatrix} \underline{\mathbf{K}}_T(\underline{\mathbf{U}}) & \underline{\mathbf{N}}^t \\ \underline{\mathbf{N}} & \mathbf{0} \end{bmatrix}^{(i-1)} \cdot \begin{bmatrix} \Delta \underline{\mathbf{U}} \\ \Delta \underline{\lambda} \end{bmatrix}^{(i)} = {}^{t+\Delta t} \begin{bmatrix} \underline{\mathbf{P}} - \underline{\mathbf{F}}(\underline{\mathbf{U}}) + \underline{\mathbf{R}}_c \\ \underline{\Delta} \end{bmatrix}^{(i-1)} \quad (3.7)$$

In order to solve Eq. (3.7), it must be iterated until the material overlapping (penetration) is eliminated

$${}^{t+\Delta t} \underline{\Delta}^{(i-1)} \rightarrow \mathbf{0} \quad (3.8)$$

and also until the so-called *out-of-balance-vector* $\Delta \underline{\mathbf{R}}^{(i-1)}$ disappears for all nodes outside the contact zone:

$$\Delta \underline{\mathbf{R}}^{(i-1)} := {}^{t+\Delta t} \underline{\mathbf{F}}(\underline{\mathbf{U}})^{(i-1)} - {}^{t+\Delta t} \underline{\mathbf{P}} \rightarrow {}^{t+\Delta t} \underline{\mathbf{R}}_c^{(i-1)} = \begin{cases} \mathbf{0} & \text{for all nodes} \\ & \text{outside contact} \\ & \text{zone} \\ {}^{t+\Delta t} \underline{\mathbf{R}}_{c,k}^{(i-1)} & \text{for all nodes } k \\ & \text{within the contact} \\ & \text{zone} \end{cases} \quad (3.9)$$

The contact algorithms implemented in commercial software work basically using the above mentioned theoretical formulation (for more information refer to [40, 41]).

The permanent glued contact capability in MSC.Nastran is a special type of contact problem because it is used to join different bodies while prohibiting any kind of motion between them. In order to establish the contact detection, a contact tolerance may be set (cf. Fig. 3-6) and any grid points falling within these tolerances will be “glued” together. [42].

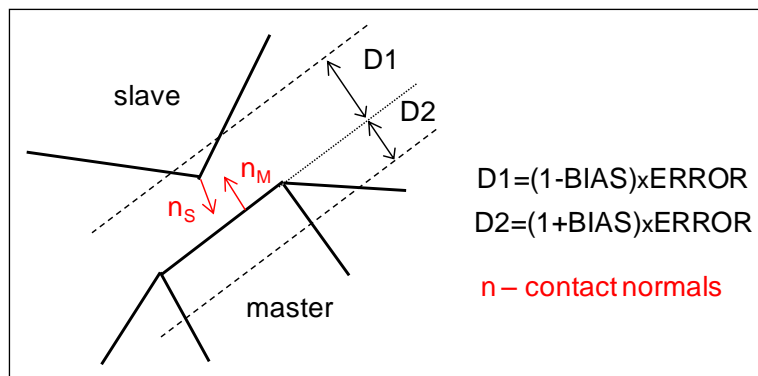


Fig. 3-6 Contact detection and tolerances [43]

After the initial contact between the bodies has been established, the permanent glued contact method creates automatically multipoint constraint (MPC) relationships between adjacent grid points. These MPC-equations are of the form

$$\sum_j A_j \cdot u_j = 0 \tag{3.10}$$

where u_j represents the degree-of-freedom C_j at grid point G_j and A_j is the correspondent coefficient [35]. Fig. 3-7 shows the FE model of a simple isogrid plate in which a stringer run-out at the lower left corner is detailed. In this case permanent glued contact creates automatically MPC-equations to join, for example, the node 23197 of the stiffener to the nodes 27221, 27222, 27272 and 27273 of the skin. The exact MSC.Nastran formulation is shown in Fig. 3-8.

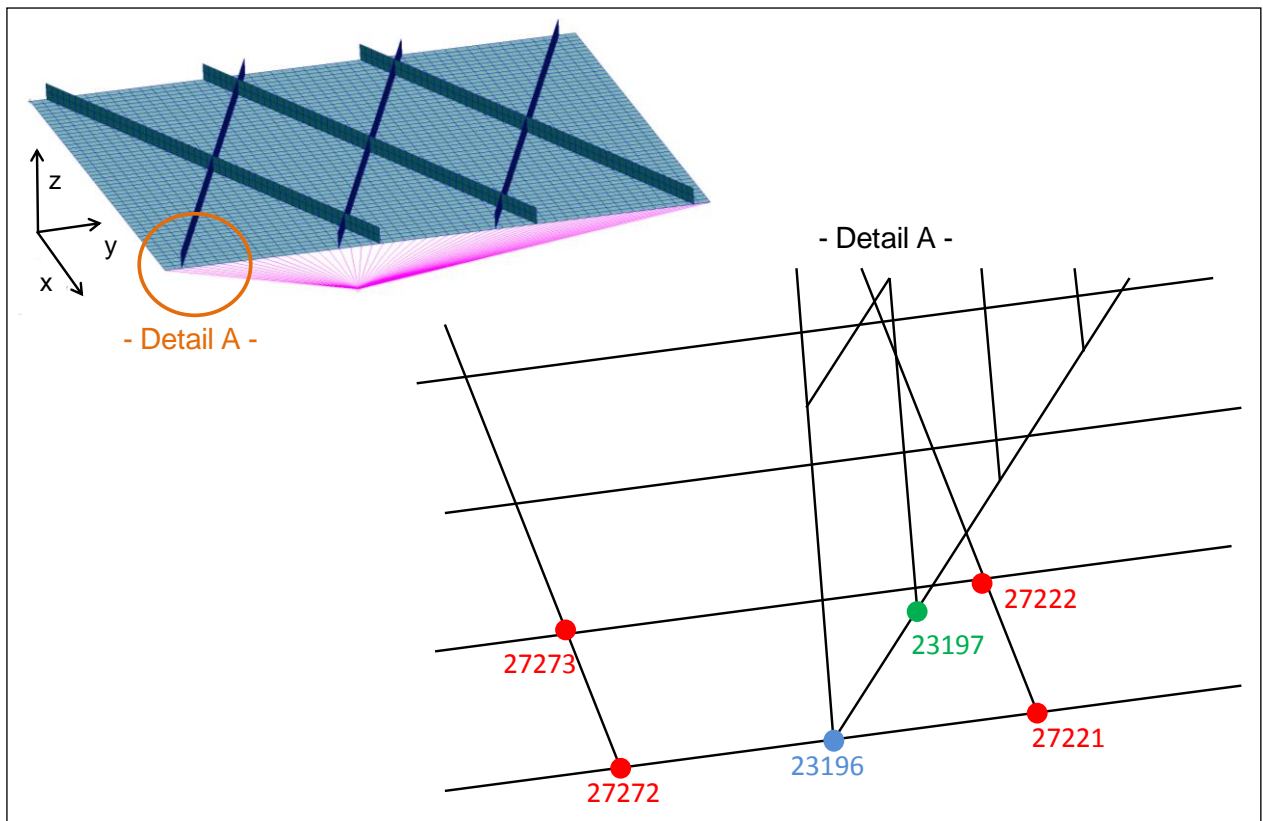


Fig. 3-7 Detail of isogrid plate FE model

MPC*	2	23197	6	0.100000000D+01
*	27221	6	-0.106247490D+00	MPC coefficient (A_j)
*	27222	6	-0.710412693D+00	
*	27273	6	-0.159487307D+00	
*	27272	6	-0.238525101D-01	

Dependent grid point: 23197
 Degree-of-freedom (C_j): 6 = z-Rotation
 Independent grid points: 27221, 27222, 27273, 27272

Fig. 3-8 MPC input created automatically for permanent glued contact

The most important entries and parameters used in MSC.Nastran to define a contact problem are described in Table 3-2.

Entry / Parameter		Description
BCONTACT		Used in a *.bdf.-file above the subcase level to initiate permanent glued contact. BCONTACT = m (m>0, m=identification number of BCTABLE)
BCTABLE		Contains all relevant parameters that define the properties of the contact. BCTABLE ID = m. An overview of the BCTABLE is given in Appendix B.1
BCTABLE	IDSLA1, IDMA1	Identification number of the slave body (IDSLA1) and of the master body (IDMA1).
	NGROUP	Define the number of pairs of slave and master used in the contact definition
	ERROR	Distance below which a slave node is considered to be in contact with the master body (cf. Fig. 3-6)
	IGLUE	Flag to activate different glue options. The glue option used throughout this thesis is IGLUE=3. The slave nodes are projected (physically moved) onto the master body. It insures full moment carrying glue.
	ISEARCH	Defines the contact searching order, from a slave to a master, vice versa or in both directions. ISEARCH = 0,1 or 2.
	ICOORD	ICOORD=1 is used to assure a stress-free initial contact (due to projection of slave nodes undesired stresses may develop)
	BIAS	Contact tolerance bias factor. Default = 0.9. (cf. Fig. 3-6)
	COPTS1, COPTM1	Flag to indicate how the slave-master pair may contact. In this thesis they are usually COPTS1= COPTM1=11061. This parameter is explained in Appendix B.2.
BCBODY		Defines a contact body. Slave: BCBODY = IDSLA1. Master: BCBODY = IDMA1. The slave (touching body) should be the body with the softer material (e.g. rubber should be a slave and steel a master) and/or the body with the finer mesh. Both slave and master are defined as "deformable bodies".

Table 3-2 Entries and parameters for contact definition in MSC.Nastran [35]

3.4 Validation of permanent glued contact method

In order to find suitable settings and to check that the glued contact method calculates feasible results, a simple assessment of the elastic deformation and buckling behavior of different stiffened plate models is performed. For this purpose, the results of a model with congruent meshes between skin and stiffeners (coincident nodes/equivalence) are compared to the results of a model with dissimilar meshes (glued contact). The models were chosen arbitrarily and do not represent any experimentally or analytically validated plate models.

Within this validation the focus is also put on the solver settings: SOL105 (linear buckling analysis) and SOL400 (advanced non-linear implicit analysis) are investigated.

3.4.1 Assessment of buckling behavior

Two configurations are used for the assessment of the buckling behavior: a parallel stiffened plate (cf. Fig. 3-9) and an isogrid-like plate (cf. Fig. 3-10). For each configuration there are two models: model A whose properties are defined so that global buckling modes are most likely to appear, and model B whose properties are defined so that local buckling modes are most likely to appear. For each model the equivalence method (congruent meshes between skin and stringers) and permanent glued contact method (dissimilar meshes) are employed.

The plates are simply supported on all edges and subjected to a combined compression-shear load (as typical for a plate on the upper wing cover). The compression load is given as a shortening of $\Delta x=0.1\text{mm}$ at one plate end by means of RBE2-elements. Based on a constant shear flow of $N_{xy}=2\text{ N/mm}$, shear forces are calculated and implemented by means of RBE3-elements at each plate edge. The normal vectors of the skin elements point in positive z -direction and the laminate offset is defined as zero. The CFC-materials are the same used for the forward swept wing model (cf. Appendix C).

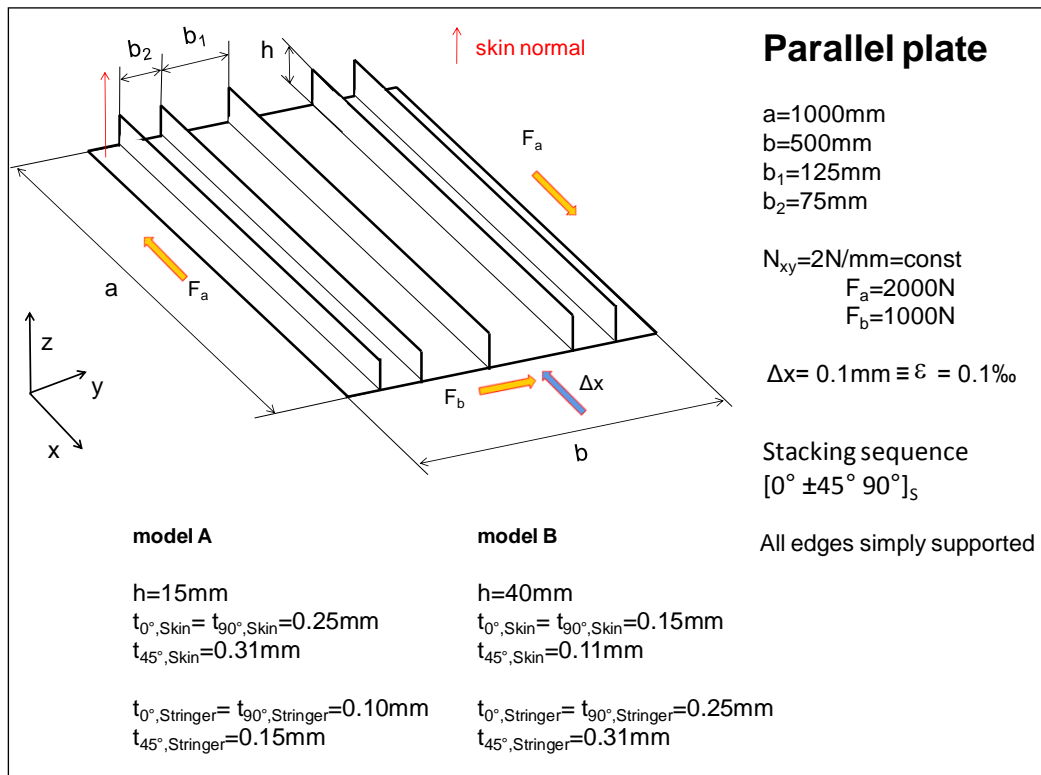


Fig. 3-9 Parallel plate configuration

A linear buckling analysis (SOL105: Lanczos method) is performed to calculate the first 15 eigenvalues ($\lambda \geq 0$). The following settings regarding the glued contact method are used:

- ERROR = 1.0
- IGLUE = 3
- ISEARCH = 1 (from slave to master)
- COPTS1= COPTM1=11061
- BCBODY: Slave \rightarrow blade stiffeners; Master \rightarrow panel skin

In order to calculate mesh-independent results, all plate models are finely meshed using CQUAD4-elements with a target element length of $l=10\text{mm}$.

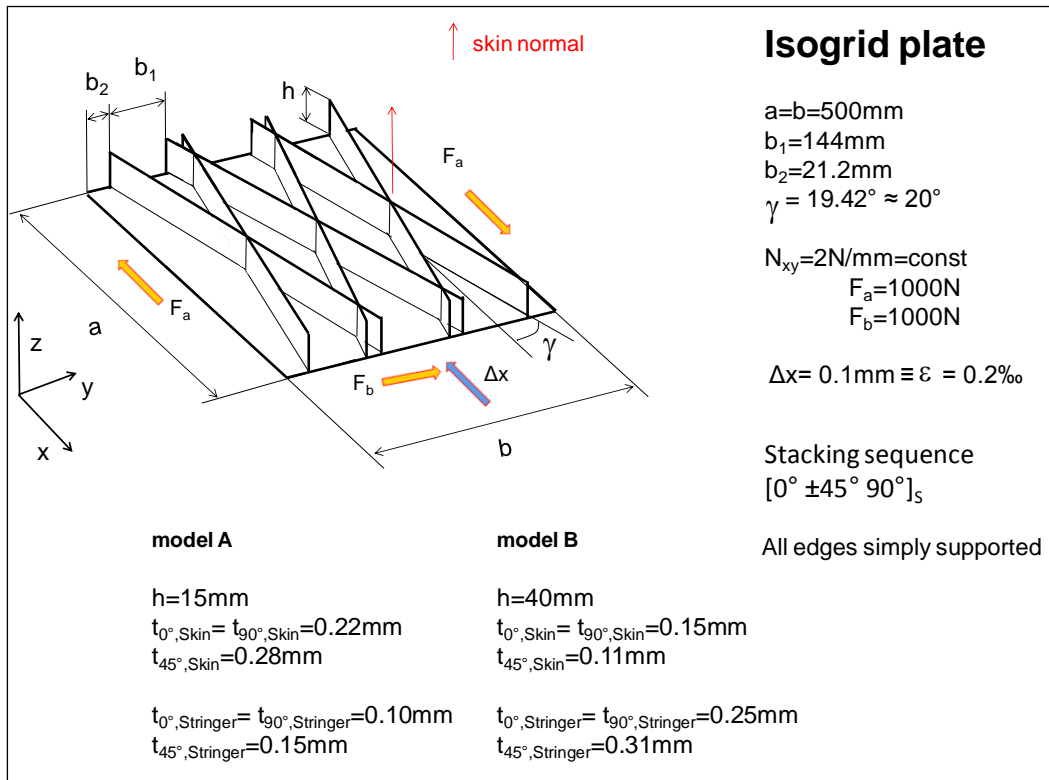


Fig. 3-10 Isogrid plate configuration

3.4.1.1 Results of parallel plate

a) Model A

Fig. 3-11 shows that the eigenvalues of the parallel plate (model A) between equivalence and glued contact coincide very well. The largest difference is $\Delta=2.1\%$ for eigenvalue 13.

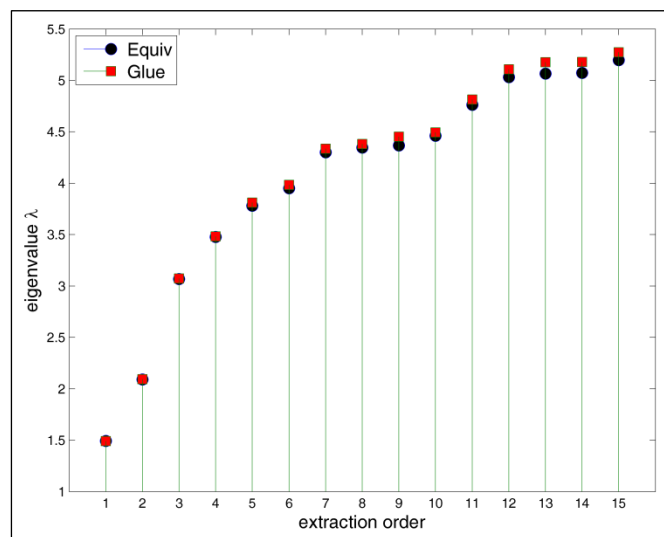


Fig. 3-11 Comparison of eigenvalues λ of parallel plate (model A)

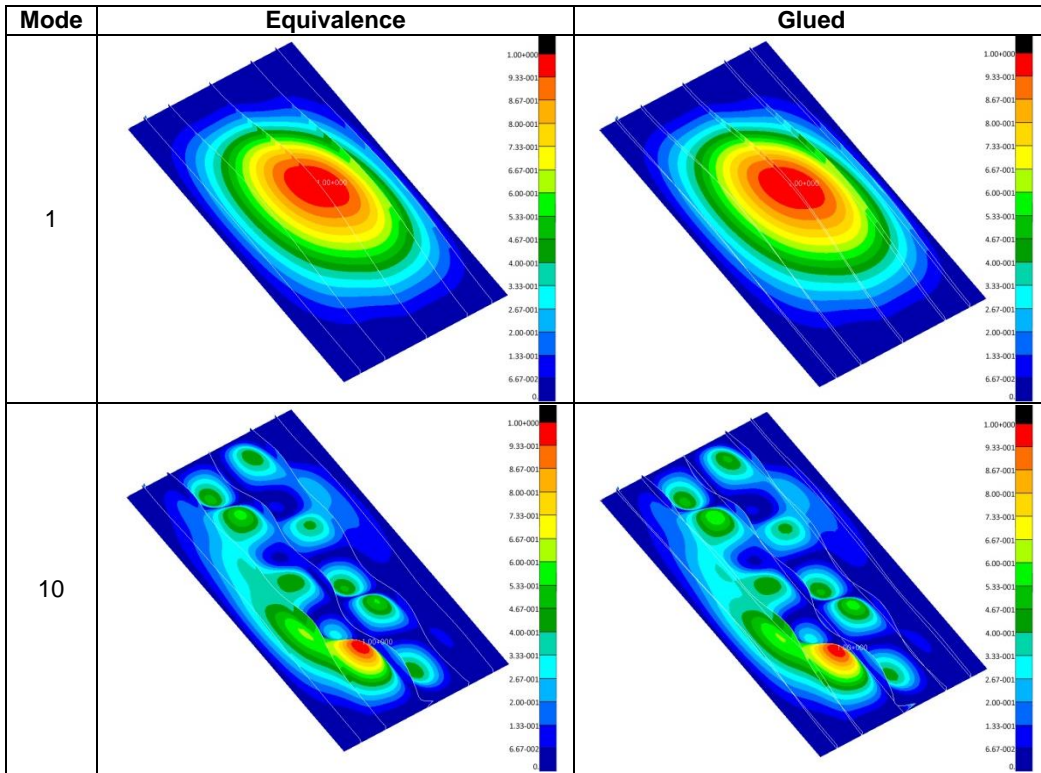


Table 3-3 Selected eigenmodes of parallel plate (model A)

b) Model B

The eigenvalues of the parallel plate (model B) between equivalence and glued contact have a largest difference of $\Delta=5.7\%$. Despite this, Fig. 3-12 shows a very good trend accordance.

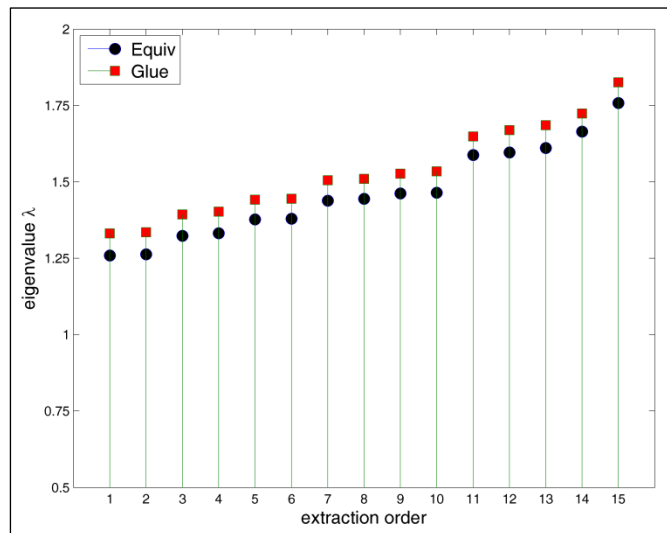


Fig. 3-12 Comparison of eigenvalues λ of parallel plate (model B)

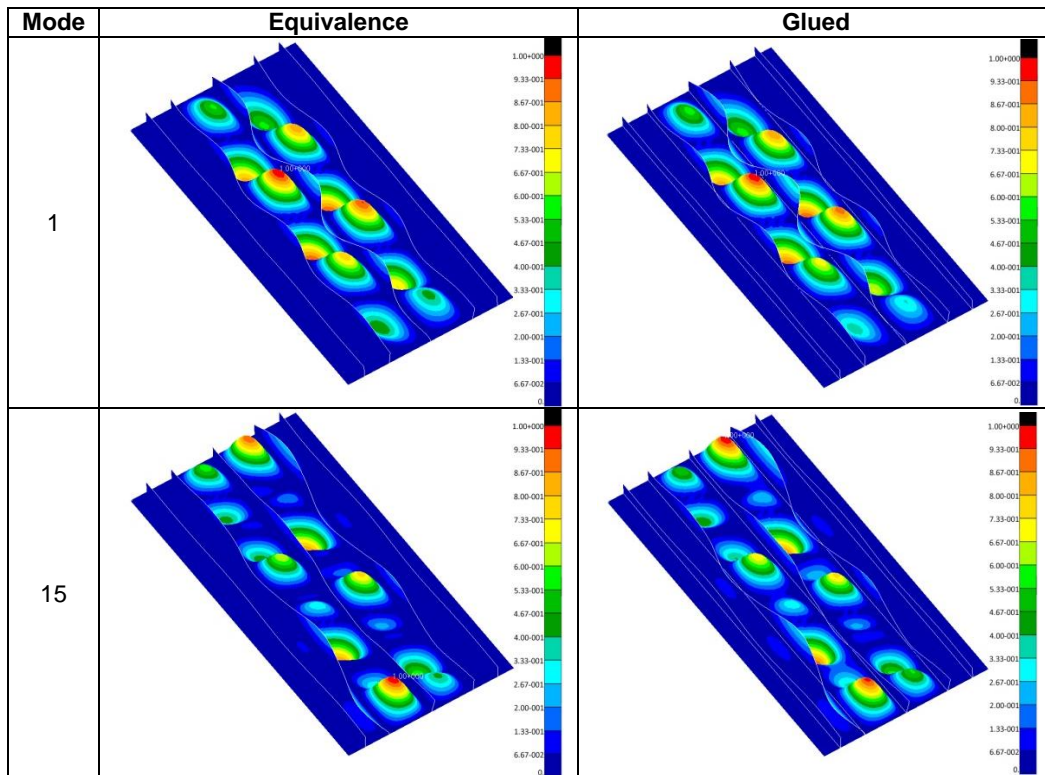


Table 3-4 Selected eigenmodes of parallel plate (model B)

3.4.1.2 Results of isogrid plate

a) Model A

The eigenvalues of the isogrid plate (model A) between equivalence and glued contact show a good accordance (cf. Fig. 3-13). The largest difference is $\Delta=4.3\%$ for eigenvalue 6.

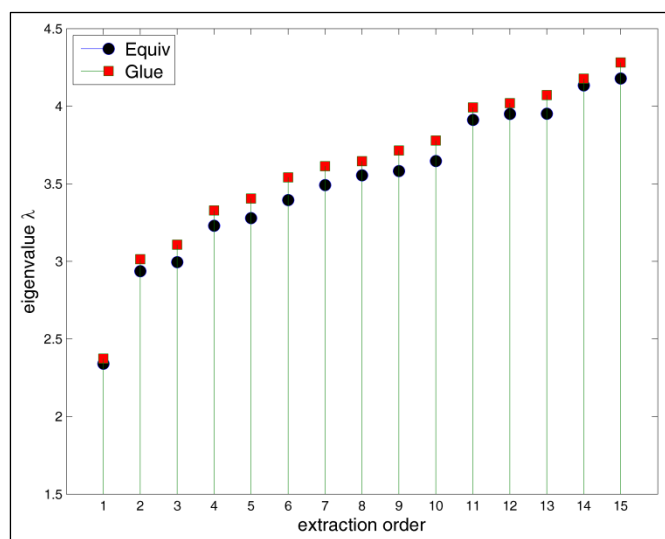


Fig. 3-13 Comparison of eigenvalues λ of isogrid plate (model A)

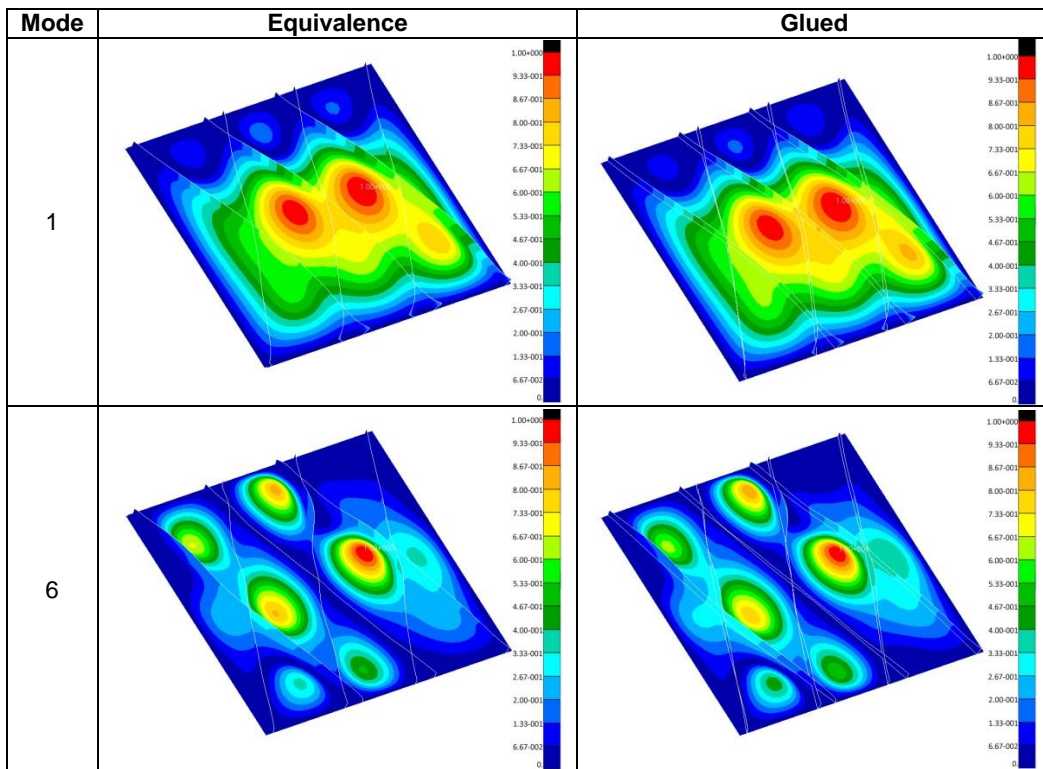


Table 3-5 Selected eigenmodes of isogrid plate (model A)

b) Model B

The eigenvalues of the isogrid plate (model B) between equivalence and glued contact show a very similar trend (cf. Fig. 3-14). However, there is a difference up to $\Delta=8.6\%$ for eigenvalue 6.

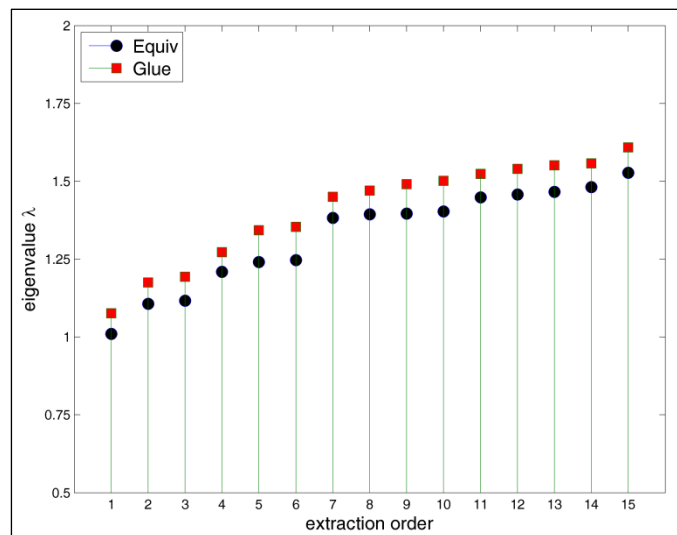


Fig. 3-14 Comparison of eigenvalues λ of isogrid plate (model B)

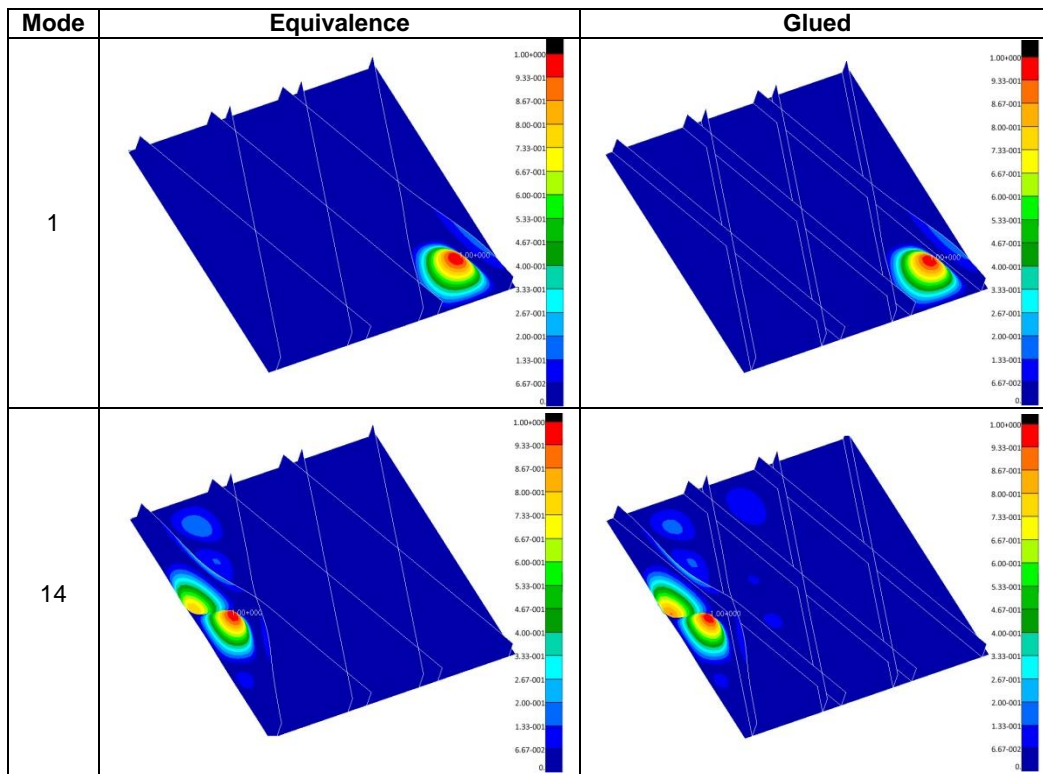


Table 3-6 Selected eigenmodes of isogrid plate (model B)

It can be seen that the permanent glued contact method using dissimilar meshes between skin and stiffeners calculates in all the cases similar eigenvalues and eigenmodes to those of the equivalence method. The results of the parallel plates show in general a better accordance than the results of the isogrid plates. Furthermore, the local buckling results coincide in general slightly better than the global buckling results. There seems to be a minor stiffness overestimation which leads in general to slightly higher glued contact eigenvalues λ . It was also observed that few eigenmodes may shift one position (extraction order) upward or downward within the examined spectrum. In spite of this, the permanent glued contact proves to be suitable to calculate feasible results and accurate eigenvalue trends. The linear buckling analysis SOL105 using permanent glued contact performs well while reducing at the same time the pre-processing effort.

3.4.2 Assessment of elastic deformations

For the assessment of the elastic deformations the two plate configurations described above (cf. Ch. 3.4.1) are used again but with some modifications. Fig. 3-15 shows the properties of the models that are now clamped at one edge and subjected to a normal force F_z at the opposite free edge. At this free edge, RBE3-elements are used to transfer the point load into the structure. In order to calculate mesh-independent results, all plate models are finely meshed using CQUAD4-elements with a target element length of $l=10\text{mm}$.

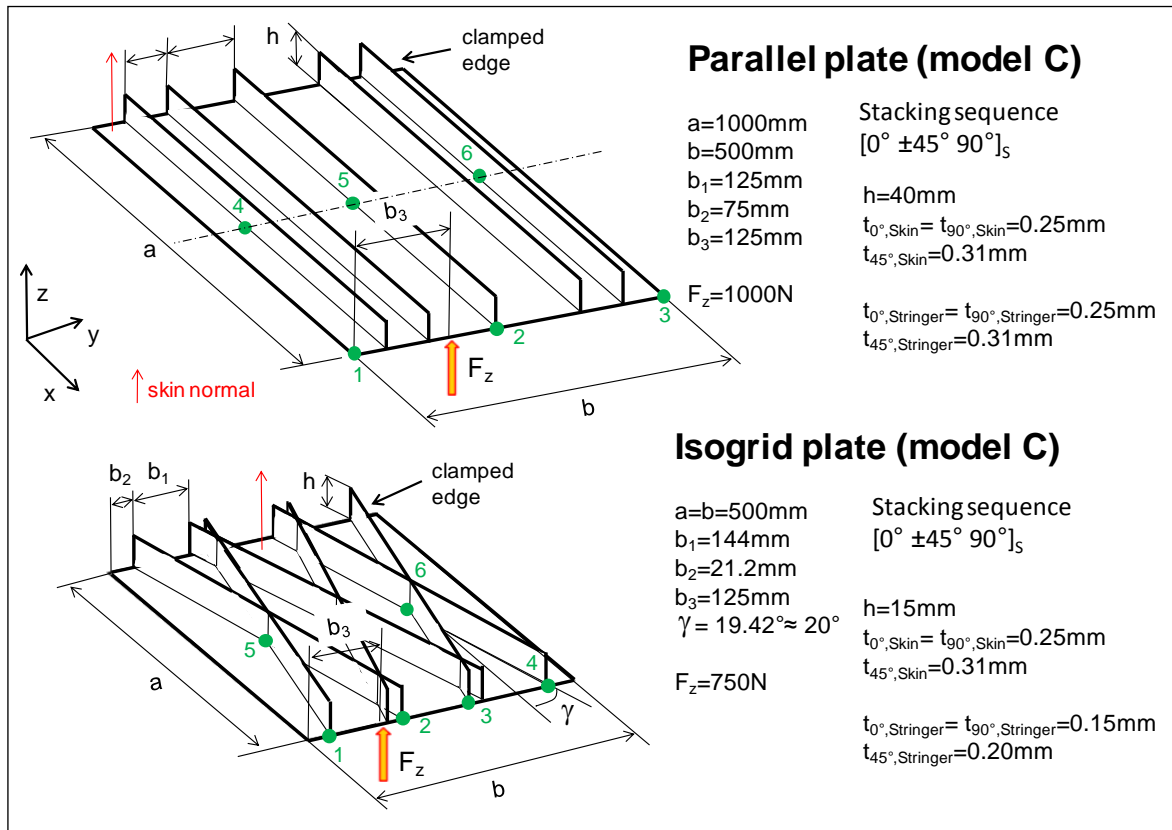


Fig. 3-15 Plate models used for assessment of elastic deformation

Within the advanced non-linear implicit solution (MSC.Nastran SOL400) a linear static analysis is performed with all models in order to find the node displacements. Regarding the solver and permanent glued contact method, the following relevant settings are used:

- RIGID= LINEAR
- ANALYSIS=STATICS
- NGROUP = 2
- ERROR = 1.0
- IGLUE = 3
- ISEARCH = 1 (from slave to master)
- COPTS1= COPTM1=11061
- BCBODY: blade stiffeners are first slave and then master; panel skin is first master and then slave (NGROUP = 2)

The displacement values at six different plate positions (see green points in Fig. 3-15) are compared, using on the one hand the equivalent method ("Equiv") and on the other hand the permanent glued contact method ("Glue"). The results of the first three plate positions are shown below.

a) Results of parallel plate (model C)

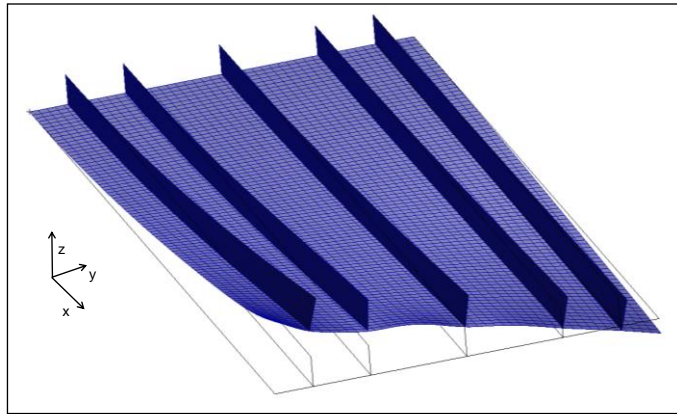


Fig. 3-16 Deformation plot of parallel plate

		Position 1 [mm]			Position 2 [mm]			Position 3 [mm]		
		Equiv	Glue	Δ [%]	Equiv	Glue	Δ [%]	Equiv	Glue	Δ [%]
DOF	T1	1.09017	1.09272	+0.23	0.40636	0.40570	-0.16	-0.18894	-0.19009	+0.60
	T2	0.84324	0.81965	-2.79	1.09955	1.10965	+0.91	1.06827	1.06043	-0.73
	T3	117.2476	118.4990	+1.06	46.9656	47.0384	+0.15	-22.8957	-23.5422	+2.82
	R1	-0.58869	-0.61944	+5.22	-0.27730	-0.26556	-4.23	-0.31353	-0.32442	+3.47
	R2	-0.31089	-0.31414	+1.04	-0.06977	-0.06967	-0.14	0.04615	0.04782	+3.62
	R3	0.00186	0.00183	-1.61	0.00143	0.00133	-6.99	0.00199	0.00198	-0.50

Table 3-7 Comparison of displacement results of parallel plate

b) Results of isogrid plate (model C)

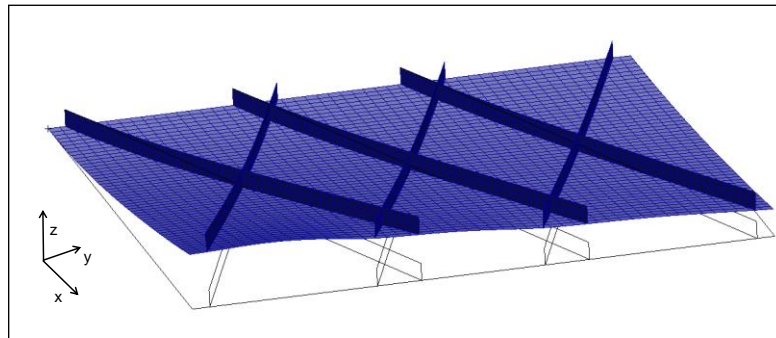


Fig. 3-17: Deformation plot of isogrid plate

		Position 1 [mm]			Position 2 [mm]			Position 3 [mm]		
		Equiv	Glue	Δ [%]	Equiv	Glue	Δ [%]	Equiv	Glue	Δ [%]
DOF	T1	0.59239	0.59353	+0.19	0.49516	0.49656	+0.28	0.38285	0.38671	+1.01
	T2	0.01610	0.03984	+147.4	-0.09870	-0.10200	+3.34	-0.15958	-0.15432	-3.30
	T3	144.5790	143.6743	-0.63	119.3426	119.5229	+0.15	96.6004	96.7736	+0.18
	R1	0.06317	0.09268	+46.72	-0.10333	-0.10715	+3.70	-0.18665	-0.18025	-3.43
	R2	-0.47487	-0.47915	+0.90	-0.35739	-0.35923	+0.51	-0.25006	-0.25586	+2.32
	R3	-0.00100	-0.00051	-49.0	0.00083	0.00093	+12.05	-0.00250	-0.00253	+1.20

Table 3-8 Comparison of displacement results of isogrid plate

As can be seen in Table 3-7 and Table 3-8, the permanent glued contact method using dissimilar meshes between skin and stiffeners calculates for all positions and for all DOF very similar displacement values to those of the equivalence method. There are only a few values of the isogrid plate that show a large difference (position 1: T2, R1 and R3), but in general it can be said that SOL400 using permanent glued contact performs very well and calculates feasible results.

Based on the conducted simulations, it can be concluded that permanent glued contact is a good alternative method for joining FE components with dissimilar meshes in an efficient way.

3.5 Further considerations about the permanent glued contact method

The permanent glued contact methodology is now to be extended to the forward swept wing model. This step requires further investigations, in order to assure an accurate FE analysis. Based on the experiences with the plate models of Ch. 3.4 and on several further test simulations, it is advisable to consider the recommendations given below.

First of all, the definition of the contact bodies has a decisive influence on the quality of the analysis results. Fig. 3-18 shows the definition of the contact bodies chosen for this thesis. Even though the upper and lower stiffeners are not physically bonded to each other, they can be defined as one single contact body. This is a practical suggestion given in [34].

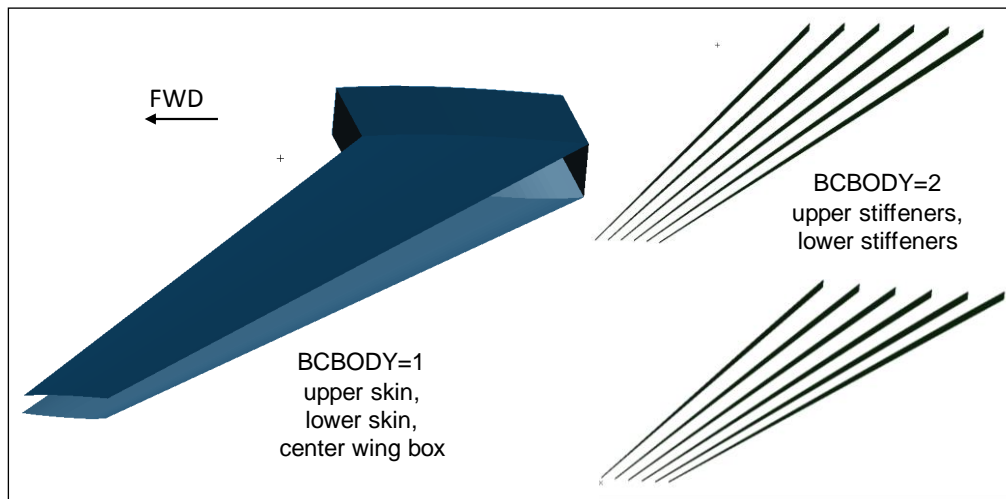


Fig. 3-18 Definition of contact bodies in forward swept wing model

Since the contact bodies have now more complex geometries, the contact tolerance is increased. A stress-free initial contact is also set. Regarding the contact direction, a double search order is chosen. This means that the search order is from the lower BCBODY ID to the higher one. If no contact is detected, then the search is continued in the opposite order [35]. This decision is based on the fact that the double search order proved to be the most robust option for detecting contact. The following settings are used:

- ERROR = 2.0
- ICOORD = 1
- ISEARCH = 0
- All other relevant parameters have the values defined in Table 3-2.

In order to visually check for a successful contact detection after the analysis has been performed, the generation of a *.MASTER-file is required. This file can be attached into a post-processing software, where a fringe plot showing the *contact status* can be created (cf. Fig. 3-19). A continuous and smooth colored line along the contact bodies signalizes a successful contact.

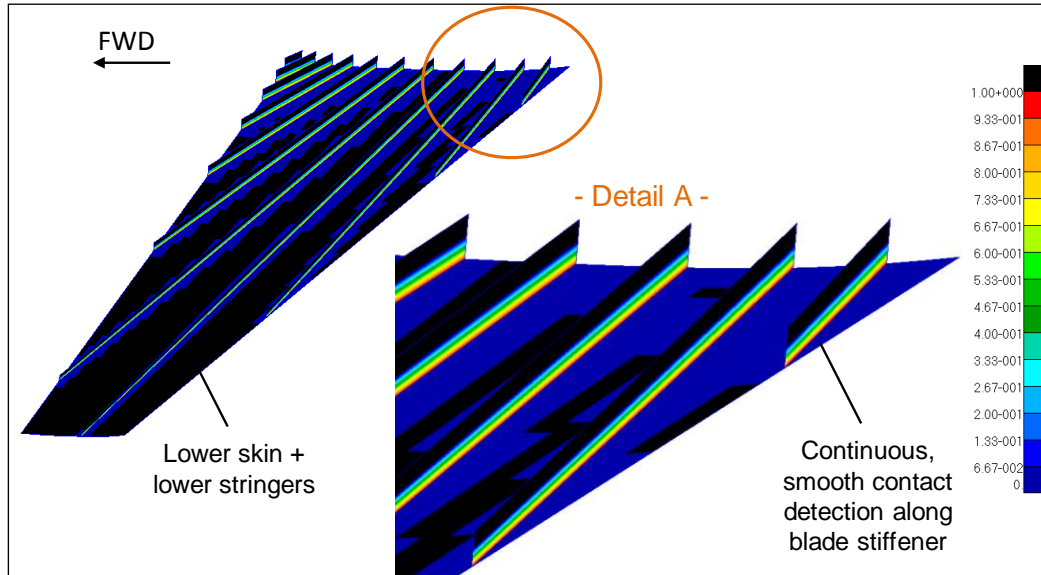


Fig. 3-19 Example of a contact status fringe plot

A comparison of the displacements between the permanent glued contact results and equivalence results is performed by means of an arbitrary forward swept wing model configuration (cf. Appendix D for model information).

Fig. 3-20 portrays the resulting wing deformation. As can be seen in Table 3-9, the maximum wing displacements for the two different load cases are very similar to each other. There is in general a better accordance among the translational DOFs than among the rotational DOFs. However, due to the magnitude of the rotational DOFs, the differences are not significant.

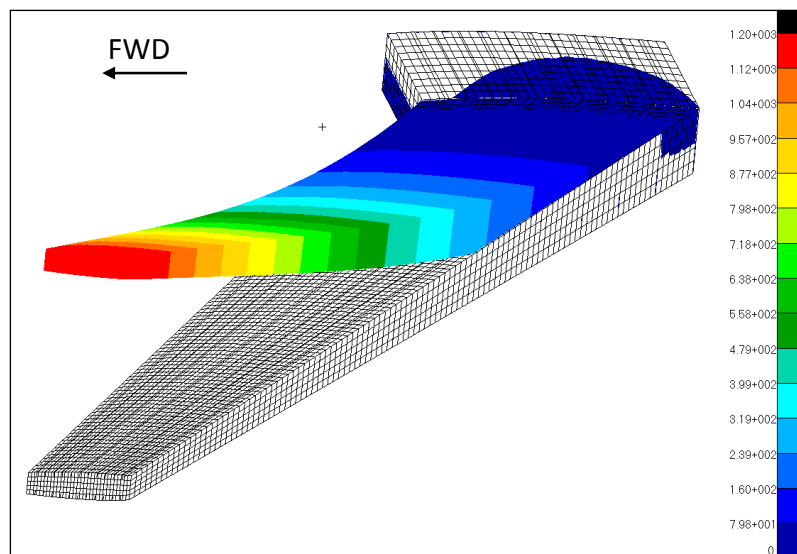


Fig. 3-20 Wing deformation plot for load case 1

		Displacements LC1 [mm]			Displacements LC2 [mm]		
		Equiv	Glue	Δ [%]	Equiv	Glue	Δ [%]
DOF	T1	11,2024	11,2173	+0,13	27,1276	27,1813	+0,20
	T2	94,8149	94,6578	-0,17	232,8366	232,4310	-0,17
	T3	1194,914	1192,859	-0,17	2921,548	2916,627	-0,17
	R1	0,09733	0,09852	+1,23	0,24116	0,24416	+1,25
	R2	0,01814	0,01971	+8,66	0,03925	0,04084	+4,05
	R3	0,01251	0,00979	-21,73	0,03086	0,02405	-22,06

Table 3-9 Comparison of maximum wing displacements

It can be concluded that the permanent glued contact method enables an accurate stiffness and load transfer for the investigation purposes of this thesis. Not only is the setup relative easy, but it also allows for a much faster FE model generation and it calculates feasible results. In the next chapter the parameterization and implementation of this method into the forward swept wing model is explained in detail.

4 Finite-element parameterization and automation

This chapter deals with the procedure providing the finite-element generation of the forward swept wing model. Special emphasis is put on the description of the parameterization concept behind the curvilinear stiffeners, which relies on *Bézier curves* and splines. Further properties about the wing model are also briefly described as well as the implementation and automation within the post-processing software MSC.Patran.

4.1 Parameterization concept of curvilinear stiffeners

Within this thesis it is very important to develop a mechanism that is able to create flexible curvilinear forms using the least number of inputs as possible, because the more inputs (design variables) an optimization problem has, the more time and resources it costs.

In order to create curvilinear paths, three *support zones* along the wing span are defined (cf. Fig. 4-1). Connecting these support zones produces a closed space: this is the *design space* of the stiffeners, or in other words, the allowable region where stiffeners can be positioned. By specifying the length of support zone #1 as the wing root chord ($l_1 = c_r$) it is guaranteed that all stiffeners always start at the wing root. This prevents that during an optimization stiffeners might disappear or new ones might be added, which could mean a significant overall stiffness jump and therefore generate unsteady gradient information. Aeroelastic tailoring in forward swept wings is achieved when the laminate stiffness direction is turned forward [1, 21]. Based on this, the length of support zone #3 is specified so that the stiffeners also have the possibility to point forward rather than backward. Finally, support zone #2 is placed in the middle of both previous zones.

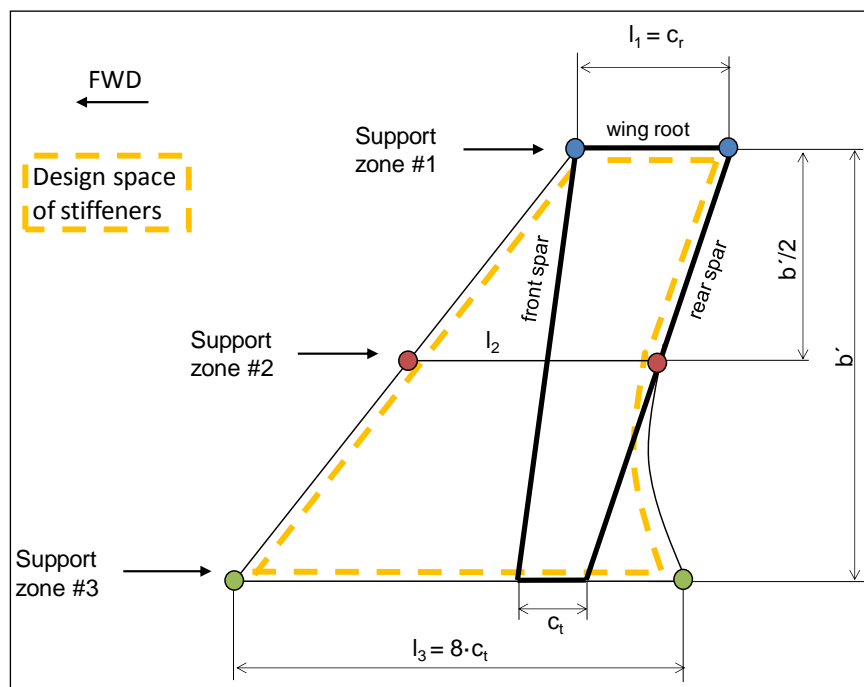


Fig. 4-1 Definition of support zones for creating curvilinear stiffeners

The form of each curvilinear stiffener is defined by three *supporting points* (one point per support zone). Once the supporting point positions are known, they can be linked to each other in order to generate a curve (within MSC.Patran the option *spline* is used to link them). Fig. 4-2 shows this exemplarily for two stringers.

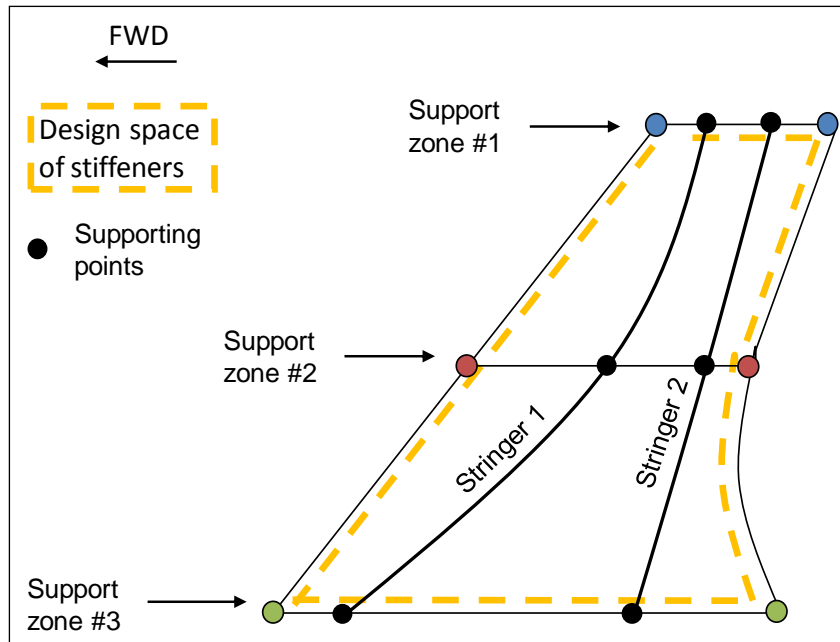


Fig. 4-2 Creation of curves (splines) between support zones

The same procedure is used to create all the desired stringers. Afterwards the stringer paths are projected from the design space onto the FE model, i.e. upper and lower wing covers (cf. Fig. 4-3). Now in the *physical space*, the projections are extruded in order to create the vertical surfaces for the blade stiffeners.

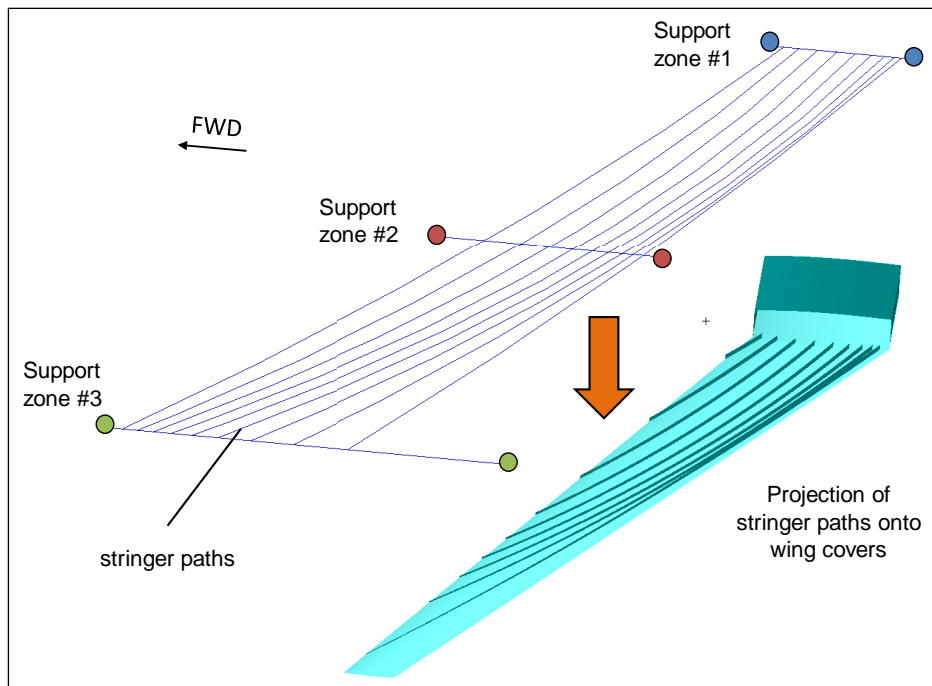


Fig. 4-3 Projection of curvilinear paths onto FE model

A key aspect of this parameterization concept is the definition of the three supporting point positions of each stringer. The solution is to use so-called *Bézier curves*. They are parametric curves developed by P. Bézier and P. de Casteljaou around 1960 at two different French car

companies and used frequently in computer graphics and CAD systems for curve and surface descriptions [44]. Such a curve is given by [44, 45]:

$$C(v) = \sum_{i=0}^n P_i \cdot B_{i,n}(v) \quad (4.1)$$

where $B_{i,n}(v)$ is a *Bernstein polynomial* of degree n defined by

$$B_{i,n}(v) = \binom{n}{i} \cdot v^i \cdot (1-v)^{n-i}, \quad i=0,1,\dots,n \text{ and } v \in [0,1]. \quad (4.2)$$

P_i are the so-called *Bézier control points*, which act as weighting factors for defining the curve path.

In this thesis fourth order Bézier curves ($n=4$) are applied. The explicit formulation is shown in Eq. (4.3) and its graphic representation is depicted in Fig. 4-4. It can be seen that the control points P_0 and P_4 are the end points of the curve, while P_1 , P_2 and P_3 do not lie on the curve.

$$C(v) = P_0 \cdot (1-v)^4 + 4 \cdot P_1 \cdot v \cdot (1-v)^3 + 6 \cdot P_2 \cdot v^2 \cdot (1-v)^2 + 4 \cdot P_3 \cdot v^3 \cdot (1-v) + P_4 \cdot v^4 \quad (4.3)$$

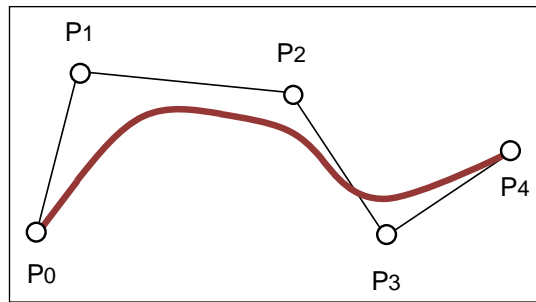


Fig. 4-4 Fourth order Bézier curve representation (adapted from [46])

There is a Bézier curve attached to each support zone in the design space. Fig. 4-5 explains this methodology by means of the support zone #1:

The Bézier control points can only adopt values between zero and one: the first control point P_0 has always a fix value of zero, which corresponds in the *physical space* to the x -position of the front spar, while the last control point P_4 has always a fix value of one and corresponds to the x -position of the rear spar. The positions of the intermediate control points define the curve path, which is then evaluated for each stringer in the model, i.e. the coordinate parameter v . Thus, a correspondent x -position is found for each stringer in the *physical space*, resulting finally in a unique supporting point arrangement at the wing root. In the example shown in Fig. 4-5a it is assumed that the wing cover has four stringers ($s_N=4$). The positions of the supporting points of the same four stringers can be easily modified just by moving one single control point, in this case P_1 a bit to the left (cf. Fig. 4-5b).

The advantage of this methodology is that actually only three control points (P_1 , P_2 and P_3) are needed to define the positions of any arbitrary number of stringers at the wing root: more stringers just mean that the same Bézier curve will be evaluated at more stations. Thus, a decoupling of the geometric design model from the actual structural analysis model is achieved.

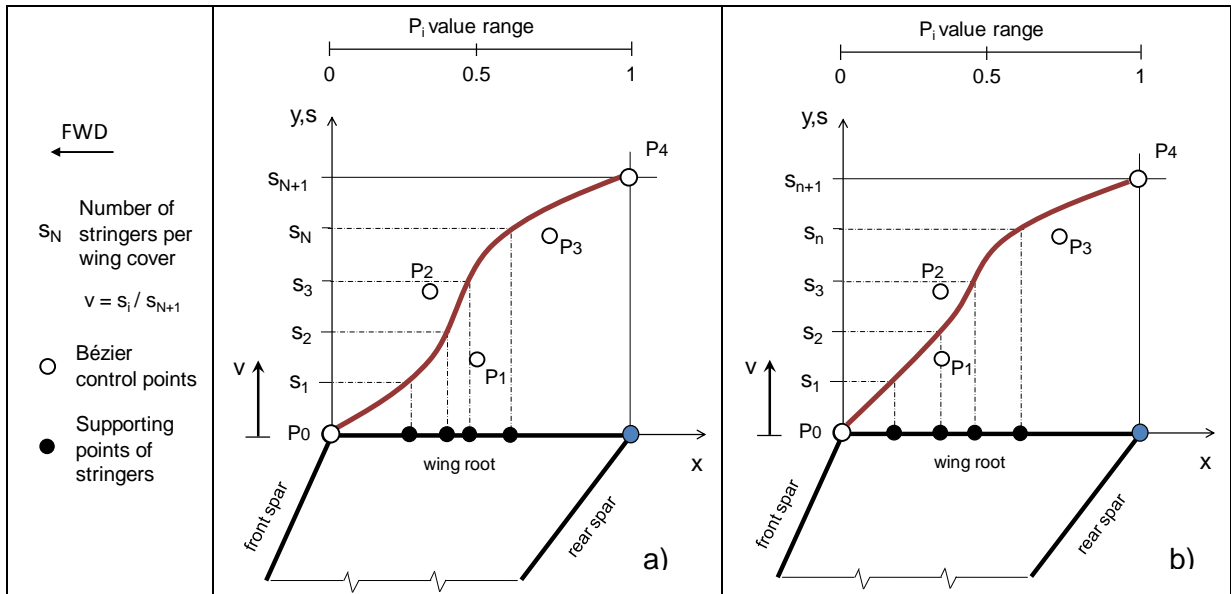


Fig. 4-5 Application of Bézier curve within support zone #1

The exact same concept is applied for the other support zones (#2 and #3) with the only difference that the *physical space* is not defined within the front and rear spar, but within their own support zone lengths l_2 and l_3 , respectively (cf. Fig. 4-6).

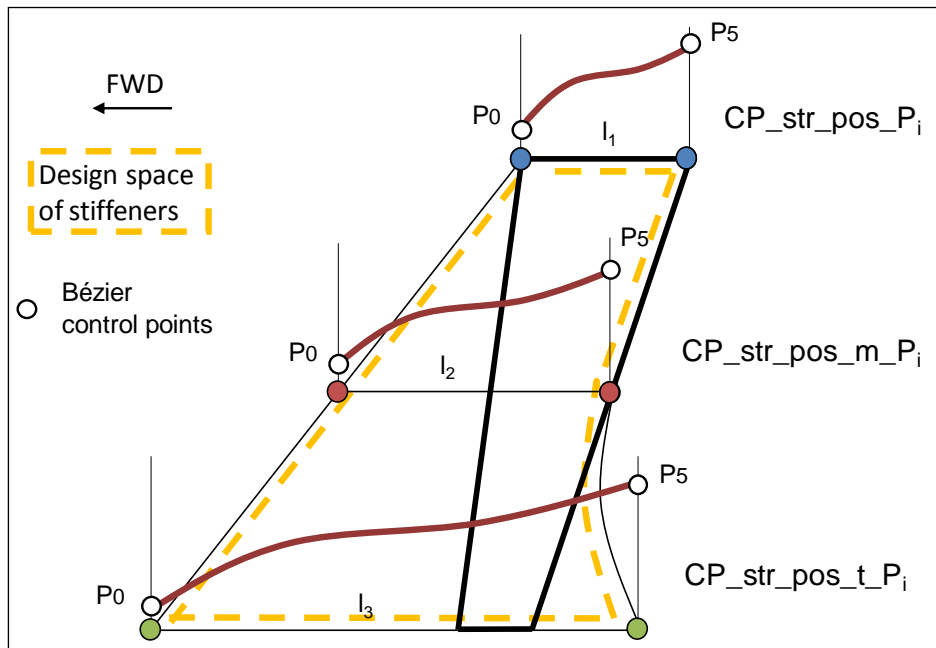


Fig. 4-6 Overview of the three Bézier curves of the design model.

At the right side: Denotation of respective control points for MSC.Patran

Apart from the curvilinear stiffeners, this design model offers the possibility to represent other stiffener configurations by means of some minor modifications as shown in Fig. 4-7. For example, the configuration 1 is achieved by using the first and third Bézier curves and at the same time reducing the length l_3 to the value of l_1 . On the other hand, the configuration 2 is achieved by internally using only the Bézier curve of support zone #1 and switching off the rest. Configuration 3 uses only support zones #1 and #3 (with its original length l_3).

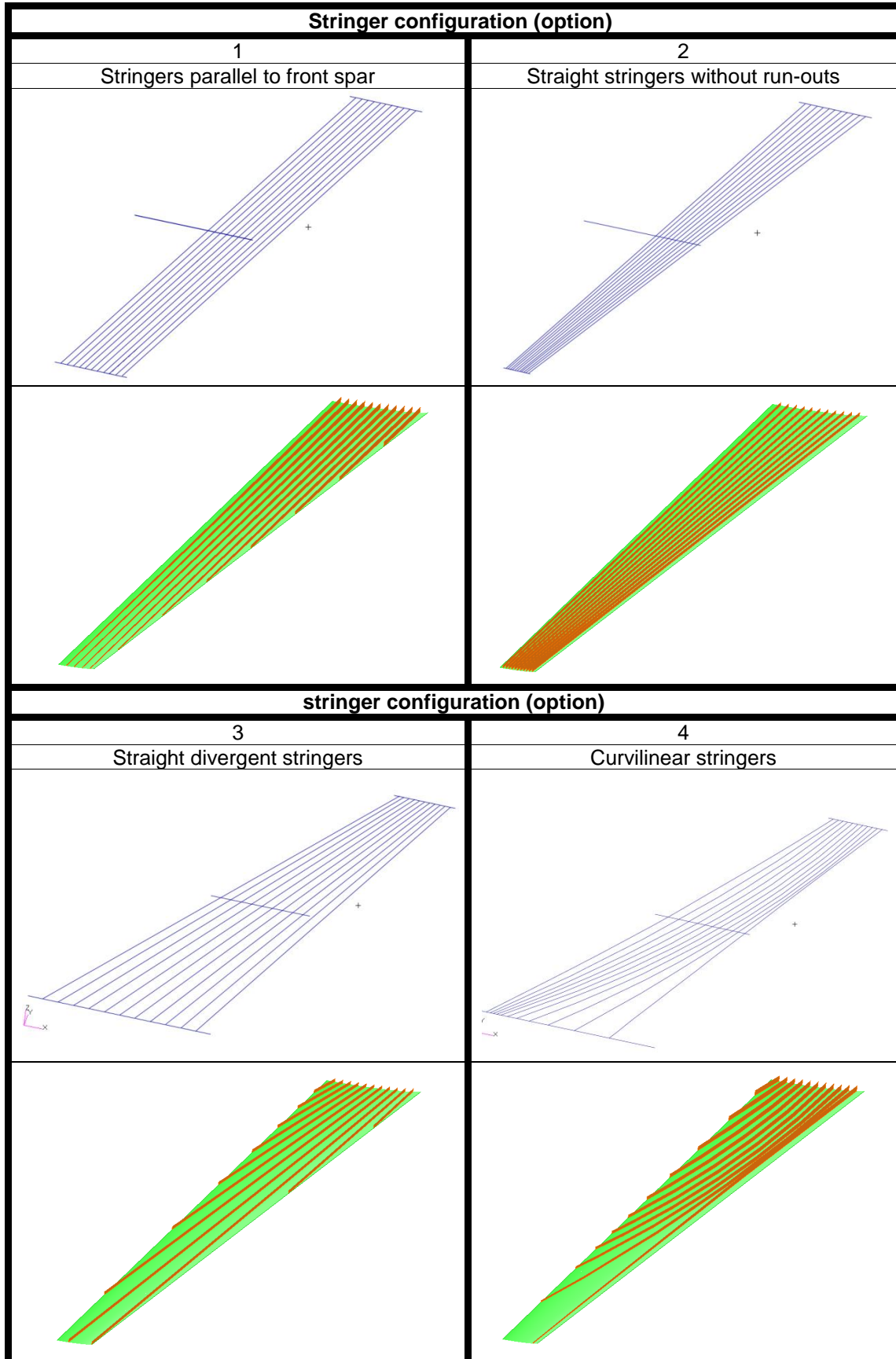


Fig. 4-7 Four different stringer configurations in the FE wing model

4.2 Further parameterized properties

The forward swept wing model used in this thesis offers more parameterized properties than just the curvilinear stiffeners. Table 4-1 shows a list containing all relevant FE model properties that are parameterized and that will be used afterwards for the definition of the optimization models in Ch. 7.

Design parameter	Description
General wing geometry	Defined by the parameters <i>wing area</i> , <i>aspect ratio</i> , <i>fuselage diameter</i> , <i>wetted half span</i> , <i>taper ratio</i> , <i>sweep angle</i> and <i>dihedral angle</i> . Based on these inputs the wing form and dimensions are calculated.
Front and rear spar positions	Defined as percentage of wing chord at two different locations: wing root and wing tip. A linear function is created that describes the spar positions in wing span direction.
Number of ribs	A desired integer number of ribs
Rib positions	Defined by one single fourth order Bézier curve. The implementation is the same as that explained by means of Fig. 4-5 using ribs instead of stringers and the wing span instead of the wing root as the <i>physical space</i> .
Number of stringers	A desired integer number of blade stiffeners (same number for upper and lower covers)
Stringer position option	Switch for defining the desired stringer configuration
Stringer positions	Defined using fourth order Bézier curves
Stringer height	Defined by a linear function between wing root and wing tip.
Meshing	Variable meshing procedure for the different wing regions based on desired element lengths or number of elements.
Composite materials	All relevant UD-Prepreg and Fabric properties are user-defined.
Stacking sequence	User-defined stacking sequence definition for all different wing regions (upper skin, lower skin, front spar, rear spar, ribs, stringers, center wing box).

Table 4-1 List of parameterized properties of the FE wing model (adapted from [49])

4.3 Implementation and automation in MSC.Patran

As the forward swept wing model is to be implemented into a structural optimization process, an automated structural analysis model procedure must be developed, which is able to precisely set up the complete FE model automatically. For this purpose the programming language of MSC.Patran (PCL = *Patran Command Language* [47]) is employed to create so-called PCL-files (*.pcl), which contain all the necessary modeling commands for building the model. Each PCL-file is responsible for a concrete task and relies on the information defined by the user in a series of input files (*.txt). For a better performance all PCL-files are compiled into a so-called library (*.plb) [48]. The modeling process is initialized by a session file (*.ses),

which opens up the library (*ForSwing_library.plb*) and then runs all compiled PCL-files sequentially (cf. Fig. 4-8). A brief description of each module can be found in Table 4-2.

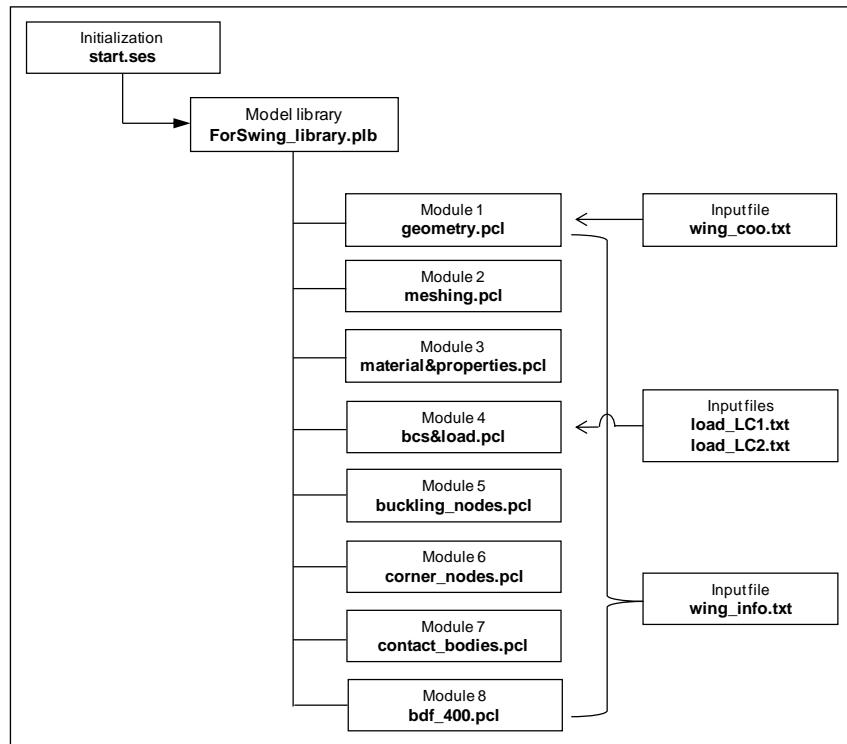


Fig. 4-8 Automated PATRAN model generator (adapted from [49])

File name	Task
start.ses	Creates a new MSC.Patran database, opens up the library and runs the compiled PCL-files
ForSwing_library.plb	Contains all compiled PCL-files (modeling commands)
geometry.pcl	Creates the complete wing geometry.
meshing.pcl	Creates the finite element mesh
material&properties.pcl	Creates the CFC-materials and laminates for the different wing regions
bcs&load.pcl	Creates the boundary conditions and the wing load distribution
buckling_nodes.pcl	Creates an external file with (<i>buckling_nodes.txt</i>) information used to identify local and global buckling modes
corner_nodes.pcl	Creates an external file (<i>corner_nodes.txt</i>) with information used to determine the wing elastic deformation (bending and torsion)
contact_bodies.pcl	Defines the contact bodies and prepares the model for permanent glued contact (cf. Fig. 3-18).
bdf_400.pcl	Creates a MSC.Nastran input file (<i>dummy.bdf</i>) for SOL400

Table 4-2 Description of PATRAN model generator modules (adapted from [49])

Regarding the input files, *wing_coo.txt* contains the point coordinates that form the wing aerodynamic profile (cf. Fig. 4-9). The module “geometry.pcl” reads these coordinates, creates the points and links them using splines. It also scales the airfoil properly in span-wise direction. The used coordinates belong to a special NLF-airfoil developed by DLR [1].

\$ Airfoil coordinates \$			
	C = CHORD		
	YU = UPPER Y-COORDINATE		
	YL = LOWER Y-COORDINATE		
NR	X/C	YU/C	YL/C
1	1.00000000	0.000000000	0.000000000
2	0.99074034	0.0030359529	0.000000000
3	0.97335893	0.0063500083	0.0003713828
4	0.95597752	0.0094291250	0.0011492009
5	0.93859612	0.0124697129	0.0015405723

Fig. 4-9 Input file containing the airfoil coordinates

On the other hand, *load_LC1.txt* and *load_LC2.txt* contain the aerodynamic coefficient distributions for two different load cases: LC1 corresponds to the load case “Cruise” ($n_z=LL=1$) and LC2 corresponds to the load case “Gust” ($n_z=LL=3.44$). Fig. 4-10 shows the structure of such a file. The used aerodynamic coefficients are provided by DLR [52].

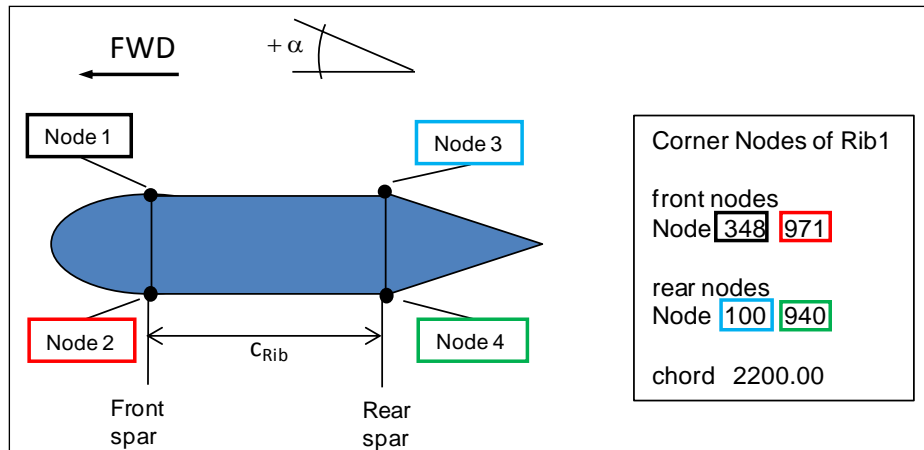
Wing span stations	Normal coefficient c_z	Pitching moment coefficient $c_{M,25}$
↓	↓	↓
2.0	0.255806169	-0.03342872
2.1	0.511612338	-0.06685744
2.3	0.517430414	-0.072839967
2.5	0.51967635	-0.07645148
3	0.521673563	-0.080992563
3.5	0.520608437	-0.081870505
4	0.523912111	-0.084352359

Fig. 4-10 Input file containing wing load information (coefficients)

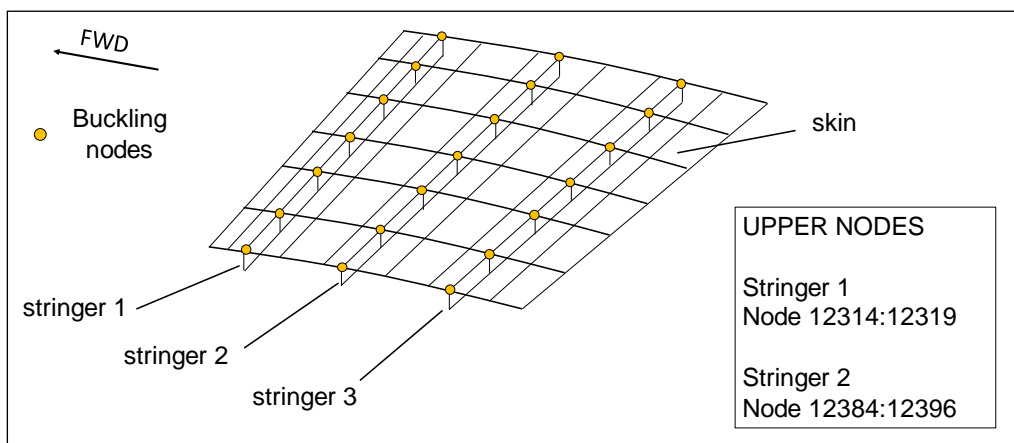
Based on the aerodynamic coefficients, loads per unit span (q_z and m_{25}) are calculated at dedicated wing span stations. By means of interpolation and numerical integration, these loads are condensed into zonal forces F_z and zonal moments M_{25} that are transferred into the structure using RBE3-elements placed at each rib (cf. Fig. 3-2). The loads are labeled according to the respective load case and rib station, e.g.: *LC1_Rib9* is the force vector at the 9th rib of LC1.

However, the most important input file is *wing_info.txt* which contains all relevant design parameters. More information about the structure of this input file can be found in Appendix E.

Three relevant output files are also produced after the model set-up. The module “corner_nodes.pcl” creates the file *corner_nodes.txt*, in which the IDs of the extreme nodes of each wing rib are listed (cf. Fig. 4-11). This information is used afterwards to calculate the wing bending and torsion at dedicated rib positions.

Fig. 4-11 Structure of input file *wing_corner_nodes.txt*

On the other hand, the module "buckling_nodes.pcl" creates the file *buckling_nodes.txt*, in which the IDs of the so-called "buckling nodes" are listed. They are all the nodes of each stringer that touch the wing cover, i.e. that come into contact with it (cf. Fig. 4-12). These nodes are used afterwards to define the buckling constraint within the optimization.

Fig. 4-12 Structure of the output file *wing_buckling_nodes.txt*

Finally, a MSC.Nastran input file (*dummy.bdf*) containing all the FE model information is created by the module "bdf_400.pcl".

The automated PATRAN model generator (PMG) described in this chapter is a self-contained module. It is used, together with several other modules and components, to create the optimization framework for this thesis. In the next chapter the architecture and properties of this framework will be detailed.

5 Optimization framework

This chapter deals with the optimization framework used for the structural optimization of the forward swept wing and therefore describes the used software, the developed architecture and modules, and the implemented design variables and constraints. The optimization framework derives from the optimization procedure developed for the research project AeroStruct - ForSwing [49, 50]. For the purposes of this thesis, several modifications and enhancements have been undertaken.

5.1 General overview of optimization process

5.1.1 Software and architecture

As can be seen in Fig. 5-1, Optimus is chosen as the overarching process coordination and optimization environment. Optimus allows the creation of automated and coordinated simulation workflows, the integration of different software tools, and the numerical optimization of simulation processes [51]. MatLab is used as the general computing software, while the industry standard MSC.Nastran together with the pre- and postprocessor MSC.Patran are used for the FE modeling and analysis. The vertical positions indicate the hierarchy and subordination of the different modules to each other. The horizontal positions indicate the chronological order within an optimization loop. Finally, the arrows represent the data transfer between the modules by means of files or function calls.

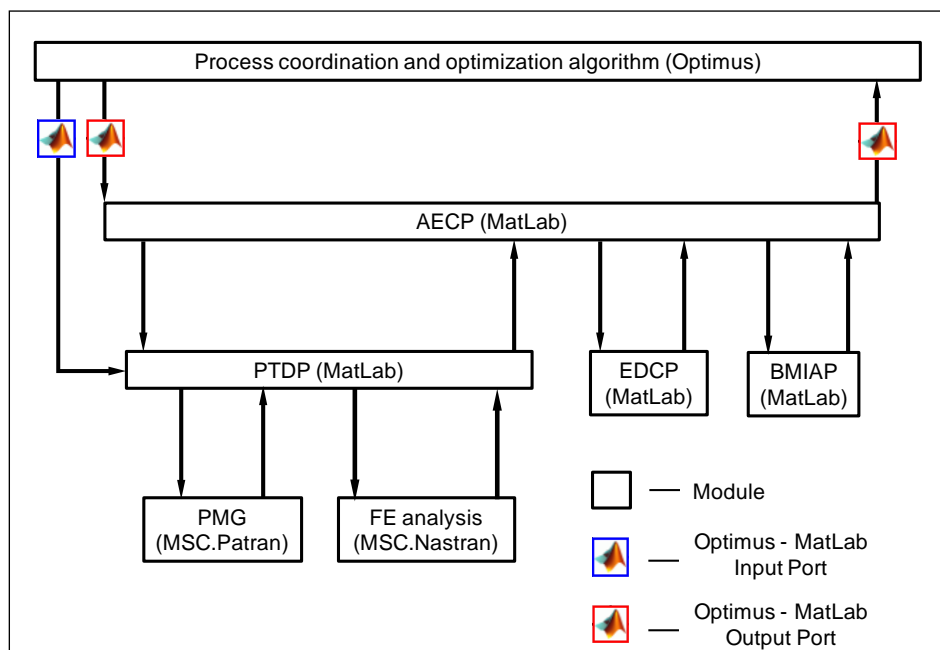


Fig. 5-1 General overview of optimization framework (adapted from [49])

The FE modeling and analysis takes place within the MatLab module PTDP (Parametric Thickness Distribution Procedure). As can be seen in Fig. 5-2 the automated PATRAN model generator module (PMG) is called up first. Based on the information defined in *wing_info.txt* the FE model is created automatically as explained in Ch. 4.3 and three relevant output files are generated (files 2, 3 and 4). Based on the file *dummy.bdf* two actual input files for MSC.Nastran are produced and sent to the solver (files 5 and 6). Finally the results files 7 and 8 are sent back to PTDP. More detailed information about the PTDP-module can be found in Ch. 5.1.2

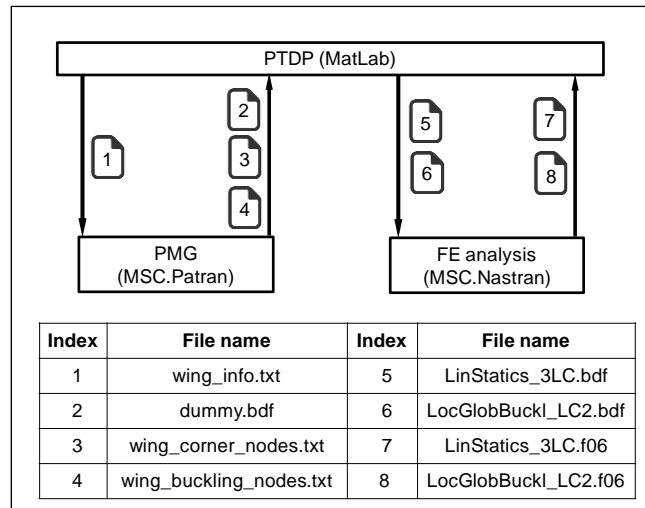


Fig. 5-2 Overview of PTDP-module and FEA (adapted from [49])

The evaluation of the design responses and the constraint formulations take place within the MatLab module AECP (Analysis Evaluation and Constraints Procedure). It also provides this information to the optimization algorithm (Optimus). The first function call is to EDCP (Elastic Deformation Constraint Procedure), which calculates the wing elastic deformations (bending and torsion) based on the information in files 1 and 2. The second function call is to BMIAP (Buckling Mode Identification and Aggregation Procedure), which uses the information in files 4 and 5 to analyze the wing buckling behavior.

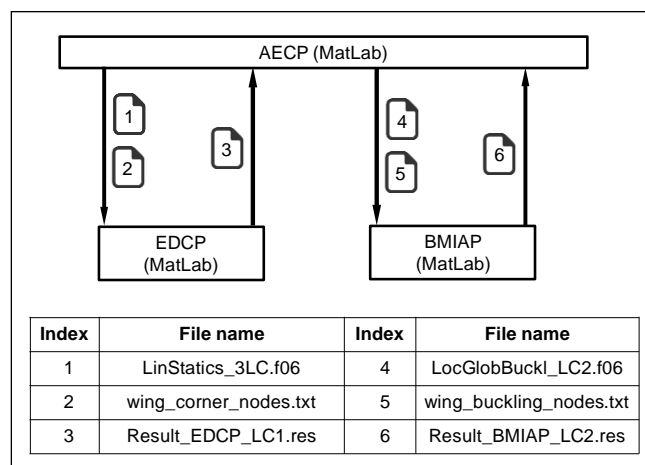


Fig. 5-3 Overview of AECP-module and function calls (adapted from [49])

5.1.2 Parametric Thickness Distribution Procedure (PTDP)

This module does not only control the FEA, but also creates parametric thickness distributions for all wing regions. Two *Bézier curves* (cf. Eq.(4.1)) can be multiplied with each other to generate a so-called *Bézier surface* [53], whose shape is also defined by a set of control points P_i . Fig. 5-4 explains this methodology for the upper cover of an arbitrary FE model. The advantage of such a surface is its FE independence, i.e. a constant number of control points is used to define the thicknesses of coarse-mesh or fine-mesh models. For this, merely the number of evaluations at different surface locations varies. Thus, a decoupling of the design model from the actual structural analysis model is also achieved.

For each of the six wing regions (upper skin, lower skin, front spar, rear spar, ribs, stringers) there are basically three parametric surfaces: one describes the element thicknesses of the 0° -layers, another describes the element thicknesses of the $\pm 45^\circ$ -layers and the third describes the element thicknesses of the 90° -layers. A typical Bézier surface configuration used in this thesis is portrayed in Appendix F.

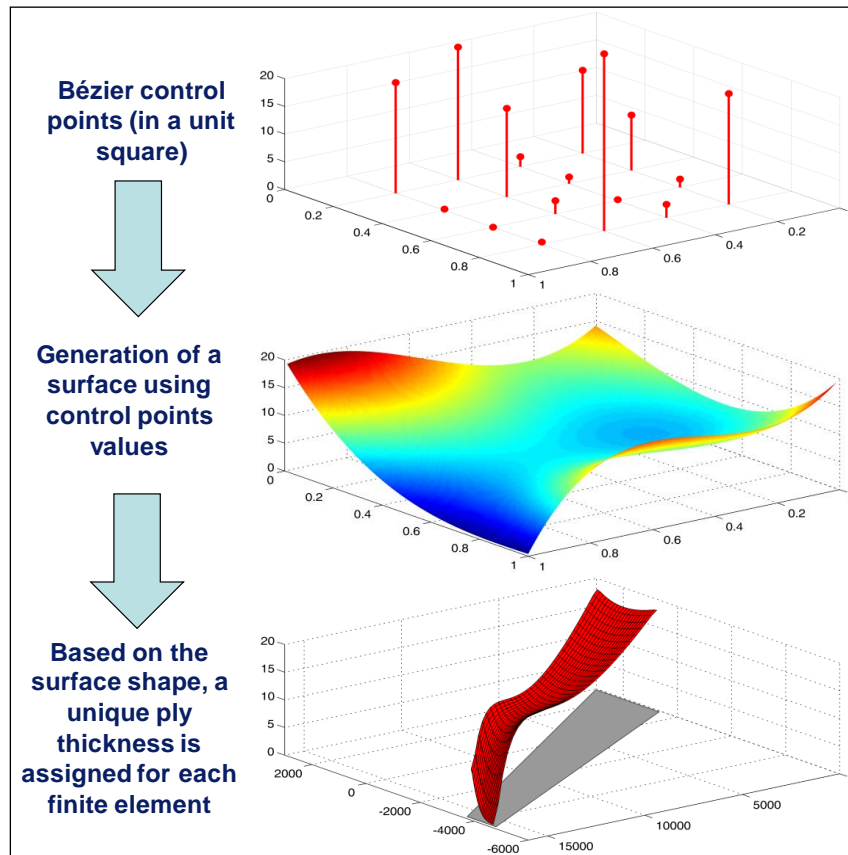


Fig. 5-4 Parametric thickness description for upper cover [50]

After the PMG-module has successfully run, PTDP builds the Bézier surfaces for all wing regions and modifies the file *dummy.bdf* by writing a separate and unique composite property card (PCOMP) for each finite element (cf. Fig. 5-5 and Fig. 5-6). Finally, two new MSC.Nastran input files are created by modifying the file header: *LinStat_3LC.bdf* is intended for a linear static analysis within SOL400, and *LocGlobBuckl_LC2.bdf* is intended for a linear buckling analysis within SOL105. After the FE analysis has been completed, the respective results files (*.f06) are sent back to PTDP.

The definition of the Bézier surfaces, i.e. composite design variables, also takes place in the input file *wing_info.txt* (cf. Appendix E, Detail 5).

```

$ Elements and Element Properties for region : Upper_Skin
$ Composite Property Record created from material record: Laminate_Upper_Skin
$ Composite Material Description :
PCOMP 1 0. SYM
      1 .25 0. YES 2 .31 45. YES
      1 .25 90. YES

$ Pset: "Upper_Skin" will be imported as: "pcomp.1"
CQUAD4 100 1 100 101 109 108 3
CQUAD4 101 1 101 102 110 109 3
CQUAD4 102 1 102 103 111 110 3

```

Fig. 5-5: Detail of *dummy.bdf* before parametric thickness description

```

$ Elements and Element Properties for region : Upper_Skin
$ Composite Property Record created from material record: Laminate_Upper_Skin
$ Composite Material Description :

PCOMP,1,0,,,,,SYM+
+,1,5.86362e+00,0.,YES+
+,2,3.00000e+00,45.,YES+
+,1,3.51200e+00,90.,YES+
CQUAD4 100 1 100 101 109 108 3

PCOMP,2,0,,,,,SYM+
+,1,5.75230e+00,0.,YES+
+,2,3.31000e+00,45.,YES+
+,1,3.42200e+00,90.,YES+
CQUAD4 101 2 101 102 110 109 3

PCOMP,3,0,,,,,SYM+
+,1,5.60769e+00,0.,YES+
+,2,3.45300e+00,45.,YES+
+,1,3.20121e+00,90.,YES+
CQUAD4 102 3 102 103 111 110 3

```

Fig. 5-6 Detail of *dummy.bdf* after parametric thickness description

5.1.3 Optimization platform Optimus

Fig. 5-7 shows the definition of the optimization process within the Optimus GUI. To the left are the parameters defined as optimization design variables; to the right are the design responses defined either as objective function or constraints. The user builds such a simulation workflow by simply dragging and dropping the different symbols and blocks into the GUI and linking them with arrows.

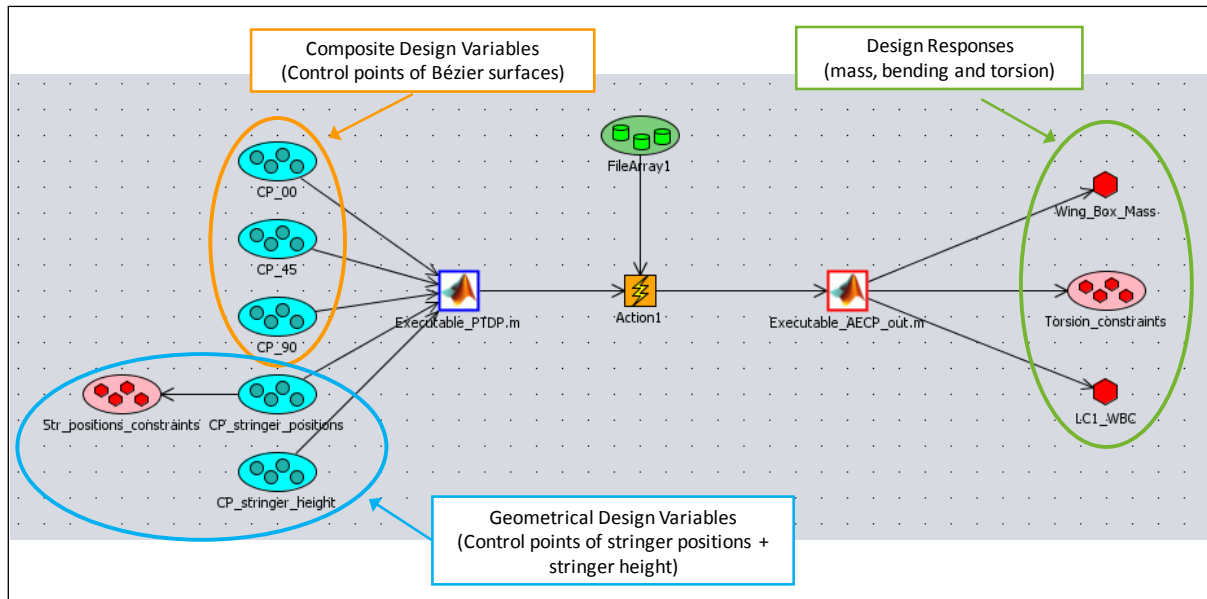


Fig. 5-7 Optimization problem definition within Optimus GUI

After setting up the simulation workflow (also called *Graph*), the optimization method among several local and global optimization algorithms must be chosen. Then, Optimus executes and coordinates the whole process automatically and in the end finds the most suitable optimum design. The optimal results can be found in the *.optimal file (cf. Fig. 5-8).

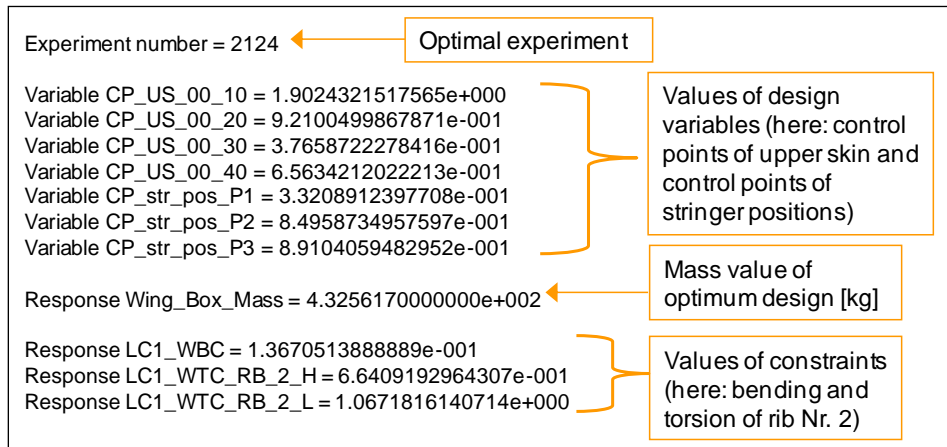


Fig. 5-8 Structure of a *.optimal file containing the optimal results

5.2 Optimization problem definition

In this section the implemented optimization design variables and design responses are presented. The nomenclature shown here corresponds to the actual nomenclature used within the optimization platform Optimus.

5.2.1 Design variables

5.2.1.1 Geometric design variables

From all the geometric design parameters incorporated in the PMG-module only the parameters directly concerning the stiffener properties are chosen as design variables (cf. Table 5-1):

Label	Description
CP_str_pos_Pi	Design variables for defining the stringer positions at support zone #1. These are the control points of the 4th order Bézier curve (cf. Fig. 4-6)
CP_str_pos_m_Pi	Design variables for defining the stringer positions at support zone #2. These are the control points of the 4th order Bézier curve.
CP_str_pos_t_Pi	Design variables for defining the stringer positions at support zone #3. These are the control points of the 4th order Bézier curve.
CP_str_hh_u_Pi	Design variables for defining the height of the upper cover stringers. These are two points that define a linear function between the wing root (P0) and wing tip (P1).
CP_str_hh_l_Pi	Design variables for defining the height of the lower cover stringers. These are two points that define a linear function between the wing root (P0) and wing tip (P1).

Table 5-1: Nomenclature (labels) of geometric design variables

5.2.1.2 Composite design variables

Table 5-2 shows the labeling system of the composite design variables, i.e. Bézier surface control points.

CP_XX_YY_ZZ	
CP	Control Point of Bézier surface.
XX	This is the wing region the control points belong to: US=Upper Skin; LS=Lower Skin; FS=Front Spar; RS=Rear Spar; RB=Ribs; SU=Upper cover stringers; SL= Lower cover stringers
YY	This denotes the layer orientation the Bézier surface is assigned to: YY=00 (0°-layers); YY=45 (±45-layers); YY=90 (90°-layers)
ZZ	Control point index, e.g.: ZZ=10 (control point Nr. 1); ZZ=40 (control point Nr. 4)
CP_RB_Cfg_X_YY_ZZ	
RB_Cfg_X	This kind of label appears only when all ribs are <u>not</u> defined by the same three Bézier surfaces, but certain ribs have their own surface distributions: Cfg=Configuration; X=1,2,...,N.
YY	See description of YY above.
ZZ	See description of ZZ above

Table 5-2 Nomenclature (labels) of composite design variables

5.2.2 Design responses

5.2.2.1 Mass

The optimization process has been especially developed for the use of the wing mass as the objective function to be minimized. The mass value is extracted from the MSC.Nastran results files (*.f06) and is labeled as “Wing_Box_Mass”. This output excludes the mass of the non-optimizable center wing box.

5.2.2.2 Elastic deformation (bending and torsion)

The wing bending is determined at the outermost rib (wing tip). The vertical displacements of the four extreme nodes of this rib (cf. Fig. 4-11) are used in Eq. (5.1):

$$w_{\text{tip}} = \frac{w_1 + w_2 + w_3 + w_4}{4} \quad (5.1)$$

The wing bending constraint is labeled as “LC1_WBC” and it has the form:

$$\text{LC1_WBC} = 1 - \frac{w_{\text{tip}}}{w_{\text{max}}} \quad (5.2)$$

In order to enable for a natural laminar flow (NLF), the wing bending is limited to a maximum value of $w_{\text{max}} = 600\text{mm}$ [50].

On the other hand, the torsion deformation in degrees [°] is determined at each wing rib using Eq. (5.3):

$$\alpha_{\text{Rib}} = \arctan\left(\frac{(w_1 + w_2)/2 + (w_3 + w_4)/2}{c_{\text{Rib}}}\right) \quad (5.3)$$

The wing torsion constraints are labeled as “LC1_WTC_RB_X_Y”, where X denotes the respective rib station ($X=1,2,\dots,N$) and Y is either H (upper boundary) or L (lower boundary). They have the form:

$$\text{LC1_WTC_RB_X_Y} = 1 - \frac{\alpha_{\text{Rib}}}{\alpha_{\text{Allow}}} \quad (5.4)$$

In order to enable for a natural laminar flow (NLF), the wing torsion is limited between the lower boundary $\alpha_{\text{Allow}} = -0.5^\circ$ and the upper boundary $\alpha_{\text{Allow}} = 0.1^\circ$ [50].

5.2.2.3 Buckling behavior

A FEM-based buckling criterion was developed in order to identify local and global buckling modes [54]. Local buckling is normally allowed at lower load levels than global buckling and hence a method for identifying the buckling modes of the forward swept wing model is necessary. The following definitions are used:

- A local buckling mode is characterized by ...
 - buckling of the skin between stringers of upper (or lower) cover
 - buckling of the stringer flanges
- A global buckling mode is characterized by ...
 - buckling of upper (or lower) cover with stringers
 - buckling of ribs
 - buckling of front or rear spar

In order to identify the wing region where buckling has occurred, the eigenvectors are analyzed. The procedure searches for the FE node with the maximum displacement value (“buckling peak”=|1.0|) and at the same time analyzes the displacement values of the so-called “buckling nodes” (cf. Fig. 4-12). Based on this information, the procedure is able to identify the buckling-endangered region and indicate if the eigenvector at hand is a local or global mode according to the above definitions.

After the identification process has been performed, the eigenvalues are aggregated by means of the Kreisselmeier-Steinhauser function [55]. Using Eq. (5.5) all eigenvalues that correspond to local buckling modes are aggregated into a single local value, as well as all “global modes” are aggregated into a single global value:

$$\lambda_{\text{aggr}} = \frac{1}{\rho_{\text{KS}}} \cdot \ln\left(\sum_i e^{\rho_{\text{KS}} \cdot (\lambda_i - \bar{x})}\right) \quad (5.5)$$

where \bar{x} is a user-defined factor that corresponds to the allowable buckling level, e.g.:

- local buckling is allowed at limit load (1·LL) $\rightarrow \bar{x}=1$
- global buckling is allowed at 1.2·LL $\rightarrow \bar{x}=1.2$.

The aggregation method is employed to reduce the number of design responses (i.e. eigenvalues) to only two meaningful values and thus relieve the optimization algorithm. Furthermore, buckling is a very unsteady phenomenon that involves eigenvalues shifting their positions within the examined spectrum or even disappearing. The aggregation is therefore used to smoothen out this problem in order to get more reliable gradient information [50].

The two aggregated values are directly used as constraints. The local buckling constraint is labeled as “LBC_LC2”, while the global buckling constraint is labeled as “GBC_LB2”:

$$\begin{aligned} \text{LBC_LC2} &= \lambda_{\text{aggr, local}} \\ \text{GBC_LB2} &= \lambda_{\text{aggr, global}} \end{aligned} \quad (5.6)$$

6 Preliminary structural assessment

6.1 Definition of parameter study

Upfront the optimizations, a preliminary structural assessment (parameter study) is performed in order to explore the design domain and identify relevant relationships and trends. This is very useful to better understand and interpret the optimization results afterwards.

In this case, the elastic deformations of the wing using four different stringer configurations are investigated. The used FE models are shown in Table 6-1 to Table 6-3. Configuration 1, i.e. model 1, is used as the reference case. The wing bending and torsion of each model are calculated using Eq. (5.1) and Eq. (5.3). The wing-box longitudinal axis is defined as the line that lies at the average value between the front and rear spar positions (in this case: 36.5%). Further properties about the models are described in Appendix D.

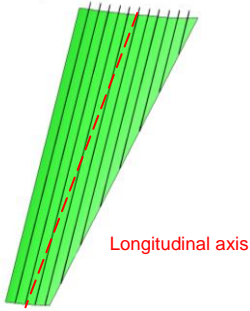
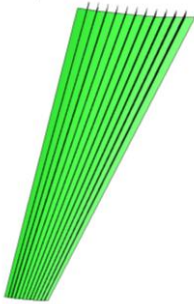
Model index / stringer configuration	Model picture	Properties	
1		Stringers	Straight stiffeners parallel to front spar
		CP_str_pos_Pi	[0 0.25 0.50 0.75 1.0]
2		Stringers	Straight stiffeners without run-outs
		CP_str_pos_Pi	[0 0.25 0.50 0.75 1.0]

Table 6-1 Basic wing model configurations


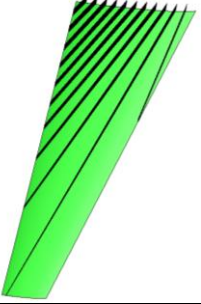
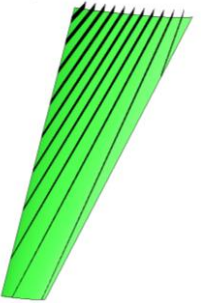
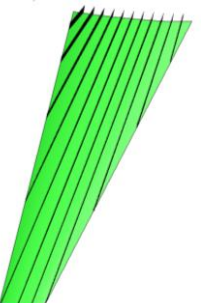
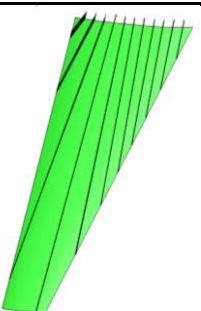
Model index / stringer configuration	Model picture	Properties	
3-A		Stringers	Straight divergent stiffeners
		CP_str_pos_Pi	[0 0.25 0.50 0.75 1.0]
		CP_str_pos_t_Pi	[0 0.1 0.1 0.1 1.0]
3-B		Stringers	Straight divergent stiffeners
		CP_str_pos_Pi	[0 0.25 0.50 0.75 1.0]
		CP_str_pos_t_Pi	[0 0.3 0.3 0.3 1.0]
3-C		Stringers	Straight divergent stiffeners
		CP_str_pos_Pi	[0 0.25 0.50 0.75 1.0]
		CP_str_pos_t_Pi	[0 0.5 0.5 0.5 1.0]
3-D		Stringers	Straight divergent stiffeners
		CP_str_pos_Pi	[0 0.25 0.50 0.75 1.0]
		CP_str_pos_t_Pi	[0 0.7 0.7 0.7 1.0]
3-E		Stringers	Straight divergent stiffeners
		CP_str_pos_Pi	[0 0.25 0.50 0.75 1.0]
		CP_str_pos_t_Pi	[0 0.9 0.9 0.9 1.0]

Table 6-2 Wing models with straight divergent stiffeners






Model index / stringer configuration	Model picture	Properties	
4-A		Stringers	Curvilinear stiffeners
		CP_str_pos_Pi	[0 0.25 0.50 0.75 1.0]
		CP_str_pos_m_Pi	[0 0.1 0.1 0.1 1.0]
		CP_str_pos_t_Pi	[0 0.1 0.1 0.1 1.0]
4-B		Stringers	Curvilinear stiffeners
		CP_str_pos_Pi	[0 0.25 0.50 0.75 1.0]
		CP_str_pos_m_Pi	[0 0.3 0.3 0.3 1.0]
		CP_str_pos_t_Pi	[0 0.1 0.1 0.1 1.0]
4-C		Stringers	Curvilinear stiffeners
		CP_str_pos_Pi	[0 0.25 0.50 0.75 1.0]
		CP_str_pos_m_Pi	[0 0.5 0.5 0.5 1.0]
		CP_str_pos_t_Pi	[0 0.1 0.1 0.1 1.0]
4-D		Stringers	Curvilinear stiffeners
		CP_str_pos_Pi	[0 0.25 0.50 0.75 1.0]
		CP_str_pos_m_Pi	[0 0.7 0.7 0.7 1.0]
		CP_str_pos_t_Pi	[0 0.1 0.1 0.1 1.0]
4-E		Stringers	Curvilinear stiffeners
		CP_str_pos_Pi	[0 0.25 0.50 0.75 1.0]
		CP_str_pos_m_Pi	[0 0.9 0.9 0.9 1.0]
		CP_str_pos_t_Pi	[0 0.1 0.1 0.1 1.0]

Table 6-3 Wing models with curvilinear stiffeners

6.2 Results of parameter study

The bending results in Fig. 6-1 are normalized using configuration 1 as a reference ($w=1200\text{mm}$). It can be seen that the orientation of the straight divergent stringers has an influence on the wing bending: the more they are turned forward, the less the wing longitudinal stiffness and the higher the bending value. Thus, model 3-A bends 14% more than configuration 1 while model 3-D bends only 4% more. However configuration 2, in which all stringers run out at the wing tip, has the lowest bending value.

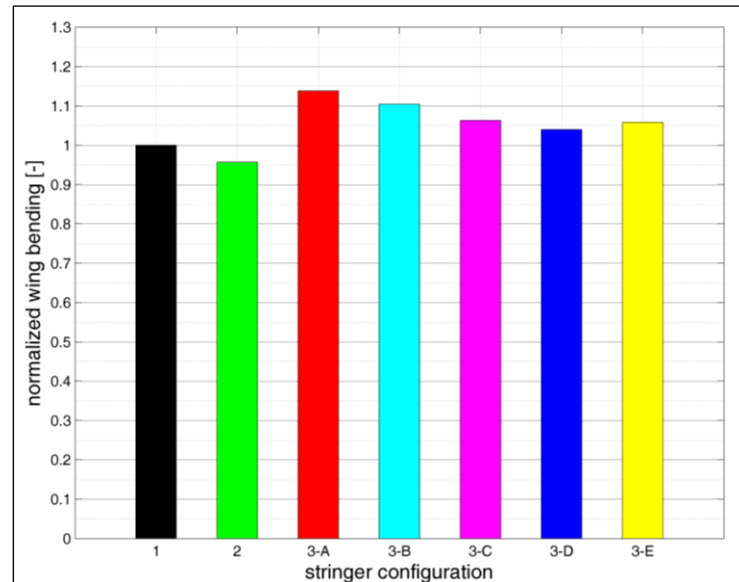


Fig. 6-1 Wing bending results of configuration 3.

In Fig. 6-2 the torsion values are normalized also using configuration 1 as reference. It can be seen that turning the stringers forward leads to an increase in the torsion stiffness. Now model 3-A has the best values, i.e. lowest torsion angle (40% reduction at wing tip). The highest torsion is measured with model 3-E, in which the stringers are slightly turned backwards. Despite similar bending, there is a large torsion difference between configurations 1 and 2.

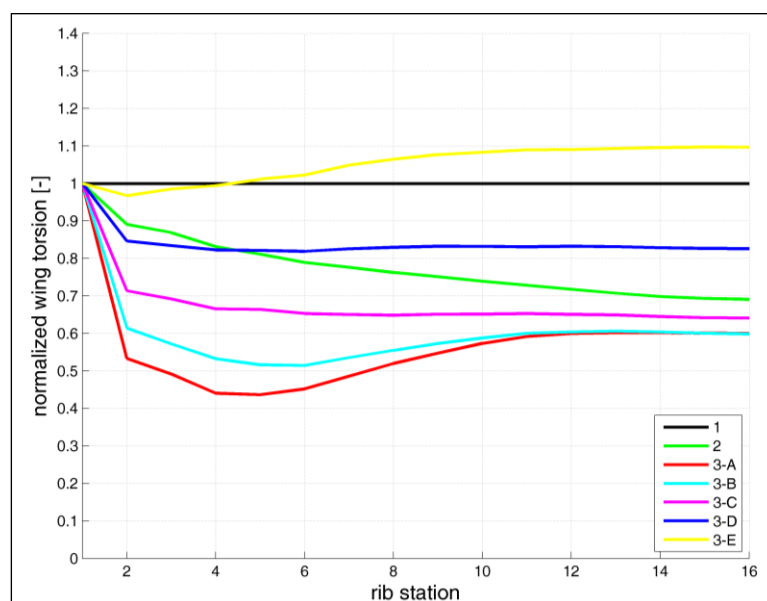


Fig. 6-2 Wing torsion results of configuration 3

Fig. 6-3 shows that configuration 4 with highly curved stiffeners contributes to control the wing bending. For example model 4-E achieves a bending value in the range of the reference case configuration 1. Nevertheless, configuration 2 exhibits a slightly lower bending value.

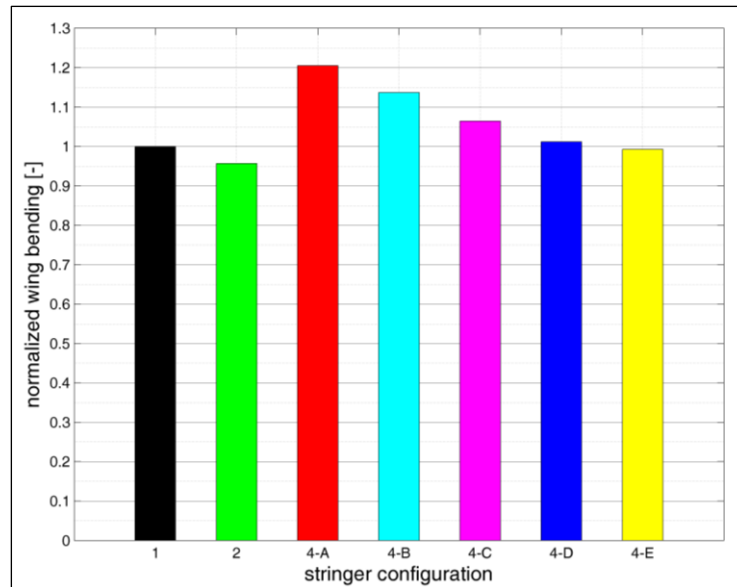


Fig. 6-3 Wing bending results of configuration 4

The curvilinear stiffeners also lead to an increase of the torsion stiffness so that the measured torsion angles are in general lower than those of configurations 1 and 2 (cf. Fig. 6-4) and of configuration 3 (cf. Fig. 6-2). Model 4-C shows a torsion reduction of approximately 50% at the wing tip in comparison to the reference case.

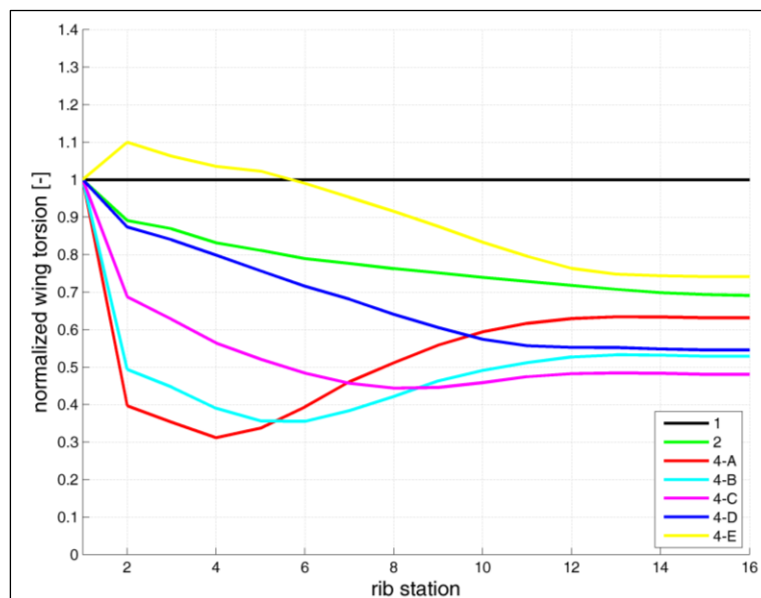


Fig. 6-4 Wing torsion results of configuration 4

When comparing all results, it seems that curvilinear stiffeners are best suited for reducing the wing torsion angle while at the same time achieving a low mass value (cf. Table 6-4). Configuration 2 is best suited for reducing the wing bending but it shows the highest mass

value. Configuration 3 is able to reduce the torsion and achieve low mass values but this increases the wing bending enormously (model 3-A). Compared to the other stringer configurations, configuration 1 shows very high torsion angles.

Model index	Torsion at wing tip [°]	Δ_{Torsion} [%]	Bending [mm]	Δ_{Bending} [%]	Wing mass [kg]	Δ_{Mass} [%]
1	1.2322	--	1240.16	--	771.28	--
2	0.8511	-30.93	1186.80	-4.303	846.97	+9.814
3-A	0.7398	-39.96	1411.65	+13.83	680.36	-11.78
3-D	1.0178	-17.40	1290.06	+4.024	739.01	-4.184
4-C	0.5920	-51.96	1320.20	+6,450	716.37	-7.119
4-D	0.6723	-45.44	1254.83	+1.183	750.65	-2.675

Table 6-4 Comparison of results of different models

Based on the parameter study results it may be concluded that:

- the configuration and orientation of the stringers have a significant influence on the wing elastic deformations. They offer the possibility of embodying directional stiffness within the wing-structure and therefore may be used for aeroelastic tailoring.
- the wing torsion deformation can be reduced when the stringers are turned or curved forward w.r.t. the wing-box longitudinal axis. This is equivalent to the investigations performed by *Weisshaar* [21] in which the directional stiffness of the cover laminates is turned forward in order to increase the divergent speed.
- turning the stringers forward increases the torsion stiffness but at the same time reduces the bending stiffness. There exists a bending-torsion coupling and the best trade-off must be found according to the wing requirements.
- curvilinear stiffeners have the potential of significantly reducing the torsion without compromising the bending stiffness or the mass (model 4-D). On the other hand, stringers parallel to front spar or turned slightly backwards are not useful for reducing the torsion at all.
- the stringer configuration used so far within ForSwing (configuration 2) shows in general good bending and torsion values in comparison to the other configurations but the highest mass.
- the torsion reduction achieved by the stringers is not equal in span-wise direction: the reducing effect seems to be more distinctive for the region near the wing root.

7 Structural optimizations

7.1 Definition of optimization models and overall settings

Table 7-1 shows the fundamental properties of the used forward swept wing model that derives from the ForSwing data set. Based on this model, three different optimization types are performed:

- Optimizations A: consideration of wing mass, bending and torsion (*A-models*)
- Optimizations B: same as A with modified design variable definitions (*B-models*)
- Optimizations C: consideration of wing mass and buckling (*C-models*)

Property	Description
General geometrical properties	Refer to Ch. 3.1
Number of ribs	16 (including root rib)
Number of stringers	22 (11 per wing cover)
Laminate definition <i>Upper Skin</i>	$[0^\circ \pm 45^\circ 90^\circ]_S$
Laminate definition <i>Lower Skin</i>	$[0^\circ \pm 45^\circ 90^\circ]_S$
Laminate definition <i>Front Spar</i>	$[0^\circ \pm 45^\circ 90^\circ]_S$
Laminate definition <i>Rear Spar</i>	$[0^\circ \pm 45^\circ 90^\circ]_S$
Laminate definition <i>Ribs</i>	$[0^\circ \pm 45^\circ 90^\circ]_S$
Laminate definition <i>Stringers</i>	$[0^\circ \pm 45^\circ 90^\circ]_S$
Material properties	Refer to Appendix C
Load cases	LC1 <i>Cruise</i> ($n_z=LL=1.0$) LC2 <i>Gust</i> ($n_z=LL=3.44$)

Table 7-1 Fundamental properties of structural model

The names of the optimization models are defined in such a way that they point out the used stringer configuration and also the used constraint levels. The following applies for all *A-models* and *B-models*:

$$\text{Model name} = \mathbf{X_WBCY_WTCZ}$$

where

- X is the stringer configuration: $\mathbf{X} = 1, 2, 3, 4$ (cf. Fig. 4-7)
- Y is the maximum wing bending in [mm]: $\mathbf{Y} = 600$ (Default), 1200, 1800
- Z is the allowable wing torsion in [°]: $\mathbf{Z} = 05_01$ for $-0.5^\circ \leq \alpha_{\text{Allow}} \leq 0.1^\circ$ (Default);
 $\mathbf{Z} = 005_001$ for $-0.05^\circ \leq \alpha_{\text{Allow}} \leq 0.01^\circ$ or $\mathbf{Z} = _01$ for $\alpha_{\text{Allow}} \leq 0.1^\circ$

On the other hand, the following applies for all *C-models*:

$$\text{Model name} = \mathbf{X_LBCY_GBCZ}$$

where

- X is the stringer configuration: $\mathbf{X} = 1, 2, 3, 4$ (cf. Fig. 4-7)
- Y is the local buckling level as a function of Limit Load: $\mathbf{Y} = 10$ for $\lambda = 1 \cdot LL$ (Default)
- Z is the global buckling level as a function of Limit Load: $\mathbf{Z} = 12$ for $\lambda = 1.2 \cdot LL$ (Default)

The robust gradient-based optimization algorithm NLPQL [56] is chosen for the structural optimization of all models (tolerance convergence value of 10^{-4}).

7.1.1 Optimizations A (elastic deformations)

For the *A-models* the following relevant options are chosen in the input file *wing_info.txt*.

- **GeomSwitch = 1**
 - Geometrical design variables are enabled. Model geometry will be updated each optimization loop.
- **RibSwitch = 3**
 - All ribs do not share the same Bézier surfaces. The first four ribs (1-4) share the same thickness distributions; the rest of the ribs (5-16) share the same thickness distributions.
- **StrSwitch = 3**
 - All stiffeners of the upper cover share the same thickness distributions; all stiffeners of the lower cover share the same thickness distributions.

Table 7-2 describes the configuration of the composite design variables of all *A-models*. Moreover, Table 7-3 shows the geometrical design variables used for each model.

Wing region	Configuration of Bézier surfaces	Total number of DVs (control points)	Initial value of all control points	Limits
Upper Skin	4x1 control point vector for each of the three ply orientations	12	3	[0.05, 10]
Lower Skin	4x1 control point vector for each of the three ply orientations	12	3	[0.05, 10]
Front Spar	3x1 control point vector for each of the three ply orientations	9	3	[0.05, 10]
Rear Spar	3x1 control point vector for each of the three ply orientations	9	3	[0.05, 10]
Ribs	Ribs 1-4: 2x1 control point vector for each of the three ply orientations	6	3	[0.05, 10]
	Ribs 5-16: 2x1 control point vector for each of the three ply orientations	6	3	[0.05, 10]
Stringers	Upper cover stringers: 2x1 control point vector for each of the three ply orientations	6	3	[0.05, 10]
	Lower cover stringers: 2x1 control point vector for each of the three ply orientations	6	3	[0.05, 10]

Table 7-2 Composite design variables of *A-models*

Model name	Number of geometrical DVs	Initial values	Limits
1_WBC600_WTC05_01 1_WBC1200_WTC05_01 1_WBC1800_WTC05_01 1_WBC1200_WTC_01	7	CP_str_pos_Pi: [0 0.25 0.50 0.75 1.0]	[0.1, 0.9]
		CP_str_hh_u_P0: 150mm	[50, 175]
		CP_str_hh_u_P1: 35mm	[15, 50]
2_WBC600_WTC05_01 2_WBC1200_WTC05_01 2_WBC1800_WTC05_01 2_WBC1200_WTC_01	7	CP_str_pos_Pi: [0 0.25 0.50 0.75 1.0]	[0.1, 0.9]
		CP_str_hh_u_P0: 150mm	[50, 175]
		CP_str_hh_u_P1: 35mm	[15, 50]
3_WBC600_WTC05_01	10	CP_str_pos_Pi: [0 0.25 0.50 0.75 1.0]	[0.1, 0.9]
		CP_str_pos_t_Pi: [0 0.25 0.50 0.75 1.0]	[0.1, 0.9]
		CP_str_hh_u_P0: 150mm	[50, 175]
		CP_str_hh_u_P1: 35mm	[15, 50]
4_WBC600_WTC05_01 4_WBC1200_WTC05_01 4_WBC1800_WTC05_01 4_WBC1200_WTC_01	10	CP_str_pos_Pi: [0 0.25 0.50 0.75 1.0]	[0.1, 0.9]
		CP_str_pos_m_Pi: [0 0.45 0.60 0.85 1.0] = const	[0.4, 0.85]
		CP_str_pos_t_Pi: [0 0.10 0.10 0.10 1.0]	[0.1, 0.5]
		CP_str_hh_u_P0: 150mm	[50, 175]
		CP_str_hh_u_P1: 35mm	[15, 50]

Table 7-3 Geometrical design variables of *A-models*

7.1.2 Optimizations B (elastic deformations, limited wing cover thicknesses)

For the *B-models* the number of design variables is reduced in order to cut down the optimization time and resources. The following relevant options are chosen in the input file *wing_info.txt*:

- **GeomSwitch = 1**
 - Geometrical design variables are enabled. Model geometry will be updated with each optimization loop.
- **RibSwitch = 2**
 - All ribs share the same Bézier surfaces.
- **StrSwitch = 3**
 - All stiffeners of the upper cover share the same thickness distributions; all stiffeners of the lower cover share the same thickness distributions.

Table 7-4 shows the configuration of the composite design variables for all *B-models*. Here the initial values and upper limit of the ply thicknesses in both wing covers is reduced. The objective is to investigate how the wing behaves now that its biggest structural components are limited in their dimensions. Moreover, Table 7-5 describes the geometrical design variables used in each model.

Wing region	Configuration of Bézier surfaces	Total number of DVs (control points)	Initial values	Limits
Upper Skin	3x1 control point vector for each of the three ply orientations	9	0° → 2	[0.05, 2]
			±45° → 1	[0.05, 1]
			90° → 1	[0.05, 1]
Lower Skin	3x1 control point vector for each of the three ply orientations	9	0° → 2	[0.05, 2]
			±45° → 1	[0.05, 1]
			90° → 1	[0.05, 1]
Front Spar	2x1 control point vector for each of the three ply orientations	6	3	[0.05, 10]
Rear Spar	2x1 control point vector for each of the three ply orientations	6	3	[0.05, 10]
Ribs	All Ribs (1-16): 2x1 control point vector for each of the three ply orientations	6	3	[0.05, 10]
Stringers	Upper cover stringers: 2x1 control point vector for each of the three ply orientations	6	3	[0.05, 10]
	Lower cover stringers: 2x1 control point vector for each of the three ply orientations	6	3	[0.05, 10]

Table 7-4 Composite design variables of *B-models*

Model name	Number of geometrical DVs	Initial values	Limits
1_WBC600_WTC005_001	7	CP_str_pos_Pi: [0 0.25 0.50 0.75 1.0]	[0.1, 0.9]
		CP_str_hh_u_P0: 150mm	[50, 175]
		CP_str_hh_u_P1: 35mm	[15, 50]
2_WBC600_WTC005_001	7	CP_str_pos_Pi: [0 0.25 0.50 0.75 1.0]	[0.1, 0.9]
		CP_str_hh_u_P0: 150mm	[50, 175]
		CP_str_hh_u_P1: 35mm	[15, 50]
3_WBC600_WTC005_001	10	CP_str_pos_Pi: [0 0.25 0.50 0.75 1.0]	[0.1, 0.9]
		CP_str_pos_t_Pi: [0 0.30 0.30 0.30 1.0]	[0.1, 0.9]
		CP_str_hh_u_P0: 150mm	[50, 175]
		CP_str_hh_u_P1: 35mm	[15, 50]
4_WBC600_WTC005_001	10	CP_str_pos_Pi: [0 0.25 0.50 0.75 1.0]	[0.1, 0.9]
		CP_str_pos_m_Pi: [0 0.45 0.60 0.80 1.0] = const	[0.4, 0.85]
		CP_str_pos_t_Pi: [0 0.30 0.30 0.30 1.0]	[0.1, 0.5]
		CP_str_hh_u_P0: 150mm	[50, 175]
		CP_str_hh_u_P1: 35mm	[15, 50]

Table 7-5 Geometrical design variables of *B-models*

7.1.3 Optimizations C (buckling behavior)

For all *C-models*, the following relevant options are chosen in the input file *wing_info.txt*:

- **GeomSwitch = 1**
 - Geometrical design variables are enabled. Model geometry is updated with each optimization loop.
- **RibSwitch = 2**
 - All ribs share the same Bézier surfaces.
- **StrSwitch = 3**
 - All stiffeners of the upper cover share the same thickness distributions; all stiffeners of the lower cover share the same thickness distributions.

The number of stringers of the *C-models* is reduced to 6 stringers per wing cover. In addition to this, the mesh is refined so that there are at least 5 FE nodes between adjacent stiffeners. This is a recommendation of MSC.Nastran [42], so that local buckling modes can be properly represented.

Table 7-6 shows the configuration of the composite design variables for all *C-models*. Moreover, Table 7-7 describes the geometrical design variables used in each model.

Wing region	Configuration of Bézier surfaces	Total number of DVs (control points)	Initial values	Limits
Upper Skin	3x1 control point vector for each of the three ply orientations	9	3	[0.05, 10]
Lower Skin	3x1 control point vector for each of the three ply orientations	9	3	[0.05, 10]
Front Spar	2x1 control point vector for each of the three ply orientations	6	3	[0.05, 10]
Rear Spar	2x1 control point vector for each of the three ply orientations	6	3	[0.05, 10]
Ribs	All Ribs (1-16): 2x1 control point vector for each of the three ply orientations	6	3	[0.05, 10]
Stringers	Upper cover stringers: 2x1 control point vector for each of the three ply orientations	6	3	[0.05, 10]
	Lower cover stringers: 2x1 control point vector for each of the three ply orientations	6	3	[0.05, 10]

Table 7-6 Composite design variables of *C-models*

Model name	Number of geometrical DVs	Initial values	Limits
1_LBC10_GBC12	7	CP_str_pos_Pi: [0 0.25 0.50 0.75 1.0]	[0.15, 0.85]
		CP_str_hh_u_P0: 150mm	[50, 175]
		CP_str_hh_u_P1: 35mm	[15, 50]
2_LBC10_GBC12	7	CP_str_pos_Pi: [0 0.25 0.50 0.75 1.0]	[0.15, 0.85]
		CP_str_hh_u_P0: 150mm	[50, 175]
		CP_str_hh_u_P1: 35mm	[15, 50]
4_LBC10_GBC12	10	CP_str_pos_Pi: [0 0.25 0.50 0.75 1.0]	[0.15, 0.85]
		CP_str_pos_m_Pi: [0 0.45 0.60 0.85 1.0] = const	[0.4, 0.85]
		CP_str_pos_t_Pi: [0 0.10 0.10 0.10 1.0]	[0.1, 0.5]
		CP_str_hh_u_P0: 150mm	[50, 175]
		CP_str_hh_u_P1: 35mm	[15, 50]

Table 7-7 Geometrical design variables of *C-models*

7.2 Optimization results

7.2.1 Optimizations A

As can be seen in Fig. 7-1, all wing models converge after approximately 50 iterations on the same mass value. Regardless the stringer configuration, all models are able to fulfill the elastic deformation requirements and the optimal forward swept wing mass becomes approximately $m=619\text{kg}$.

The aeroelastic tailoring capability of the stiffeners (cf. parameter study results in Ch. 6.2) disappears for the optimum design. During the optimization, the height and thickness of the stiffeners are reduced to the minimum values, so that they become negligible in comparison to other structural components. Fig. 7-2 shows for the model *4_WBC600_WTC05_01* the reduction of the percentage mass share of the stringers to a minimum, while the mass of both wing covers makes up more than 90% of the total amount in the optimum design.

In fulfilling the deformation requirements it seems that the most weight-efficient approach is investing in the cross-sectional stiffness, i.e. wing covers. Fig. 7-3 shows for the same model

the optimal thickness distributions. It can be seen that only the thickness of the 0° -layers of the wing covers near the wing root has largely increased. The resulting elastic deformations are depicted in Fig. 7-4. Practically the same behavior and results are observed for the rest of the models.

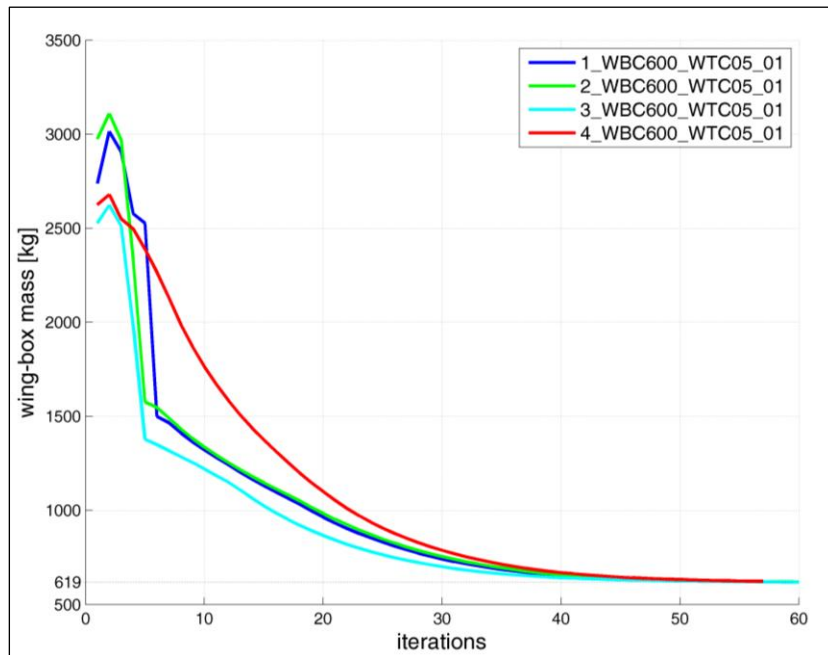


Fig. 7-1 Comparison of optimal mass of *A-models*

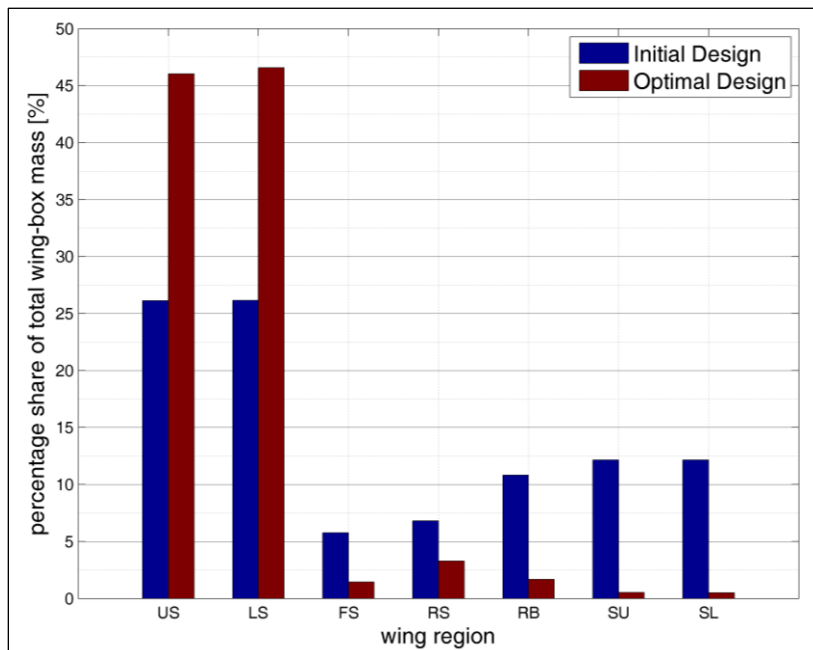


Fig. 7-2 Mass breakdown of model *4_WBC600_WTC05_01*
 US: Upper Skin, LS: Lower Skin, FS: Front Spar, RS: Rear Spar,
 RB: Ribs, SU: Stringers of upper cover, SL: Stringers of lower cover

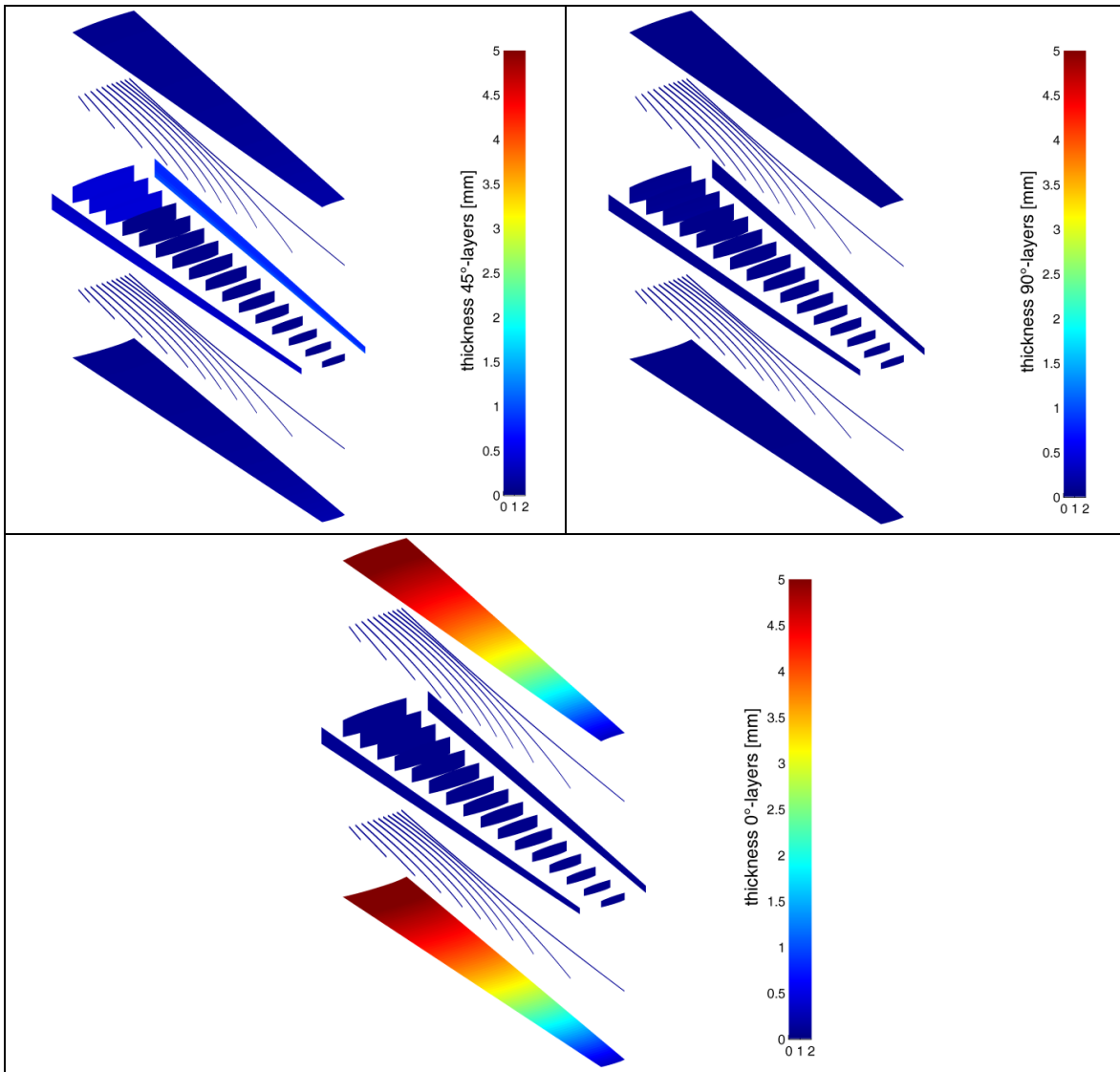


Fig. 7-3 Optimal thickness values of model 4_WBC600_WTC05_01

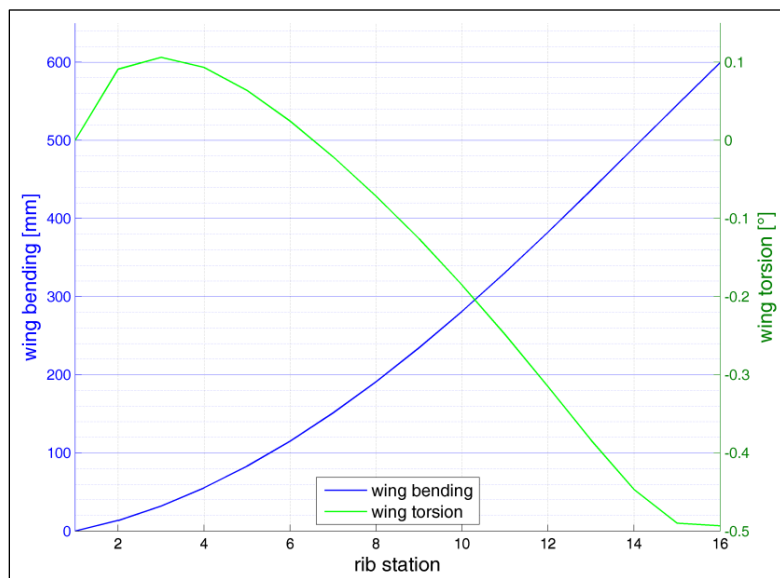
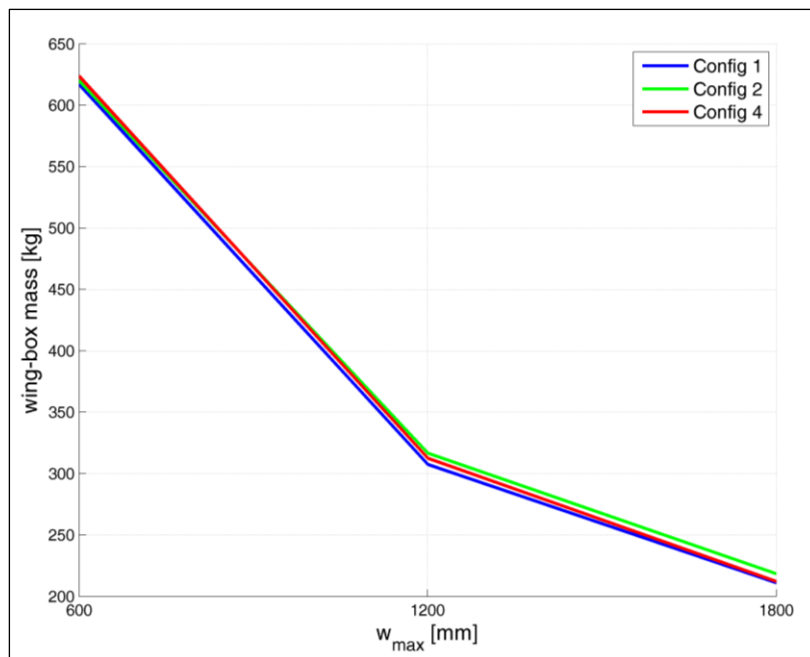


Fig. 7-4 Elastic deformations of optimum design

Geometrical DV	Initial value	Optimal value		
		4_WBC600_ WTC05_01	4_WBC1200_ WTC05_01	4_WBC1800_ WTC05_01
CP_str_pos_P1	0.250	0.289	0.386	0.466
CP_str_pos_P2	0.500	0.629	0.797	0.637
CP_str_pos_P3	0.750	0.746	0.872	0.823
CP_str_pos_t_P1	0.100	0.136	0.132	0.100
CP_str_pos_t_P2	0.100	0.137	0.103	0.103
CP_str_pos_t_P3	0.100	0.147	0.105	0.105
CP_str_hh_u_P0 [mm]	150.0	50.98	51.31	50.49
CP_str_hh_u_P1 [mm]	35.0	30.28	30.92	30.78
CP_str_hh_l_P0 [mm]	150.0	50.94	54.14	50.53
CP_str_hh_l_P1 [mm]	35.0	30.05	30.76	30.66

Table 7-8 Values of geometrical DVs of *A-models* using configuration 4

Using the configurations 1, 2 and 4 the functional relationship between the optimal mass and the allowable bending value is investigated. Fig. 7-5 shows that the different stiffeners configurations still calculate practically the same optimal mass results: doubling w_{\max} leads to a 50% reduction of the optimal mass; a triplication of w_{\max} leads to a 65% reduction of the optimal mass.

Fig. 7-5 Optimal mass as a function of allowable bending value w_{\max}

The results of configuration 4 (curvilinear stiffeners) are described here exemplarily: Table 7-8 shows that increasing the allowable wing bending leads in general to the stringers moving towards the rear spar near the wing root. Nevertheless, the stringer height for $w_{\max}=1200\text{mm}$ and $w_{\max}=1800\text{mm}$ is reduced to the same small values as for $w_{\max}=600\text{mm}$. In addition to this, the stringer thickness is again reduced to minimum values so that the stringers become negligible compared to other structural components. Fig. 7-6 shows that the thicknesses of the 0° -layers in the covers are increased the most, giving the wing the required stiffness. The thickness of the 45° - and 90° -layers are almost zero and therefore not shown here.

Based on the results, it can be stated that the bending constraint level does not have any influence on the performance of the stiffeners configurations. Curvilinear stiffeners do not show any advantageous properties.

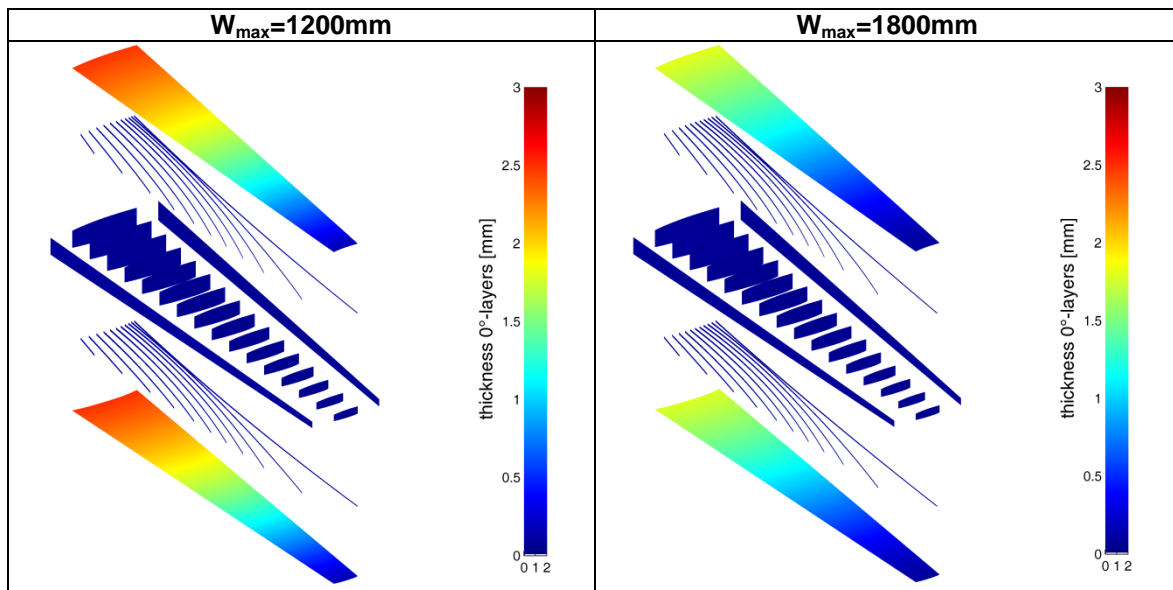


Fig. 7-6 Optimal thickness distribution of 0°-layers using curvilinear stiffeners

In order to investigate the influence of the torsion constraint, this is modified so that only the upper boundary ($\alpha_{\text{Allow}} \leq 0.1^\circ$) must be fulfilled. Probably having such a tight allowable torsion range near zero degrees does not allow the stiffeners to properly display their torsion-reducing effect during the optimization. The higher boundary remains untouched because it is imperative for a forward swept wing that the positive torsion is constrained. Therefore, the lower boundary of -0.5° is not considered.

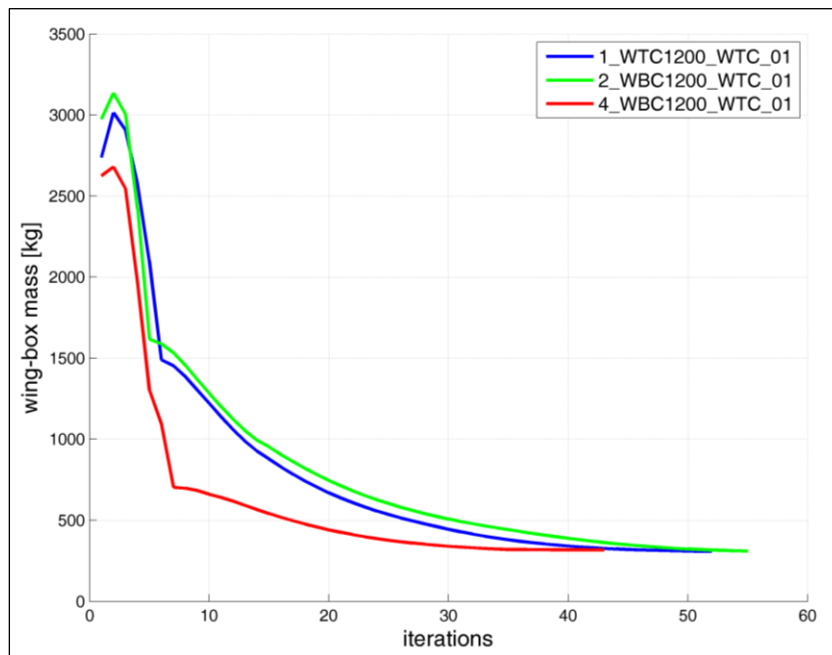


Fig. 7-7 Comparison of optimal mass values using only the upper torsion limit

As can be seen in Fig. 7-7, the modified torsion constraint does not have any influence on the optimal mass either. Despite the fact that the models exhibit now a different torsion angle distribution in span-wise direction (curvilinear stiffeners achieve the lowest torsion angle, cf. Fig. 7-8), the optimizations converge practically towards the same mass result ($m \approx 310\text{kg}$). In this case, the thickness of the wing covers is again the decisive stiffness property.

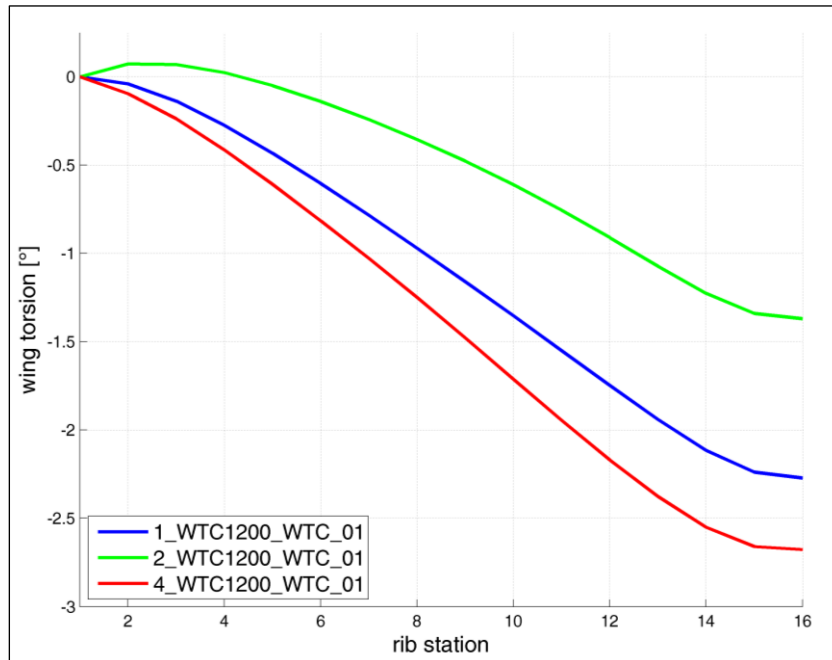


Fig. 7-8 Torsion angle of optimal designs using only the upper torsion limit

7.2.2 Optimizations B

For all *B-models* the stiffness influence of the wing covers is reduced on purpose by limiting the allowable ply thicknesses to small values. Now, in order to fulfill the deformation requirements, the optimization algorithm increases the dimensions of other structural components, especially stringers and spars. In doing so, different optimum designs are found according to the selected stiffener configuration (cf. Fig. 7-9). Straight divergent stringers (configuration 3) achieve the lowest optimal mass while configuration 2 (continuous stringers from wing root till wing tip) exhibits the highest optimal mass.

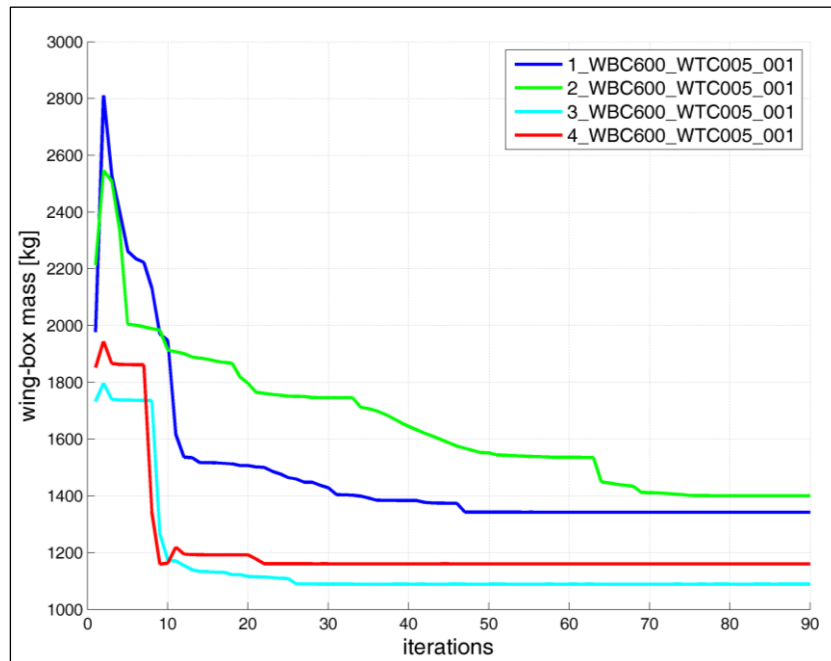


Fig. 7-9 Comparison of optimal mass of *B-models*

In configuration 2 the thickness of the front spar is largely increased and makes up more than 20% of the total optimal mass (cf. Fig. 7-10 and Fig. 7-11). This means that configuration 2 relies on the stiffness of the front spar for fulfilling the deformation requirements. It can be seen that the 0° -layers of the stringers near the wing root are also increased as well as the 0° -layers of the rear spar.

Regarding the geometrical DVs Table 7-9 shows that the stringer height is again reduced to a minimum. Furthermore, the stringers are moved a bit towards the front spar.

Geometrical DV	Initial value	Optimal value
CP_str_pos_P1	0.250	0.145
CP_str_pos_P2	0.500	0.456
CP_str_pos_P3	0.750	0.737
CP_str_hh_u_P0 [mm]	150.0	50.09
CP_str_hh_u_P1 [mm]	35.0	15.79
CP_str_hh_l_P0 [mm]	150.0	54.75
CP_str_hh_l_P1 [mm]	35.0	15.0

Table 7-9 Values of geometrical DVs of model *2_WBC600_WTC005_001*

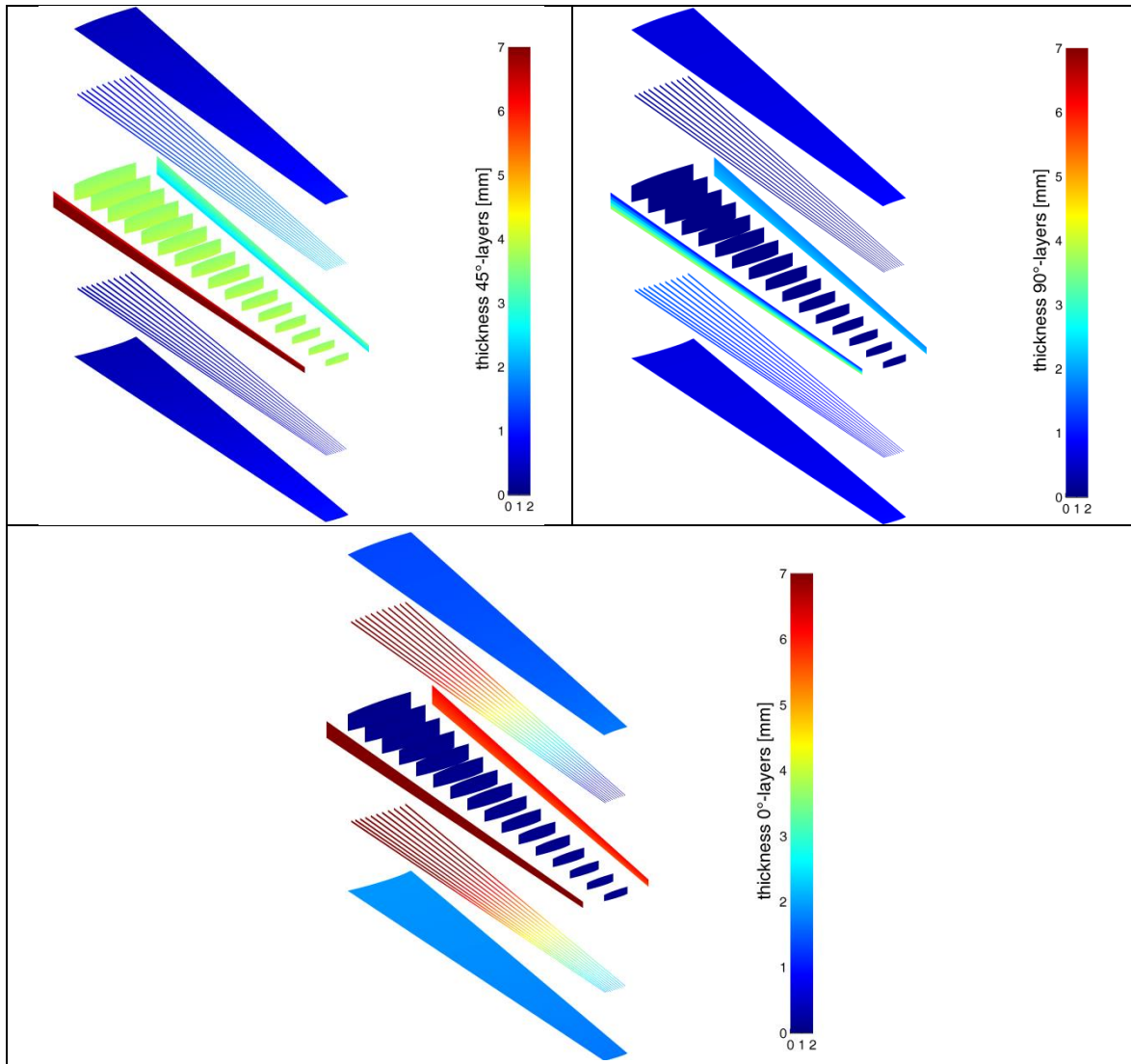


Fig. 7-10 Optimal thickness values of model 2_WBC600_WTC005_001

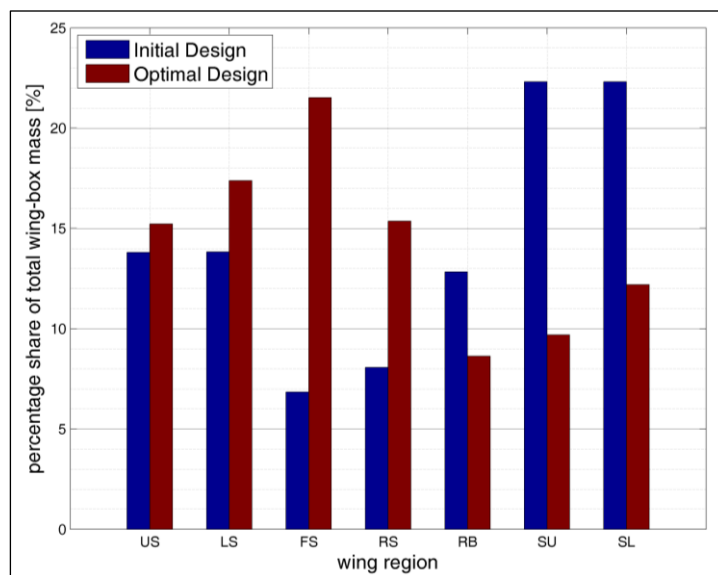


Fig. 7-11 Mass breakdown of model 2_WBC600_WTC005_001

On the other hand, the straight divergent stringers (configuration 3) prove to be very useful for the wing: near the root the stringers are moved towards the front spar, near the tip the stringers are spread, and their height is not reduced to the lower limits (cf. Table 7-10). Now the 0°-layer thickness of the stringers is increased the most (cf. Fig. 7-12) and the spars, as opposite to configuration 2, do not play a key role for the wing stiffness anymore.

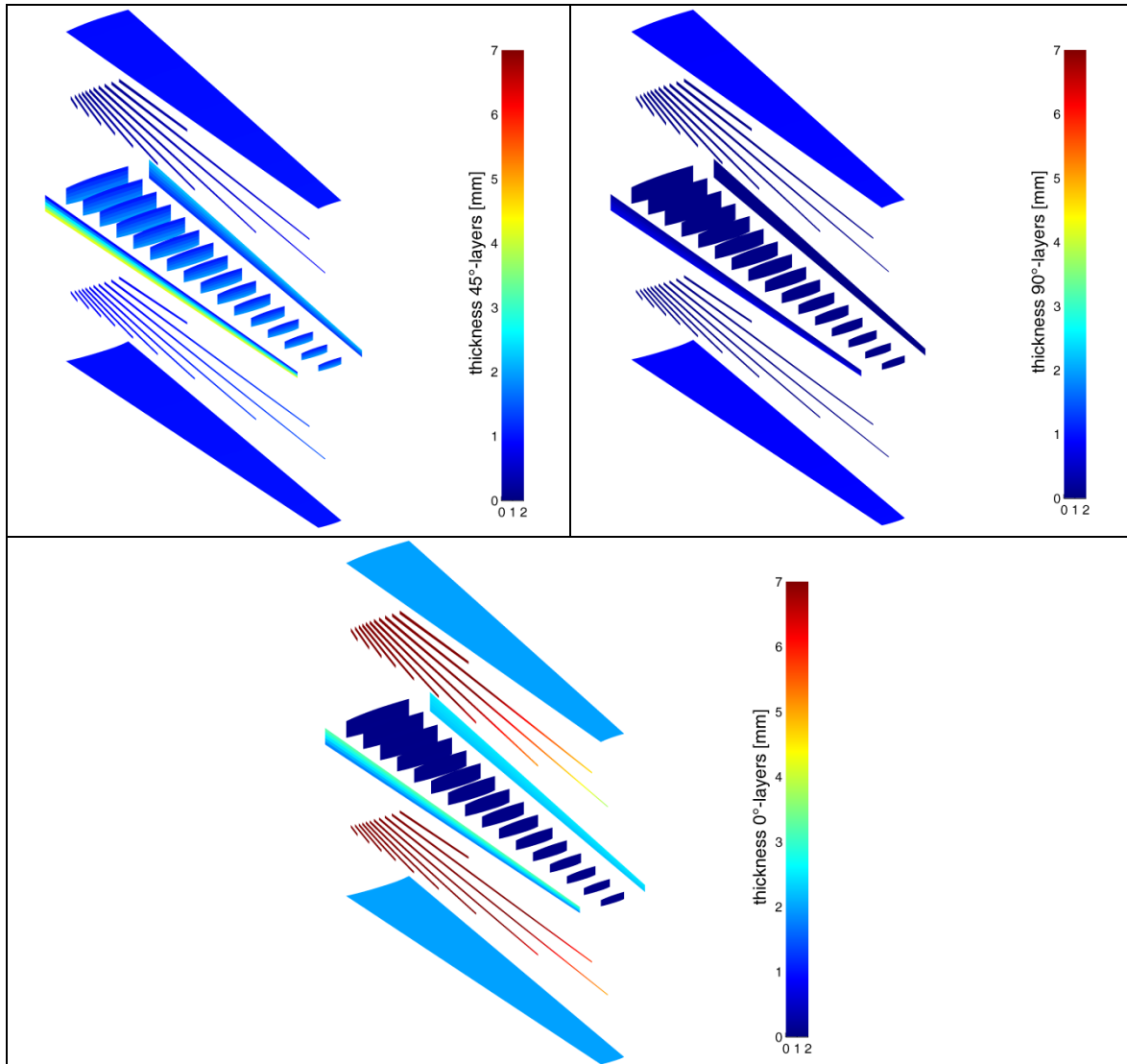


Fig. 7-12 Optimal thickness values of model 3_WBC600_WTC005_001

Geometrical DV	Initial value	Optimal value
CP_str_pos_P1	0.250	0.253
CP_str_pos_P2	0.500	0.309
CP_str_pos_P3	0.750	0.530
CP_str_pos_t_P1	0.300	0.249
CP_str_pos_t_P2	0.300	0.331
CP_str_pos_t_P3	0.300	0.622
CP_str_hh_u_P0 [mm]	150.0	97.57
CP_str_hh_u_P1 [mm]	35.0	31.41
CP_str_hh_l_P0 [mm]	150.0	74.07
CP_str_hh_l_P1 [mm]	35.0	31.89

Table 7-10 Values of geometrical DVs of model 3_WBC600_WTC005_001

The massive divergent stringers running sequentially out at the front spar lead now to an unsteady torsion angle trend in span-wise direction (cf. Fig. 7-13)

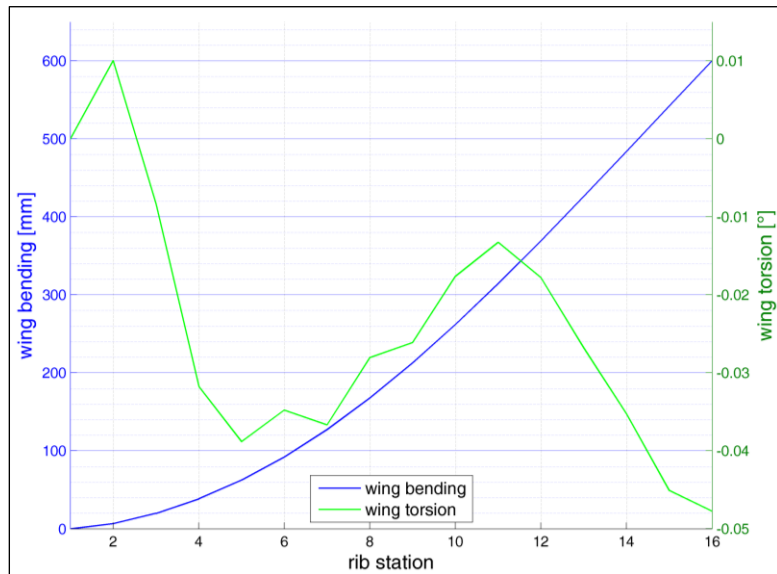


Fig. 7-13 Elastic deformations of optimal design of model 3_WBC600_WTC005_001

The covers make up over 50% of the total mass (cf. Fig. 7-14), followed by the stringers with approximately 27%. The model with curvilinear stiffeners achieves a similar mass breakdown.

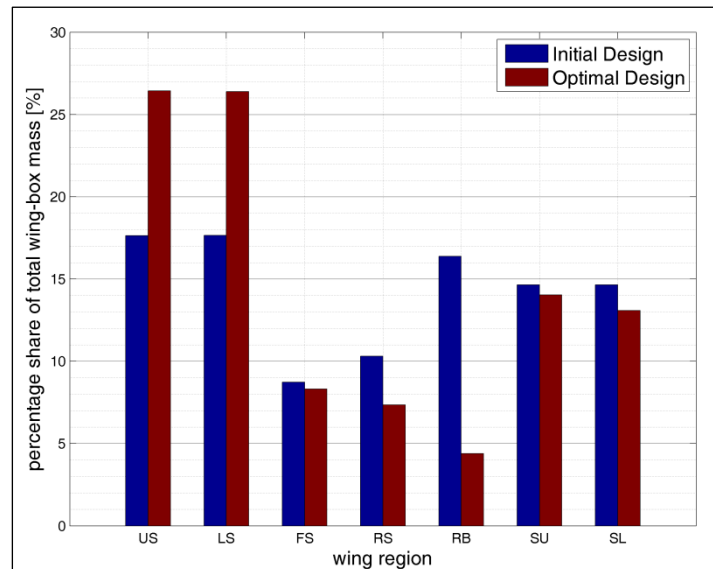


Fig. 7-14 Mass breakdown of model 3_WBC600_WTC005_001

Limiting the maximum ply thickness of the wing covers leads to different optimal results of the ForSwing reference wing according to the stiffener configuration. In this case, curvilinear stiffeners are not the best suited configuration but rather straight divergent stringers. However, the best optimal mass of the *B-models* is $m=1113\text{kg}$, while the optimal mass of the *A-models* is $m=619\text{kg}$. Despite the fact that the A- and B-optimization models are not completely identical the magnitude difference between these two results proves that limiting the cover thickness leads definitely to higher optimal mass values. In other words, the cover thickness (and not the stiffener arrangement) is the most effective property to optimally fulfill the deformation requirements of the ForSwing reference wing.

7.2.3 Optimizations C

As the primary task of the stringers is to support the covers against buckling, the C-models are optimized using the buckling constraints defined in Eq. (5.6). Fig. 7-15 shows that the stiffener configuration has an influence on the optimal wing mass: configuration 1 (stringers parallel front spar) achieves the lowest optimal mass, while configuration 4 (curvilinear stiffeners) exhibits the highest optimal mass.

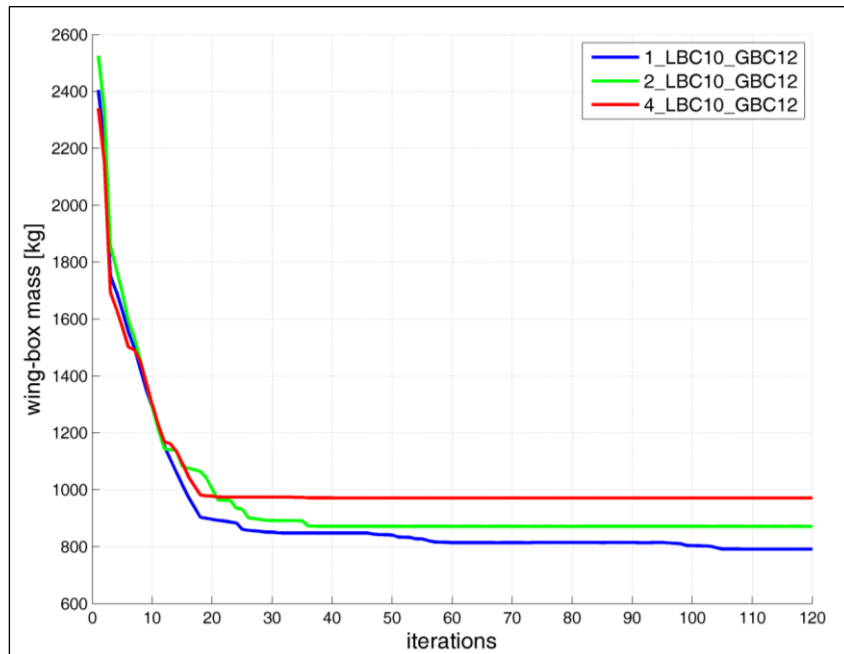


Fig. 7-15 Comparison of optimal mass of C-models

Table 7-11 shows that the optimal stringer positions are in general not very different from the initial positions. The stringer height at the wing root seems to play an important role because it remains at a high value. In all models, the region near the wing root turns out to be the most buckling endangered region and therefore, high stiffeners are necessary to achieve the desired critical buckling loads.

DV	Initial value	Optimal value		
		1_LBC10_GBC12	2_LBC10_GBC12	4_LBC10_GBC12
CP_str_pos_P1	0.250	0.254	0.305	0.285
CP_str_pos_P2	0.500	0.508	0.406	0.464
CP_str_pos_P3	0.750	0.712	0.710	0.672
CP_str_pos_t_P1	0.100	-	-	0.106
CP_str_pos_t_P2	0.100	-	-	0.107
CP_str_pos_t_P3	0.100	-	-	0.115
CP_str_hh_u_P0 [mm]	150.0	123.78	125.15	134.79
CP_str_hh_u_P1 [mm]	35.0	32.75	32.25	36.51
CP_str_hh_l_P0 [mm]	150.0	116.66	112.49	118.35
CP_str_hh_l_P1 [mm]	35.0	33.13	31.66	33.78

Table 7-11 Values of geometrical DVs of C-models

Depending on the stiffener configuration different buckling modes are calculated as shown in Fig. 7-16: (a) shows the first local mode of configuration 1 in which dents between the

stiffeners (yellow lines) at the wing root are visible; (b) displays the first global mode of configuration 1 with big dents extending over several stiffener positions (stiffeners are deflected together with the skin); (c) shows the first local mode of configuration 4 detected at a higher λ -value and at a different position as configuration 1; (d) displays the first global mode of configuration 4 which is not as pronounced as in configuration 1.

It seems as if curvilinear stiffeners make the wing too stiff against buckling and therefore it is not possible to find local modes at the desired level $\lambda = 1.00$. The same phenomenon can also be observed for configuration 2. On the other hand, configuration 1 seems to exploit the design domain properly and achieves the constraint levels successfully, leading to a lower optimal mass.

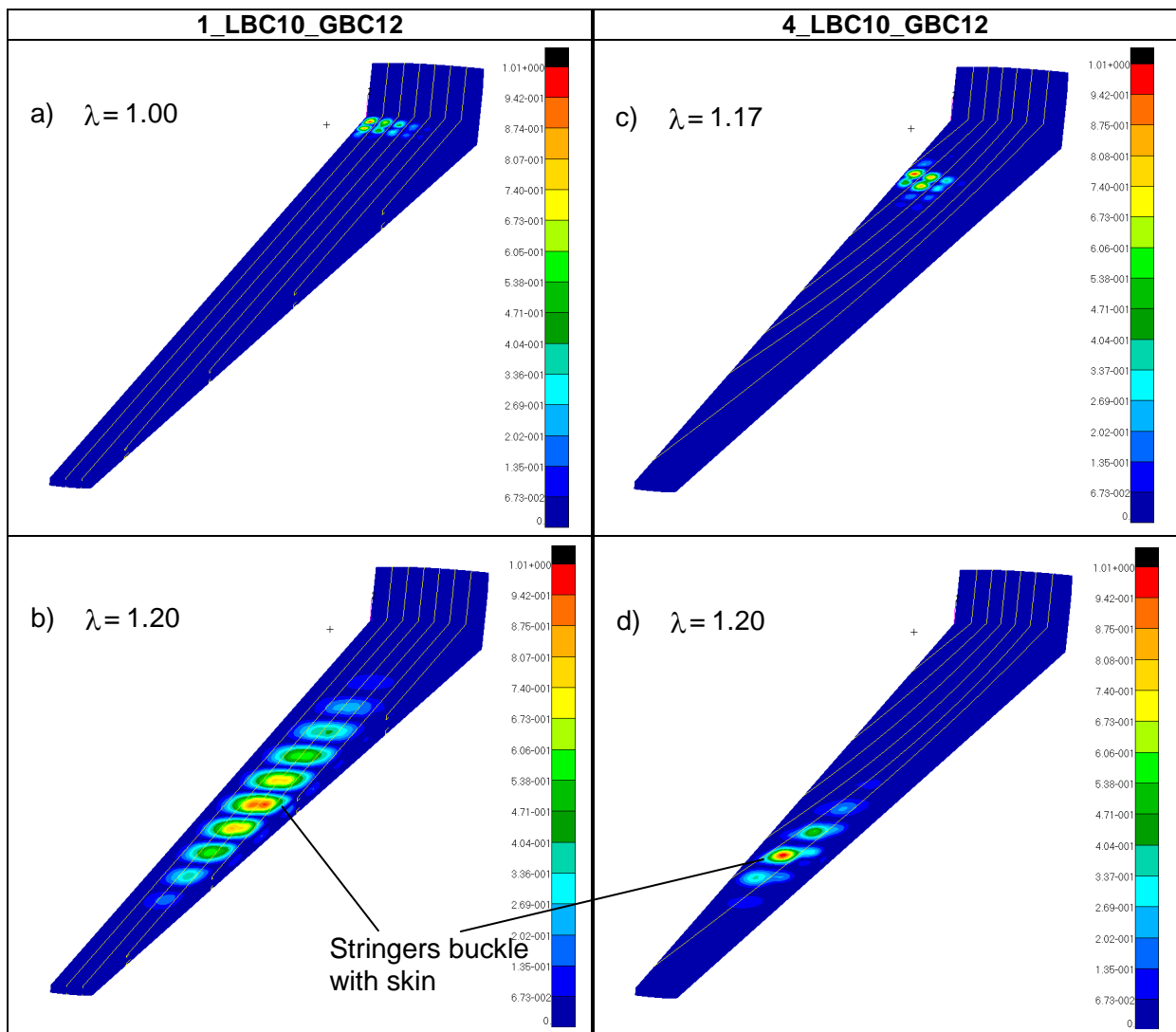


Fig. 7-16 Comparison of buckling modes between configurations 1 and 4

Regarding the laminate thicknesses, the 0° -layers of the upper cover stiffeners are increased the most as well as the 90° -layers of the upper cover near the wing root (cf. Fig. 7-17). It can be concluded that a traditional stiffener arrangement (straight stringers parallel to front spar) seems to be best suited for optimizing the buckling behavior of the ForSwing reference wing.

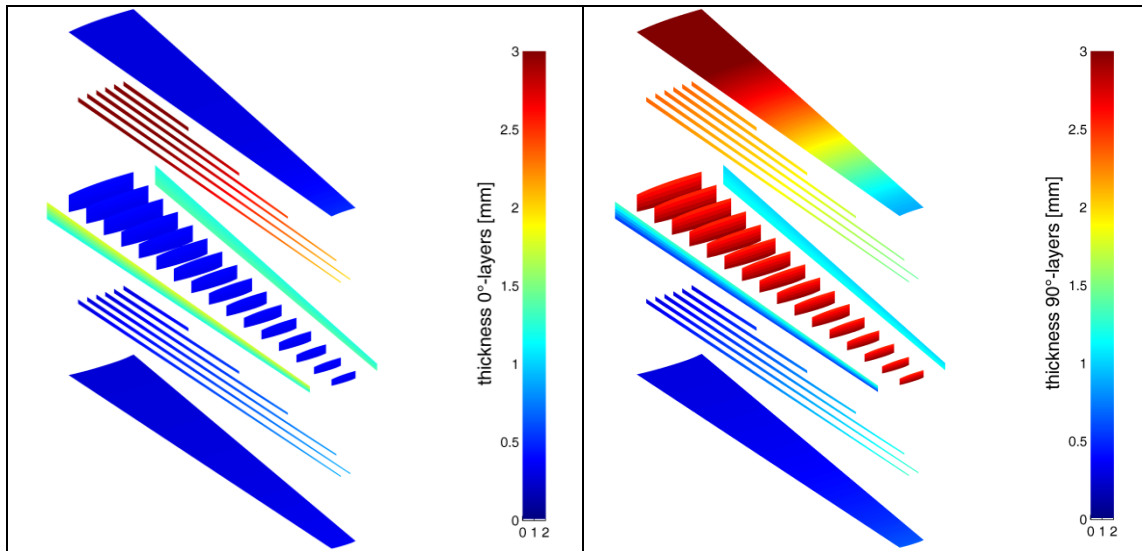


Fig. 7-17 Optimal thickness values of model 1_LBC10_GBC12

8 Conclusions and outlook

This thesis deals with the investigation of the influence of curvilinear stiffeners on the structural behaviour of a forward swept wing design. For this purpose, the structural analysis is performed by means of the finite-element-method and integrated into a numerical optimization procedure in order to find optimum wing designs.

First, a suitable FE assembly method for modeling the forward swept wing structure is investigated. The permanent glued contact method proves to be a precise and efficient method for joining the blade stiffeners to the wing covers. Secondly, a parameterization concept based on Bézier curves is developed to define the curvilinear stringer paths. This concept along with other parameterized properties is implemented into an automated wing modeling procedure. Thirdly, an optimization framework is defined that allows for the use of composite and geometrical design variables and of the design responses mass, elastic deformations and buckling. Finally, after performing a small preliminary structural assessment in order to explore the design domain, several optimizations using traditional and curvilinear stiffener arrangements are performed and the optimum design results are compared.

The benefits of implementing curvilinear stiffeners w.r.t. the structural responses elastic deformations and buckling are investigated. For this, three different optimization types are performed:

- Optimizations A: consideration of wing mass, bending and torsion (*A-models*)
- Optimizations B: same as A with limited wing cover thicknesses (*B-models*)
- Optimizations C: consideration of wing mass and buckling (*C-models*)

A preliminary structural assessment shows that stiffeners have the potential of influencing the elastic deformations of the forward swept wing, i.e. are capable of aeroelastic tailoring. The wing torsion deformation can be reduced when the stringers are turned or curved forward w.r.t. the wing-box longitudinal axis. Specially using curvilinear stiffeners leads to a significant reduction of the wing torsion in comparison to traditional stiffener arrangements. However, they lead in general to an increase of the wing bending.

The optimization of the ForSwing reference wing shows that the beneficial twist-reducing effect of curvilinear stiffeners does not have any influence on the optimum wing design (*A-models*). With curvilinear or straight stiffeners, the most weight-efficient approach for fulfilling the bending and torsion requirements is to increase the thickness, i.e. stiffness, of the wing covers. Thus, the model with curvilinear stiffeners achieves practically the same optimal mass as the models with traditional stiffeners.

For selected *A-models*, the rigorous bending constraint was softened with the result that the higher the allowable bending is, the lower the wing mass becomes. However, it is shown that for different bending constraint levels the models with curvilinear stiffeners still achieve very similar optimal mass values to those of the models with traditional stiffener arrangements. When the torsion constraint is modified, the models feature different twist angle distributions in span-wise direction. In this case, the model with curvilinear stiffeners exhibits the lowest twist but this does not lead to a lower optimal mass.

Using curvilinear stiffeners leads to a significant lower optimal mass only when the maximum allowable cover thickness is limited to small values (*B-models*). In this case, the stiffeners and/or spars become very massive but this is not as weight-efficient as thick wing covers. In other words, using curvilinear stiffeners is not the most effective approach to optimally fulfill the deformation requirements of the ForSwing reference wing.

Concerning the C-models, the commonly used straight stiffeners parallel to the front spar are best suited for optimizing the buckling behavior. The model with curvilinear stiffeners achieves a higher optimal mass and is not able to fulfill the buckling constraints successfully.

Based on the investigations performed in this thesis, it can be concluded that implementing curvilinear stiffeners in the design and optimization of the ForSwing reference wing is not beneficial from a structural point of view. They do not help to better fulfill the wing bending and twisting requirements, neither do they prove to be advantageous for the buckling behavior.

However, the concept of using curvilinear stiffening members is a very innovative idea that should be investigated more in detail. Further research should be therefore carried out that takes into account more parameters, e.g.:

- Wing sweep angle:
 - A higher sweep angle means a stronger geometrical bending-torsion coupling, i.e. higher wing torsion that must be reduced.
- Wing-box dimensions:
 - Different spar positions should be investigated as they have an enormous influence on the cross-sectional stiffness.
- Stiffeners type:
 - Perform optimizations using not only blade stiffeners, e.g. I-profile or omega-profile.

In addition to this, more refined parameterization concepts might possibly deliver better results and/or sensitivities, e.g.:

- Curvilinear stiffeners that are able to cross each other
- Define the stiffener height in span-wise direction using a more complex function than the so far implemented linear approach.

In a further step, a more realistic aerodynamic load calculation should also be implemented. This would require the integration of a CFD-based software into the optimization process that on the one hand would calculate very good aerodynamic data but on the other hand would largely increase the computational effort. Other relevant design responses like strength and damage tolerance should be considered in a further step as well.

Despite the fact that the gradient-based algorithm used in this thesis showed in general a satisfactory performance, other algorithms should also be employed to validate the results. For example, evolutionary algorithms [57] are able to explore the design space more extensively and might find a different (and better) optimum design. Maybe defining a multi-objective optimization, in which not only the wing mass but also the wing torsion is minimized at the same time, could lead to the curvilinear stiffeners significantly influencing the optimum design of a forward swept wing. In addition to this, a two-level optimization approach as recommended by *Hansen* [13], in which geometrical design variables are separated from sizing (thickness) design variables, might show a better performance.

When it comes to composite structures, manufacturing aspects play a very important role, too. For a curvilinear stiffener arrangement, like the one presented in this thesis, each stiffener has unique dimensions, i.e. curvature and length. This means that all stiffeners cannot be produced in mass as opposite to straight stringers which undergo the same manufacturing process. Thus, the manufacturing of curvilinear stiffeners would definitely lead to higher costs.

In addition to this, probably the most suited method of giving the stiffeners their curved forms is through a hot bending process [58]. Stiffeners are normally made up of a large share of 0°-plies in longitudinal direction (high longitudinal stiffness to transfer axial loads). For sharp curved stiffeners, the bending process would cause that outermost plies are elongated, while

internal plies are compressed. Only the outermost plies would be highly loaded and eventually fail. Then, the plies beneath would transfer the whole load and eventually fail too, and so on (cf. Appendix G). Furthermore, compatibility problems between sharp curved stiffeners and the wing covers could also arise because of the very different orientation angles [58]. A proper load transfer in this area is imperative and should be investigated in detail. Thus, from a manufacturing point of view, curvilinear stiffeners do not exhibit any advantages in comparison to traditional straight stringers. In this context, perhaps new manufacturing methods, like a new Boeing-method of manufacturing curved composite structural elements [59], can lead in the future to a more adequate production of curvilinear stiffeners.

On the whole, this thesis serves as a first step towards investigating the potential of implementing curvilinear stiffeners into the design of a forward swept wing and it should be regarded as a cornerstone for further research.

References

- [1] Kruse, M.; Wunderlich, T.; Heinrich, L. (2012): *A conceptual study of a transonic NLF transport aircraft with forward swept wings*. AIAA paper, 30th AIAA Applied Aerodynamics Conference, New Orleans, Louisiana, 25 – 28 June
- [2] Chun-Yung Niu, M. (1999): *Airframe structural design*, 2nd edition. Hong Kong Conmilit Press Ltd., Hong Kong, pp. 263-264
- [3] Airbus S.A.S: *A320-100 Airframe Certification Document*, Vol. 2: *Structural Description*. Issue 1 – January 1987
- [4] Airbus S.A.S: *A350 XWB wing production start, Broughton MSN1* [Web Photo from January 24, 2013]
Retrieved from <http://www.airbus.com/galleries/photo-gallery/?p=58#open=galleries/photo-gallery/dg/idp/28423-a350-xwb-wing-production-start-broughton-msn1/?backURL=galleries/photo-gallery/?p=58> (March 17, 2014)
- [5] Michell, A.G.M. (1904): *The limits of economy of materials in frame structures*. Philosophical Magazine Series 6, Vol. 8, No. 47, pp. 589-597
- [6] Haftka, R.T.; Gürdal, Z.; Kamat, M.P. (1990): *Elements of Structural Optimization*. Kluwer Academic Publishers
- [7] Arora, J.S. (2004): *Introduction to optimum design*, 2nd edition. Elsevier Academic Press, London
- [8] Kirsch, U. (1993): *Structural Optimization*. Springer-Verlag, Berlin – Heidelberg
- [9] Starnes Jr., J.H.; Haftka, R.T. (1979): *Preliminary design of composite wings for buckling, strength and displacement constraints*. Journal of Aircraft, Vol. 16, No.8, pp. 564-570
- [10] Hürlimann, F. (2010): *Mass estimation of transport aircraft wingbox structures with a CAD/CAE-based multidisciplinary process*. Dissertation submitted to ETH Zürich (Nr. 19458)
- [11] Venter, G.; Sobieszczanski-Sobieski, J. (2002): *Multidisciplinary optimization of a transport aircraft wing using particle swarm optimization*. Presented as paper 2002-5644, 9th AIAA/ISSMO Symposium on Multidisciplinary Analysis and Optimization, Atlanta, Georgia, 4 – 6 June
- [12] Liu, B.; Haftka, R.T.; Akgün, M.A. (2000): *Two level composite wing structural optimization using response surfaces*. Structural and Multidisciplinary Optimization, Vol. 20, pp. 87-96
- [13] Hansen, L.U.; Horst, P. (2008): *Multi-level optimization in aircraft structural design evaluation*. Computers & Structures, Vol. 86, pp. 104-118
- [14] Zhao, Q.; Ding, Y.; Jin, H. (2011): *A layout optimization method of composite wing structures based on carrying efficiency criterion*. Chinese Journal of Aeronautics, Vol. 24, pp. 425-433

-
- [15] Chintapalli, S.; Elsayed, M.; Sedaghati, R.; Abdo, M. (2010): *The development of a preliminary structural design optimization method of an aircraft wing-box skin-stringer panels*. Aerospace Science and Technology, Vol. 14, pp. 188-198
- [16] Almeida, F.S.; Awruch, A.M. (2009): *Design optimization of composite laminated structures using genetic algorithms and finite element analysis*. Composite Structures, Vol. 88, pp. 443-454
- [17] Eschenauer, H.A.; Geilen, J.; Wahl, H.J. (1993): *SAPOP – An optimization procedure for multicriteria structural design*. International series of numerical mathematics, Vol. 110, Birkhäuser Verlag, Basel, pp. 207-227
- [18] Schittkowski, K. (2005): *Optimization in industrial engineering: SQP-methods and applications*. Radioss User Meeting, Mecalog, Nice, 20 – 22 June
Retrieved from <http://www.klaus-schittkowski.de/refercs.htm> (March 30, 2014)
- [19] Schittkowski, K.; Zillober, C.; Zotemantel, R. (1994): *Numerical comparison of nonlinear programming algorithms for structural optimization*. Journal of Structural Optimization, Vol. 7, No. 1, pp. 1-28
Retrieved from <http://www.klaus-schittkowski.de/refercs.htm> (March 30, 2014)
- [20] Shirk, M. H.; Hertz, T. J.; Weisshaar, T. A. (1986): *Aeroelastic Tailoring - Theory, Practice, and Promise*. Journal of Aircraft, Vol. 23, No. 1, pp. 6-18
- [21] Weisshaar, T. A. (1981): *Aeroelastic Tailoring of forward swept composite wings*. Journal of Aircraft, Vol. 18, No. 8, pp. 669-676
- [22] Isogai, K. (1992): *Transonic flutter/divergence characteristics of aeroelastically tailored and non-tailored high-aspect-ratio forward-swept wings*. Journal of Fluids and Structures, Vol. 6, No. 5, pp. 525-537
- [23] Gleichmar, R. (2004): *Approximationen und paralleles Rechnen bei der multidisziplinären Strukturoptimierung*. Dissertation submitted to Technical University Munich (TUM), Lehrstuhl für Leichtbau
- [24] Kobler, P. (2006): *Strukturoptimierung mittels aeroelastic tailoring und evolutionären Algorithmen*. Thesis submitted to ETH Zürich, Zentrum für Strukturtechnologien (Nr. 05-189)
- [25] Guo, S.; Cheng, W.; Cui, D. (2006): *Aeroelastic tailoring of composite wing structures by laminate layup optimization*. AIAA Journal, Vol. 44, No. 12, pp. 3146-3149
- [26] Dems, K.; Mróz, Z.; Szelag, D. (1987): *Optimal design of rib-stiffeners in disks and plates*. International Journal of Solids and Structures, Vol. 25, No. 9, pp. 973-998
- [27] Brubak, L.; Hellesland, J.; Steen, E. (2006): *Semi-analytical buckling strength analysis of plates with arbitrary stiffener arrangements*. Journal of Constructional Steel Research, Vol. 63, pp. 532-543
- [28] Gürdal, Z.; Gendron, G. (1993): *Optimal design of geodesically stiffened composite cylindrical shells*. Composites Engineering, Vol. 3, No. 12, pp. 1131-1147
- [29] McDonnell Douglas Astronautics Company: *Isogrid Design Handbook*. NASA-CR-124075 Revision A, February 1973
-

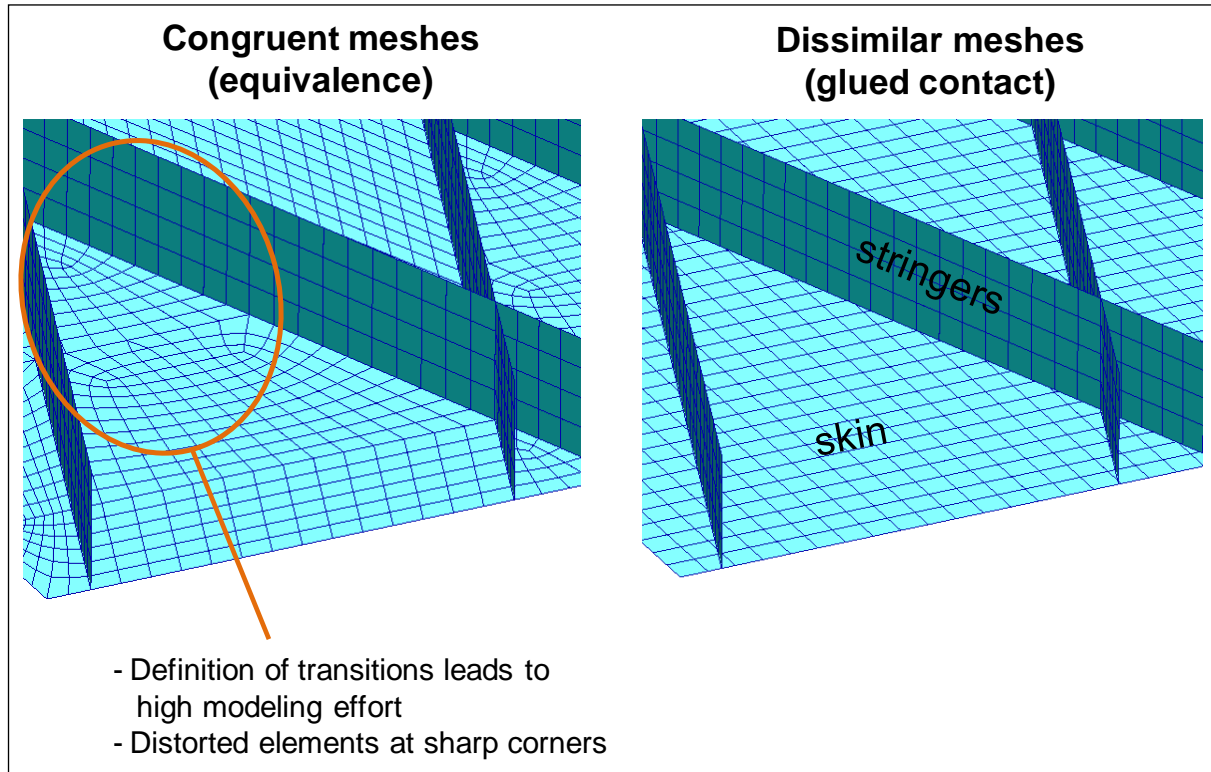
-
- [30] Slemp, W.H.C.; Bird, R.K.; Kapania, R.K.; et al. (2011): *Design, Optimization and Evaluation of Integrally Stiffened Al 7075 Panel with Curved Stiffeners*. NASA Technical Publication, NASA/TP-2011-217178, Langley Research Center
- [31] Locatelli, D. (2012): *Optimization of supersonic aircraft wing-box using curvilinear SpaRibs*. Dissertation submitted to the Faculty of the Virginia Polytechnic Institute and State University, Blacksburg, Virginia
- [32] Kobayashi, M.H.; Kolonay, R.M; LeBon, A.; et al. (2010): *On a cellular division model for multi-disciplinary optimization*. AIAA paper No. 2010-2989, 51st AIAA/ASME/ASCE/AHS/ASC Structures, Structural Dynamics, and Materials Conference, Orlando, Florida, 12 - 15 April
- [33] MSC.Software Corporation: *Choosing the right finite element | MSC Nastran* [Web documentation from July 11, 2013]
Retrieved from <http://simulatemore.mscsoftware.com/choosing-the-right-finite-element-msc-nastran/> (January 10, 2014)
- [34] MSC.Software Corporation: *Simplify assembly level analysis* [Web video from March 14, 2013]
Retrieved from <http://www.youtube.com/watch?v=7o84wAqe4yQ> (April 13, 2014)
- [35] MSC.Software Corporation: *MD/MS Nastran 2010 Quick Reference Guide*, Revision 1 – October 2010
- [36] Palmonella, M.; Friswell, M.I.; Motthershead, J.E., et al. (2004): *Guidelines for the implementation of the CWELD and ACM2 spot weld models in structural dynamics*. Finite Elements in Analysis and Design, Vol. 41, pp. 193-210
- [37] Palmonella, M.; Friswell, M.I.; Motthershead, J.E., et al. (2005): *Finite element models of spot welds in structural dynamics: review and updating*. Composite and Structures, Vol. 83, pp. 648-661
- [38] Jegley, D.; Velicki, A. (2013): *Status of advanced stitched unitized composite aircraft structures*. AIAA paper No. 2013-0410, 51st AIAA Aerospace Sciences Meeting including the New Horizons Forum and Aerospace Exposition, Grapevine, Texas, 7 - 10 January
- [39] MSC.Software Corporation: *Making meshing easier with permanent glued contact | MSC Nastran* [Web documentation from July 2, 2013]
Retrieved from <http://simulatemore.mscsoftware.com/making-meshing-easier-with-permanent-glued-contact-msc-nastran/> (January 10, 2014)
- [40] Wriggers, P. (2001): *Nichtlineare Finite-Element-Methoden*. Springer-Verlag, Berlin – Heidelberg, pp.429-433
- [41] Klein, B. (2007): *FEM - Grundlagen und Anwendungen der Finite-Elemente-Methode im Maschinen- und Fahrzeugbau*, 7. Verbesserte Auflage. Vieweg Verlag, Wiesbaden, pp.182-201
- [42] MSC.Software Corporation: *MD Nastran 2011 & MSC Nastran 2011 Linear static analysis user's guide*, Revision 0 – March 2011
- [43] MSC.Software Corporation: *SOL400 Training Course Notes – MD Nastran R3, partly 2011*, Revision 0 – March 2011
-

-
- [44] Böhm, W.; Farin, G; Kahmann, J. (1984): *A survey of curve and surface methods in CAGD*. Journal of Computer Aided Geometric Design, Vol. 1, pp. 1-60
- [45] Weisstein, E.W.: *Bézier Curve*. From MathWorld – A Wolfram Web Resource. Retrieved from <http://mathworld.wolfram.com/BezierCurve.html> (May 13, 2014)
- [46] Wikipedia: *Bézier Curve*. Retrieved from http://en.wikipedia.org/wiki/Bézier_curve (May 14, 2014)
- [47] MSC.Software Corporation: *The PATRAN Command Language (PCL) Introduction*. Retrieved from http://www.mssoftware.com/training_videos/patran/Reverb_help/index.html#page/PCL%2520and%2520Customization/pcl_topics.03.01.html (May 9, 2014)
- [48] MSC.Software Corporation: *PCL functions*. Retrieved from http://www.mssoftware.com/training_videos/patran/Reverb_help/index.html#page/PCL%2520and%2520Customization/pcl_topics.03.07.html (May 24, 2014)
- [49] Seibel, M.; Velasquez, H.; Goanta, H. (2013): *Support to implement achieved MDO-strategies into the optimization process*. AeroStruct Milestone Report Nr. 2, Hamburg University of Applied Sciences [non-published documentation]
- [50] Seibel, M.; Velasquez, H.; Goanta, H. (2013): *Robust MDO-strategies for the design of airframe structures made of fiber-reinforced plastics*. AeroStruct Milestone Report Nr. 1, Hamburg University of Applied Sciences [non-published documentation]
- [51] Noesis Solutions: *Optimus*. Retrieved from <http://www.noessolutions.com/Noesis/about-optimus> (May 16, 2014)
- [52] Heinrich, L. (2013): *Microsoft Excel Tool: QMM_aus_cp_neuer9*. Research project AeroStruct–ForSwing, German Aerospace Center, Braunschweig [non-published documentation]
- [53] Schuhmacher, G. (1995): *Multidisziplinäre, fertigungsgerechte Optimierung von Faserverbund-Flächentragwerken*. TIM Forschungsberichte (Nr. T07-03.95). FOMAAS, Universität-Gesamthochschule Siegen, pp. 116-127
- [54] Seibel, M.; Velasquez, H.; Goanta, H. (2013): *Investigation of the buckling behavior of the forward swept wing FE-model used within the ForSWING structural optimization process*. AeroStruct Action Item Report – Action Items Nr. 1.12 and 3.2, Hamburg University of Applied Sciences [non-published documentation]
- [55] Wrenn, G. A. (1989): *An Indirect Method for Numerical Optimization Using the Kreisselmeier-Steinhausser Function*. NASA Contractor Report Nr. 4220, prepared for NASA Langley Research Center under contract NAS1-18000.
- [56] Schittkowski, K. (1985/86): *NLPQL: A Fortran subroutine solving constrained nonlinear programming problems*. Annals of Operations Research, Vol. 5, pp. 485-500
- [57] Goldberg, D.E. (1989): *Genetic Algorithms in Search, Optimization & Machine Learning*. Addison-Wesley Publishing Company
-

- [58] Personal interview with M. Kleineberg, Head of the Department Composite Technology, Institute of Composite Structures and Adaptive Systems (DLR-FA), Braunschweig (April 1, 2014)
- [59] 4-traders: *Boeing: "Method of Manufacturing Curved Composite Structural Elements" in Patent Application Approval Process.*
- Retrieved from
<http://www.4-traders.com/THE-BOEING-COMPANY-4816/news/Boeing--Method-of-Manufacturing-Curved-Composite-Structural-Elements-in-Patent-Application-Approv-18161850/> (May 23, 2014)

Appendix A

Example of congruent and dissimilar meshes



Appendix B

B.1 Structure of a BCTABLE [35]

BCTABLE	ID			NGROUP	COPTS	COPTM		
	"SLAVE"	IDSLA1	ERROR			CINTERF	IGLUE	
		ISEARCH	ICOORD					
		"FSBH"		BIAS			COPTS1	COPTM1
	"MASTER"	IDMA1	IDMA2	IDMA3	IDMA4	IDMA5	IDMA6	IDMA7
		IDMA8	IDMA9	...				

B.2 Definition of parameters COPTS1 and COPTM1 [35]

$$\text{COPTX1} = A + 10 \cdot B + 1000 \cdot C$$

- A = 1: the outside of the solid elements will be in the contact description (Default)
- B = 6: both top and bottom faces will be in the contact description, shell thicknesses will be ignored. This means that the slave nodes contact the reference plane of the CQUAD4-elements and not the laminate (PCOMP) external surfaces. This decision is based on practical experience.
- C = 11: not only beam/bar edges but also shell edges are included in the contact description. In the forward swept wing model the blade stiffeners and the covers form a shell edge-to-face contact (cf. Fig. 3-4).

Appendix C

Properties of used CFC-materials [50]

Name	T800/M21	HTA-M21
Type	UD-Prepreg	Fabric-Prepreg
Layers	0°,90°	±45°
E_{11} [MPa]	150000	65000
E_{22} [MPa]	8000	65000
G_{12} [MPa]	4000	4000
ν_{12}	0.35	0.05
t_{nom} [mm]	0.25	0.31
ρ [g/cm ³]	1.6	1.55
$R_{ }^t$ [MPa]	2500	740
$R_{ }^c$ [MPa]	-1400	-715
R_{\perp}^t [MPa]	50	740
R_{\perp}^c [MPa]	-270	-715
$R_{\perp }$ [MPa]	100	100

Appendix D

Properties of forward swept wing model used for validation and parameter study

<p>General geometrical characteristics:</p> <ul style="list-style-type: none"> - Wing area = 132m² - Aspect ratio = 9.71 - Taper ratio = 0.371 - Sweep angle = -19.8°
<p>Structural characteristics:</p> <ul style="list-style-type: none"> - 16 ribs - 22 stringers (11 upper and 11 lower) <p style="margin-left: 40px;">Height at root: 150 mm</p> <p style="margin-left: 40px;">Height at tip: 35 mm</p>
<p>Loadcases:</p> <ul style="list-style-type: none"> - LC1 (Cruise): $n_z=LL=1.0$ Air density = 0.38773 kg/m³ Air velocity = 231.874 m/s Mach number = 0.78 Aircraft mass = 71500 kg - LC2 (Gust): $n_z=LL=3.44$ Air density = 1.225 kg/m³ Air velocity = 227.660 m/s Mach number = 0.67 Aircraft mass = 56100 kg
<p>Laminate stacking sequence:</p> <p style="margin-left: 40px;">Upper Skin, Lower Skin, Front Spar, Rear Spar:</p> <ul style="list-style-type: none"> - [0°₂ ±45° 90°₂ ±45° 0°₂ 90°₂]_s <p style="margin-left: 40px;">Ribs:</p> <ul style="list-style-type: none"> - [0° ±45° 90°₂]_s <p style="margin-left: 40px;">Stringers:</p> <ul style="list-style-type: none"> - [0°₂ ±45° 90°₂ ±45° 0°₂ 90°₂ 0°]_s
<p>CFC material properties:</p> <ul style="list-style-type: none"> - Refer to Appendix B

Appendix E

Structure of input file *wing_info.txt*


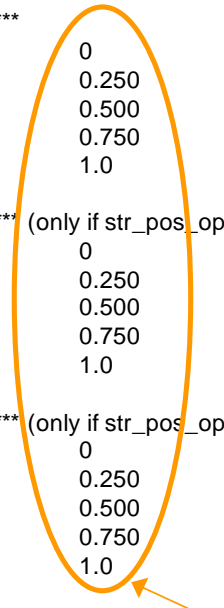
Detail 1

\$ Wing geometrical information \$		
wing_area	132	in m ² .
aspect_ratio	9.71	
fuselage_diameter	4000	in mm.
wetted_half_span	15900	in mm (from wing-fuselage-interface till wing tip).
number_of_points	59	number of points used to create airfoil (see wing_coo.txt").
taper_ratio	0.371	
phi_25	-19.8	in ° (ATTENTION! Forward sweep is negative. Domain = [-45;0]).
dihedral_angle	4	in ° (ATTENTION! Domain = [-30;30]).
\$ Spars \$		
FS_pos_root	0.150	in percent of chord at the wing root
RS_pos_root	0.580	in percent of chord at the wing root
FS_pos_tip	0.150	in percent of chord at the wing tip
RS_pos_tip	0.580	in percent of chord at the wing tip
\$ Ribs \$		
number_of_ribs	15	(without taking into account root rib). Max. number = 40
rib_pos_option	4	define y-positions of ribs: 4 → use a polynomial (Bézier) curve
**** rib position option 4: polynomial (Bézier) curve ****		
CP_rib_pos_P0	0	control point 1 (ATTENTION! This value must always be 0)
CP_rib_pos_P1	0.250	control point 2
CP_rib_pos_P2	0.500	control point 3
CP_rib_pos_P3	0.750	control point 4
CP_rib_pos_P4	1.0	control point 5 (ATTENTION! This value must always be 1)

Position of front spar (FS) and rear spar (RS)

Bézier control points of rib positions

Detail 2

\$ Stringers \$																	
number_of_str	11	number of stringers for upper and lower cover. Max. number = 30															
str_pos_option	1	define position of stringers:															
		1 for straight stringers parallel to front spar; 2 for straight stringers without run-outs; 3 for straight divergent stringers; 4 for curvilinear stringers															
<div style="border: 1px solid orange; padding: 5px; display: inline-block; margin-bottom: 10px;">Stringer configurations (cf. Fig 4-7)</div> 																	
<p>***** Support zone #1 ***</p> <table border="0"> <tr> <td>CP_str_pos_P0</td> <td>0</td> <td>control point 1 (ATTENTION! This value must always be 0)</td> </tr> <tr> <td>CP_str_pos_P1</td> <td>0.250</td> <td>control point 2</td> </tr> <tr> <td>CP_str_pos_P2</td> <td>0.500</td> <td>control point 3</td> </tr> <tr> <td>CP_str_pos_P3</td> <td>0.750</td> <td>control point 4</td> </tr> <tr> <td>CP_str_pos_P4</td> <td>1.0</td> <td>control point 5 (ATTENTION! This value must always be 1)</td> </tr> </table>			CP_str_pos_P0	0	control point 1 (ATTENTION! This value must always be 0)	CP_str_pos_P1	0.250	control point 2	CP_str_pos_P2	0.500	control point 3	CP_str_pos_P3	0.750	control point 4	CP_str_pos_P4	1.0	control point 5 (ATTENTION! This value must always be 1)
CP_str_pos_P0	0	control point 1 (ATTENTION! This value must always be 0)															
CP_str_pos_P1	0.250	control point 2															
CP_str_pos_P2	0.500	control point 3															
CP_str_pos_P3	0.750	control point 4															
CP_str_pos_P4	1.0	control point 5 (ATTENTION! This value must always be 1)															
<p>***** Support zone #2 *** (only if str_pos_option = 4)</p> <table border="0"> <tr> <td>CP_str_pos_m_P0</td> <td>0</td> <td>control point 1 (ATTENTION! This value must always be 0)</td> </tr> <tr> <td>CP_str_pos_m_P1</td> <td>0.250</td> <td>control point 2</td> </tr> <tr> <td>CP_str_pos_m_P2</td> <td>0.500</td> <td>control point 3</td> </tr> <tr> <td>CP_str_pos_m_P3</td> <td>0.750</td> <td>control point 4</td> </tr> <tr> <td>CP_str_pos_m_P4</td> <td>1.0</td> <td>control point 5 (ATTENTION! This value must always be 1)</td> </tr> </table>			CP_str_pos_m_P0	0	control point 1 (ATTENTION! This value must always be 0)	CP_str_pos_m_P1	0.250	control point 2	CP_str_pos_m_P2	0.500	control point 3	CP_str_pos_m_P3	0.750	control point 4	CP_str_pos_m_P4	1.0	control point 5 (ATTENTION! This value must always be 1)
CP_str_pos_m_P0	0	control point 1 (ATTENTION! This value must always be 0)															
CP_str_pos_m_P1	0.250	control point 2															
CP_str_pos_m_P2	0.500	control point 3															
CP_str_pos_m_P3	0.750	control point 4															
CP_str_pos_m_P4	1.0	control point 5 (ATTENTION! This value must always be 1)															
<p>***** Support zone #3 *** (only if str_pos_option = 3 or 4)</p> <table border="0"> <tr> <td>CP_str_pos_t_P0</td> <td>0</td> <td>control point 1 (ATTENTION! This value must always be 0)</td> </tr> <tr> <td>CP_str_pos_t_P1</td> <td>0.250</td> <td>control point 2</td> </tr> <tr> <td>CP_str_pos_t_P2</td> <td>0.500</td> <td>control point 3</td> </tr> <tr> <td>CP_str_pos_t_P3</td> <td>0.750</td> <td>control point 4</td> </tr> <tr> <td>CP_str_pos_t_P4</td> <td>1.0</td> <td>control point 5 (ATTENTION! This value must always be 1)</td> </tr> </table>			CP_str_pos_t_P0	0	control point 1 (ATTENTION! This value must always be 0)	CP_str_pos_t_P1	0.250	control point 2	CP_str_pos_t_P2	0.500	control point 3	CP_str_pos_t_P3	0.750	control point 4	CP_str_pos_t_P4	1.0	control point 5 (ATTENTION! This value must always be 1)
CP_str_pos_t_P0	0	control point 1 (ATTENTION! This value must always be 0)															
CP_str_pos_t_P1	0.250	control point 2															
CP_str_pos_t_P2	0.500	control point 3															
CP_str_pos_t_P3	0.750	control point 4															
CP_str_pos_t_P4	1.0	control point 5 (ATTENTION! This value must always be 1)															
<div style="border: 1px solid orange; padding: 5px; display: inline-block; margin-bottom: 10px;">Bézier control points for stiffener positions (cf. Fig 4-6)</div> 																	
Stringer height: upper cover																	
CP_str_hh_u_P0	150.000	in mm (stringer height at the wing root).															
CP_str_hh_u_P1	35.000	in mm (stringer height at the wing tip).															
Stringer height: lower cover																	
CP_str_hh_l_P0	150.000	in mm (stringer height at the wing root).															
CP_str_hh_l_P1	35.000	in mm (stringer height at the wing tip).															

Detail 3

```

$ Wing meshing information $

**** span-wise direction per rib bay ****

seed_option_span      2      mesh seed option: 1 for number of elements; 2 for element length
num_seed_span         10     /* number of elements in span-wise direction per rib bay */
length_seed_span      150    /* length of elements in span-wise direction per rib bay */

**** span-wise direction center wing box ****

seed_option_cbox      1      mesh seed option: 1 for number of elements; 2 for element length
num_seed_cbox         10     /* number of elements in spanwise-direction for
center wing box */
length_seed_cbox      200    /* length of elements in spanwise-direction for center wing box */

**** vertical direction of spars ****

num_seed_spars        5      /* number of elements in vertical (z-)direction of spars */

**** chord (x-) direction of wing covers ****

seed_option_chord     2      mesh seed option: 1 for number of elements; 2 for element length
num_seed_chord        2      /* number of elements for wing cover in chord direction */
length_seed_chord     70     /* length of elements for wing cover in chord direction */

**** stringer height ****

num_seed_strh         2      /* number of elements for height of stringers */

**** stringer length ****

length_seed_curvstr   150    /* length of elements in longitudinal direction of stringers */
    
```

Detail 4

```

$ Composite material information $
**** UD-Prepreg ****
name_UD          T800_M21
t_UD             0.25      ply thickness in mm

$ Material values
E11_UD          150000     in N/mm2
E22_UD          8000      in N/mm2
NU12_UD         0.40
G12_UD          4000      in N/mm2
G23_UD          10000000  in N/mm2
G13_UD          10000000  in N/mm2
RHO_UD          1.6       in g/cm3

$ **** Material values for center wing box **** $
mat_factor      8
t_plies         0.75      in mm

$ Laminate information $

$ Left column : define ply orientations (positive and negative angles are permissible)
$ Right column: define material type for each ply: 1 --> UD-Prepreg, 2 --> Fabric

Upper_Skin
Stacking sequence definition (one half of laminate only)

          0      1
          45     2
          90     1

Lower_Skin
Stacking sequence definition (one half of laminate only)

          0      1
          45     2
          90     1

```

Detail 5

\$ Load cases information/constraints \$

load_case_2	LC2		
rho	1.225	reference air density in kg/m3	
velocity	227.66	reference free stream velocity in m/s	
LL	3.44	limit load	
f_UL	1.5	factor to multiply by LL in order to define ultimate load	
Y	1.2 LL	factor for defining global buckling constraint	
Z	1 LL	factor for defining local buckling constraint	

\$ Buckling constraint/information \$

Desired number of eigenvalues (only positive eigenvalues considered) = 30
 threshold value for identifying local and global buckling phenomena = 0.15 (Default)

\$ Geometrical Optimization Switch \$

GeomSwitch = 1 0 = geometrical design variables are disabled;
 1 = geometrical design variables are enabled

\$ Bézier definition of ribs \$

RibSwitch = 3 2 = all ribs share the same thickness distributions;
 3 = individual thickness distributions for certain ribs

\$ Bézier definition of stringers \$

StrSwitch = 3 2 = all stringers share the same thickness distribution
 3 = all upper cover stringers share the same distributions, all lower cover stringers share the same distributions

\$ Definition of Control Points of parametric thickness distributions (Bézier surfaces) \$

Column A : 1 = Surface controlled by a vector of control points (the other direction will be held constant)
 2 = Surface controlled by a matrix of control points.

Column B : Determines the polynomial order of Bézier surface
 (Number of control points = polynomial order + 1)

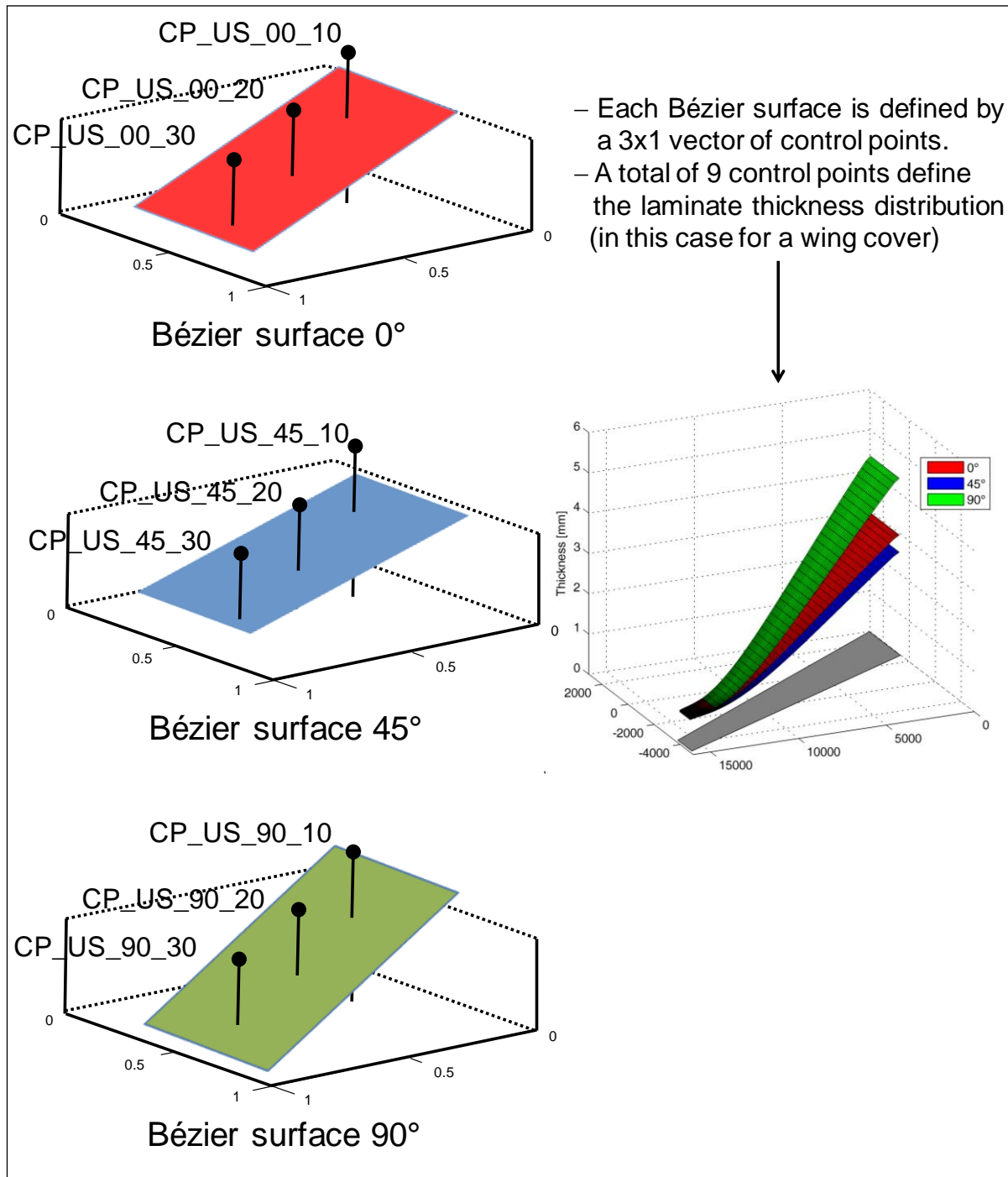
Column C : Start thickness value of 0° layers [mm]
 Column D : Start thickness value +45° layers [mm]
 Column E : Start thickness value 90° layers [mm]

Row 1 : Entries for the upper skin
 Row 2 : Entries for the lower skin
 Row 3 : Entries for the front spar
 Row 4 : Entries for the rear spar
 Row 5 : Entries for the ribs
 Row 6 : Entries for the stringers

	A	B	C	D	E
1	1	3	3	3	3
2	1	3	3	3	3
3	1	2	3	3	3
4	1	2	3	3	3
5	1	1	3	3	3
6	1	1	3	3	3

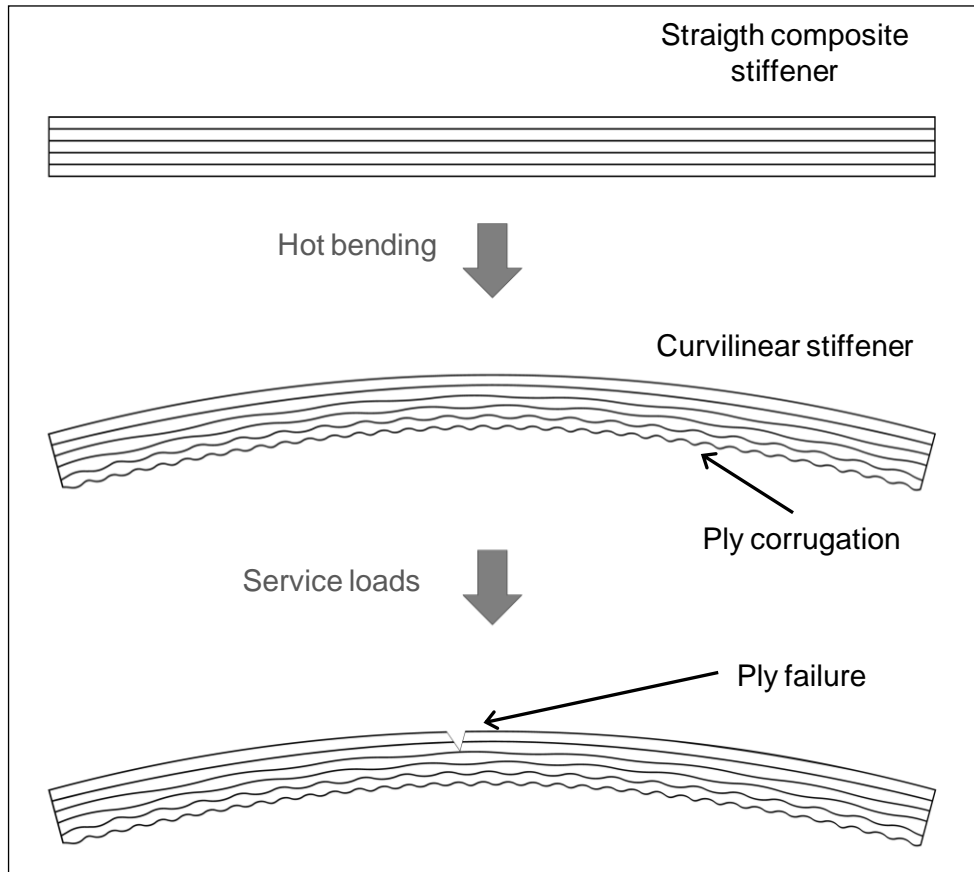
Appendix F

Visualization of a 3x1 Bézier surface configuration as used in this thesis

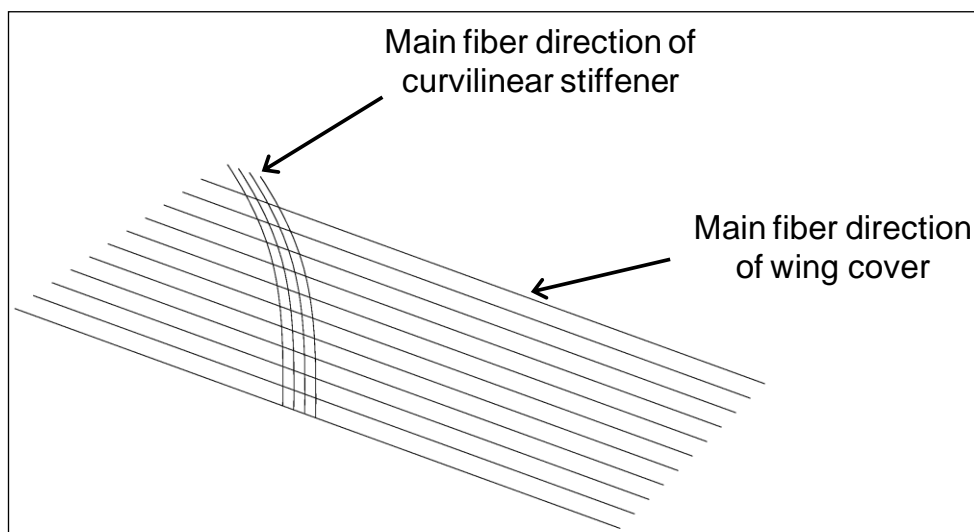


Appendix G

Manufacturing aspects: forming the curvilinear stiffeners



Manufacturing aspects: different fiber orientations between covers and curvilinear stiffeners may lead to compatibility problems



Last Page